

MEMOIRS
OF THE
FACULTY OF ENGINEERING
OSAKA CITY UNIVERSITY

VOL. 59

DECEMBER 2018

PUBLISHED BY THE
GRADUATE SCHOOL OF ENGINEERING
OSAKA CITY UNIVERSITY

This series of Memoirs is issued annually. Selected original works of the members of the Faculty of Engineering are compiled in the first part of the volume. Abstracts of papers presented elsewhere during the current year are compiled in the second part. List of conference presentations delivered during the same period is appended in the last part.

All communications with respect to Memoirs should be addressed to:

Dean of the Graduate School of Engineering
Osaka City University
3-3-138, Sugimoto, Sumiyoshi-ku
Osaka 558-8585, Japan

Editors

Akira TERAJ

Hayato NAKATANI

Kai CAI

Eriko SATO

Tetsu TOKUONO

Nagahiro YOSHIDA

MEMOIRS OF THE FACULTY OF ENGINEERING
OSAKA CITY UNIVERSITY

VOL. 59

DECEMBER 2018

CONTENTS

Regular Articles 1

Applied Chemistry and Bioengineering

Applied Chemistry and Bioengineering

Elemental analysis of three kinds of teas by tabletop XRF analyzer

Jingyuan ZHU, Haruna TAKAHASHI and Kouichi TSUJI 1

Urban Engineering

Urban Design and Engineering

Micro Traffic Simulation to Examine Congestion-control Measures Using Pace Maker Lights

Takahiro IGAKI and Takashi UCHIDA 7

A Study on the effect of Motorcycle Traffic Safety Workshop using Travel Speed and Vehicle Density in Phnom Penh, Cambodia

Toshiki KOYANAGI and Nagahiro YOSHIDA 19

Latent Opportunities for the Use of Two-Rider Bicycles and Associated Challenges by Welfare Service Providers

Takuya KONISHI and Nagahiro YOSHIDA 27

Abstracts of Papers Published in Other Journals	31
<i>Mechanical and Physical Engineering</i>	
<i>Mechanical Engineering</i>	33
<i>Electronics and Informatics</i>	
<i>Applied Physics and Electronics</i>	45
<i>Electrical and Information Engineering</i>	52
<i>Applied Chemistry and Bioengineering</i>	
<i>Applied Chemistry and Bioengineering</i>	55
<i>Urban Engineering</i>	
<i>Architecture and Building Engineering</i>	72
<i>Urban Design and Engineering</i>	75
List of Presentations at International Conferences	87
<i>Mechanical and Physical Engineering</i>	
<i>Mechanical Engineering</i>	89
<i>Electronics and Informatics</i>	
<i>Applied Physics and Electronics</i>	90
<i>Applied Chemistry and Bioengineering</i>	
<i>Applied Chemistry and Bioengineering</i>	93
<i>Urban Engineering</i>	
<i>Urban Design and Engineering</i>	98

MEMOIRS
OF THE
FACULTY OF ENGINEERING
OSAKA CITY UNIVERSITY

VOL. 59

DECEMBER 2018

PUBLISHED BY THE
GRADUATE SCHOOL OF ENGINEERING
OSAKA CITY UNIVERSITY

Elemental analysis of three kinds of teas by tabletop XRF analyzer

Jingyuan ZHU*, Haruna TAKAHASHI** and Kouichi TSUJI***

(Received October 31, 2018)

Synopsis

In this research, we investigated three kinds of tea samples by using tabletop XRF analyzer JSX-1000S (JEOL Company, Japan). Each tea sample was tested in original state, powder state and tablet state with different mass values. We could show the minimum mass for quantitative XRF analysis. By analyzing the X-ray spectrum recorded for these samples, we found the possibility of XRF analysis as a method of tea quality control and detecting tea producing area.

KEYWORDS: Tabletop XRF analyzer, EDXRF, Quantitative XRF analysis

1. Introduction

With the growth of the global economy, food trade is becoming more frequent than ever before. Consumers are willing to pay a high price for organic and non-polluting foods. Especially in tea industry, the price of famous brand tea made from specific regions is much higher than that of the ordinary brand. Therefore, the certification of the tea origin is commercially important. In addition, depending on elemental composition of tea, drinking it has risk of side effect to human organism. Therefore, it is very necessary to qualitatively and quantitatively analyze the elemental composition of teas.

According to Salvador's research¹⁾, Fe, Ni and Cu have been successfully characterized in tea samples using energy-dispersive X-ray fluorescence (EDXRF) technique. This paper shows that EDXRF method is useful for quality control to obtain 'chemical fingerprints' of tea products. Meanwhile, in Rajapaksha's research²⁾, X-ray fluorescence spectrometry (XRF) technique effectively gave us the concentrations of 13 elements (Mg, P, S, Cl, K, Ca, Mn, Fe, Cu, Zn, Br, Rb and Sr) in tea samples. This result helps to confirm the origin of 58 tea samples from four production districts in Sri Lanka.

These two research groups mentioned above inspired us to consider the possibility of use a tabletop XRF analyzer to acquire element composition and concentration of tea products. This XRF analyzer provides quick, easy elemental analysis that is non-destructive and available for different kinds of solid and liquid samples³⁾. By the analysis of the XRF intensity and the comparison with standard sample, we can obtain the concentrations of several elements detected in tea samples, leading to certification of the origin of tea products.

2. Experimental

We measured three kinds of tea products-green tea (ITOEN Company, Japan), roasted tea (ITOEN Company, Japan) and barley tea (Top Value Company, Japan). Every tea product was tested in original state, powder state and tablet state. In each state, we tested samples mass values of 0.3 g, 0.5 g, 0.7 g and 0.9 g. Therefore, we prepared 36 pieces of tea samples for investigation. To prepare the powder samples, we smashed the tea and then sieved the powder to have a diameter less than 0.46 mm particles. To prepare tablet samples, we put tea powder (same material as powder samples) into a tableting machine and put it in the pressure pump for 5 minutes under a pressure of 10 MPa. Fig.1 shows the grinder for preparing powder samples and the tableting machine for preparing tablet samples.

* Student, Master Course of Department of Applied Chemistry & Bioengineering

** Engineer, JEOL Ltd.

*** Professor, Department of Applied Chemistry & Bioengineering



(a) M20 (IKA Company, Germany)



(b) PT-20 (JASCO Corporation, Japan)

Fig.1 (a) Grinder for making powder state samples and (b) tableting machine for making tablet state samples.

We used a tabletop EDXRF instrument: JSX-1000S (JEOL Company, Japan) as an XRF analyzer. Fig.2 shows the appearance and internal structure of JSX-1000S. As an EDXRF instrument, an X-ray tube and an X-ray detector are installed below a sample chamber. This EDXRF analyzer enables a quick and easy elemental analysis with an easy software for operation. The functions for conventional qualitative and quantitative analysis are equipped. Including solution-based applications, the desired analysis can be executed automatically according to pre-recorded recipes. The new smart fundamental parameter (FP) method makes it possible to obtain high accurate quantitative results without preparing a standard sample. This FP method includes automatic correction for thickness and residual ingredient balance.

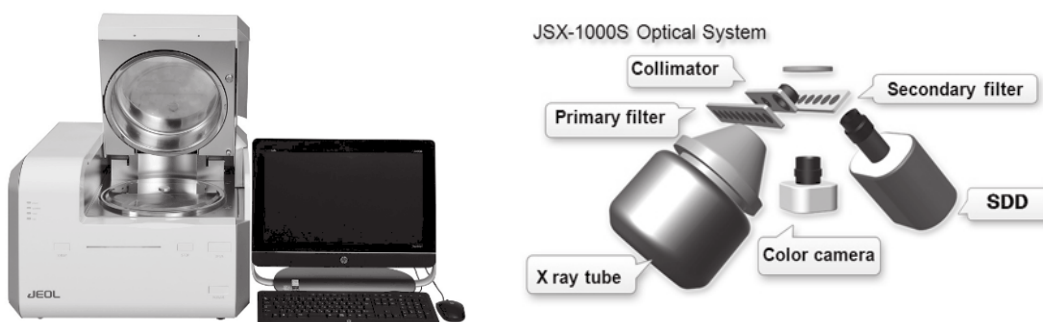


Fig.2 Tabletop EDXRF instrument, JSX-1000S (JEOL Company, Japan)

Samples were put into a holder (a white plastic hollow tube with transparency film covered under bottom, shown in Fig. 3(a)) and set in sample chamber shown in Fig. 3(b). By using an auto sample changer (Fig. 3 (b)), up to twelve samples can be analyzed at one time. For EDXRF analysis, an X-ray tube (Rh target) was operated with a voltage of 30 kV, and a current of 0.030 mA. EDXRF measurement was performed for an acquisition time of 1000 second with a collimator size of 9.0 mm.



(a)



(b)

Fig.3 (a) Sample holder and (b) auto sample changer.

3. Results and Discussion

3.1. X-ray spectrum

Fig.4 shows the X-ray spectrum of three kinds of tea products tested in powder status with a mass of 0.5 g. Elements of P, S, K, Ca, Mn, Fe, Cu, and Zn were detected. Same elements were also detected in other samples with different status and mass. The peak originated from Rh was mainly observed, because it is the primary X-rays emitted from the X-ray tube. Although we set an acquisition time in 1000 seconds for each sample, a clear X-ray spectrum appeared very quickly in less than 200 seconds.

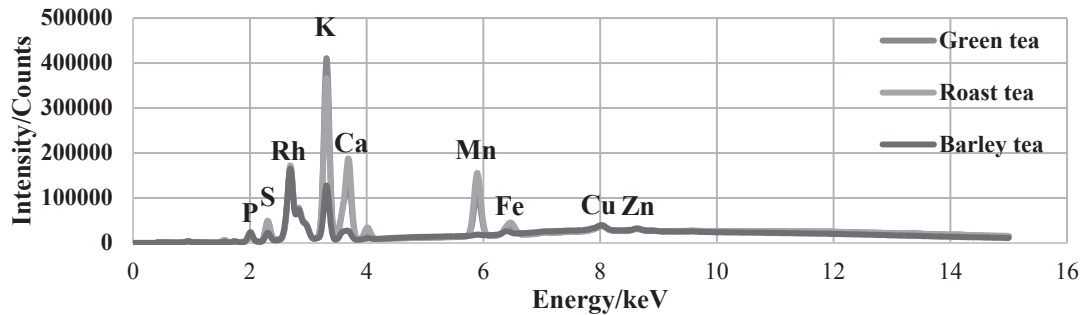


Fig.4 X-ray spectrum of three kinds of tea products (0.5g samples in powder status)

3.2. Green tea

Fig.5 shows the XRF intensities of K, Fe and Zn detected for green tea samples (original status). There is significant increase of these three elements when sample mass increased from 0.3 g to 0.5 g. However, XRF intensities of P, S, Ca, Mn and Cu did not show so much change by the increase of mass in original status. We considered that the minimum mass of green tea samples would be more than 0.5 g. As for powder and tablet status, the XRF intensities of elements were almost the same for different mass samples. Therefore, the concentration of elements in green tea would be evaluated for the mass more than 0.5 g by using calibration curve.

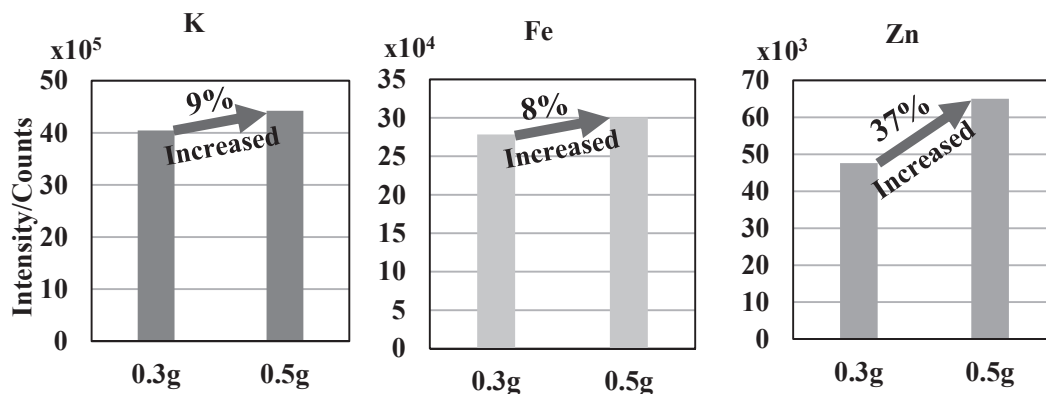


Fig.5 XRF intensities of K, Fe and Zn detected in green samples (original status)

3.3. Roasted tea

Fig.6 shows XRF intensities of elements detected for the roasted tea samples (powder status) in different mass samples. Except Mn, XRF intensities for all other elements were almost the same for different mass samples. Besides powder status samples, XRF intensities of original status and tablet status samples almost has no change with the change of mass. All roasted tea samples were dry, and this may be the reason why the same XRF intensities were detected for different mass and status of samples. Because of no significant change in XRF intensities, therefore, the concentration of elements in roasted tea would be evaluated by using calibration curve.

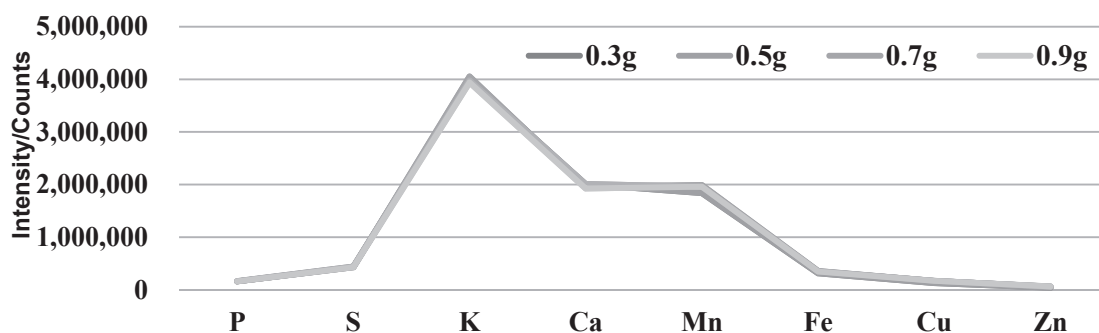


Fig.6 XRF intensities of several elements detected in roasted tea samples (powder status)

3.4. Barley tea

Fig.7 shows XRF intensities of K and Ca element detected in 0.3 g barley tea samples. Concerning K and Ca element, original status showed a highest XRF intensity. This may be because these two elements existed in the shell of barley tea seed and therefore could be easily detected in original status samples. This phenomenon does not show up in 0.5 g, 0.7 g and 0.9 g samples. In three status of barley tea samples, as the mass increases, the XRF intensities does not increase proportionally concerning the mass. Therefore, the quantitative XRF analysis would be possible for elements in barley tea by using calibration curve.

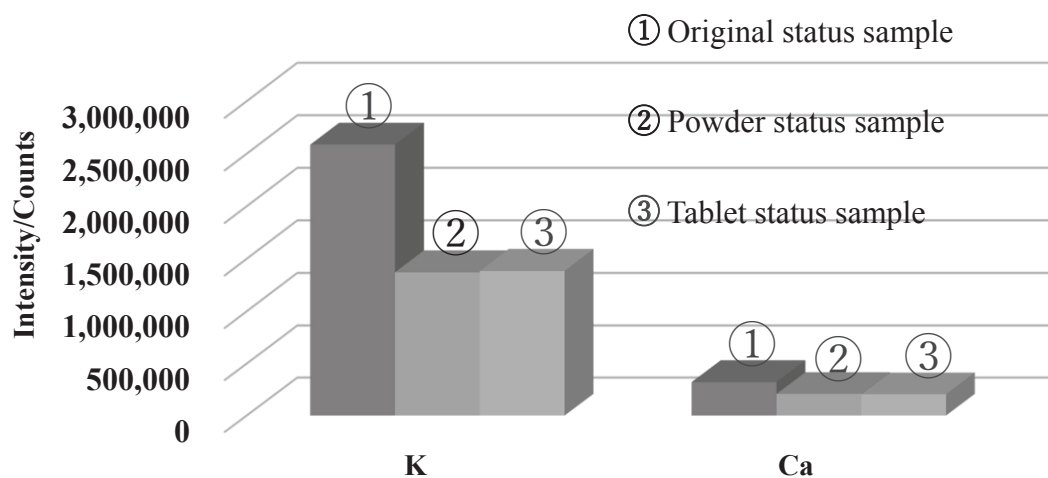


Fig.7 XRF intensities of K and Ca elements detected in 0.3 g barley tea samples.

4. Conclusions and future works

Using JSX-1000S XRF analyzer, it was possible to detect elements in tea products. We measured tea samples with different sample conditions. It was found that the minimum sample mass depended on the element (energy of X-ray fluorescence) analyzed. The qualitative analysis of tea products would be possible by applying a calibration curve with standard tea sample. The EDXRF spectrometer can be applied not only for solid samples but also for liquid samples⁴. Thus, a drinking tea solutions will be the next sample using a tabletop EDXRF spectrometer. After the tea leaves are put into boiling water, the liquid tea samples would be measured by the same XRF spectrometer at a room temperature. Comparison of both solid and liquid samples will be helpful for safety and tea quality control.

5. Acknowledgement

This work was supported by JSPS KAKENHI (17H03080, 18H01755, 171000132).

6. References

- 1) M. Salvador, G. Lopes, V. Filho, O. Zucchi, *X-ray Spectrometry*, **31**, 141 (2002).
- 2) D. Rajapaksha, V. Waduge, R. Alvarez, M. Kalpage, R. Rathnayake, A. Migliori, R. Frew, S. Abeysinghe, A. Abraham, T. Amarakoon, *X-ray Spectrometry*, **46**, 220 (2017).
- 3) R. Van Grieken and A.A Markowicz, *Handbook of X-ray Spectrometry*, Marcel Dekker Inc., New York (2002).
- 4) K. Tsutsumimoto and K. Tsuji, *BUNSEKI KAGAKU*, **56**, 499 (2007).

Micro Traffic Simulation to Examine Congestion-control Measures Using Pace Maker Lights

Takahiro IGAKI* and Takashi UCHIDA**

(Received October 31, 2018)

Synopsis

One cause of congestion on highways is “sag”: a section where the road gradient changes gradually from downward to upward. Drivers unconsciously reduce speed without anticipating the uphill part of this section. That speed reduction is imitated by other drivers, creating congestion. Some attempts to use pace maker lights have been undertaken as measures against traffic congestion occurring at a sag. Some trial operations are being conducted on various highways.

For this study, a micro traffic simulation using a car-following model with pace maker lights installed. Then a simulation was conducted of traffic conditions at the sag using time–space diagrams. Results confirmed the characteristics of the car-following model. Results demonstrated that different driving behaviors among drivers affect congestion.

KEYWORDS: expressway, numerical experiments, sag, Time–space diagram, traffic capacity

1. Research Background and Objectives

(1) Research background

A sag, a section at which the vertical gradient changes gradually from downward to upward, is a major cause of traffic congestion. As one example, the section of the Hanshin Expressway including the Hukae sag accounts for the worst (down line) and second worst (up line) in rankings of traffic congestion among Japan urban expressways ¹⁾.

The mechanism by which congestion at sag occurs is the following (Fig. 1).

1. A car approaches uphill of the sag. The driver decelerates without noticing the uphill section.
2. The driver of the following car notices slowing of the lead car and slows the vehicle by applying the brakes.
3. Subsequently, the following car driver slows by applying the brakes. Eventually, a group of cars moving at reduced speed is formed and congested. At the head of the congestion that passes the sag, the congestion gradually gets resolved.

The Hanshin Expressway is carrying out measures using pace maker lights (PMLs) for traffic congestion that occurs at sags (Fig. 2). The PMLs produce a pattern suggesting forward light flow by switching LEDs on and off sequentially at the road side or at a tunnel wall. The apparatus uses driver consciousness of driving along with the flow. It is hoped that PMLs can restrain speed reduction and support prompt speed restoration.

Past studies have assessed PMLs on actual highways. They have also measured speed and traffic capacity ²⁾, with follow-up experiments using the simulator and the actual road to measure distances between vehicles. They have confirmed the effects of PML for improving congestion ³⁾. Nevertheless, these experiments have not addressed individual driver characteristics and their effects on traffic flow.

* Student, Master Course of Department of Urban Engineering

** Professor, Department of Urban Engineering

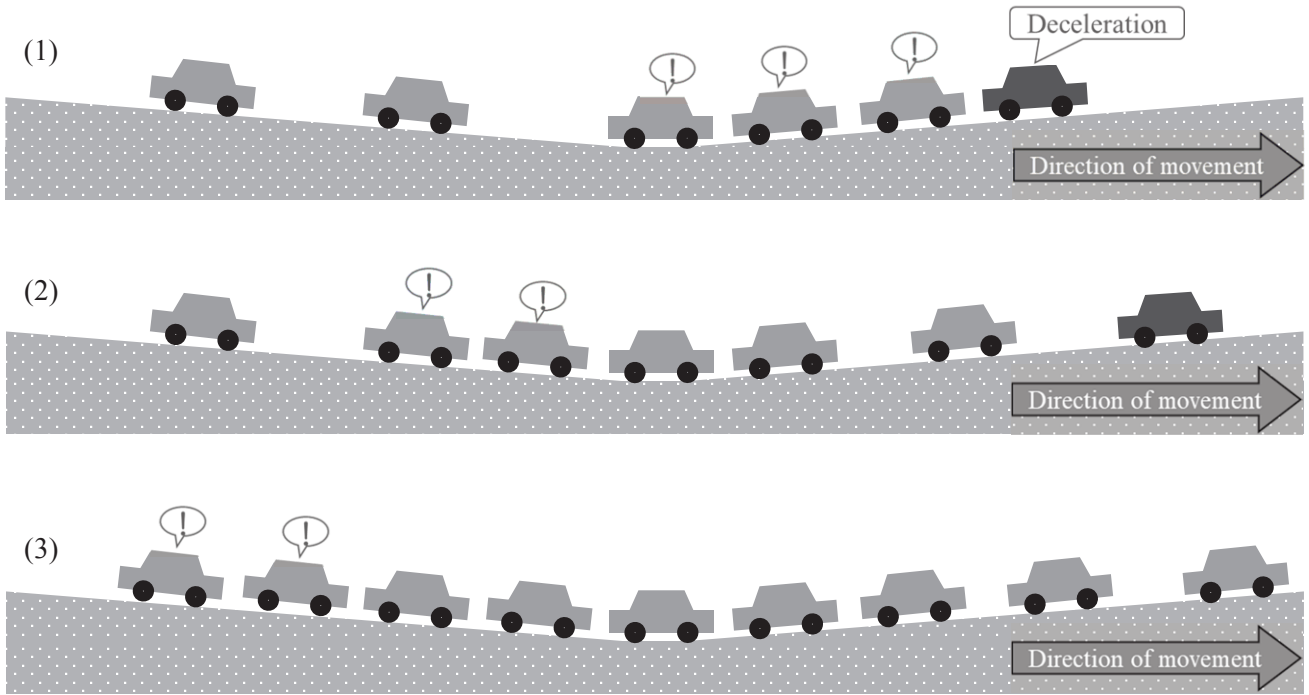


Figure 1 Mechanism of congestion occurring at a sag.

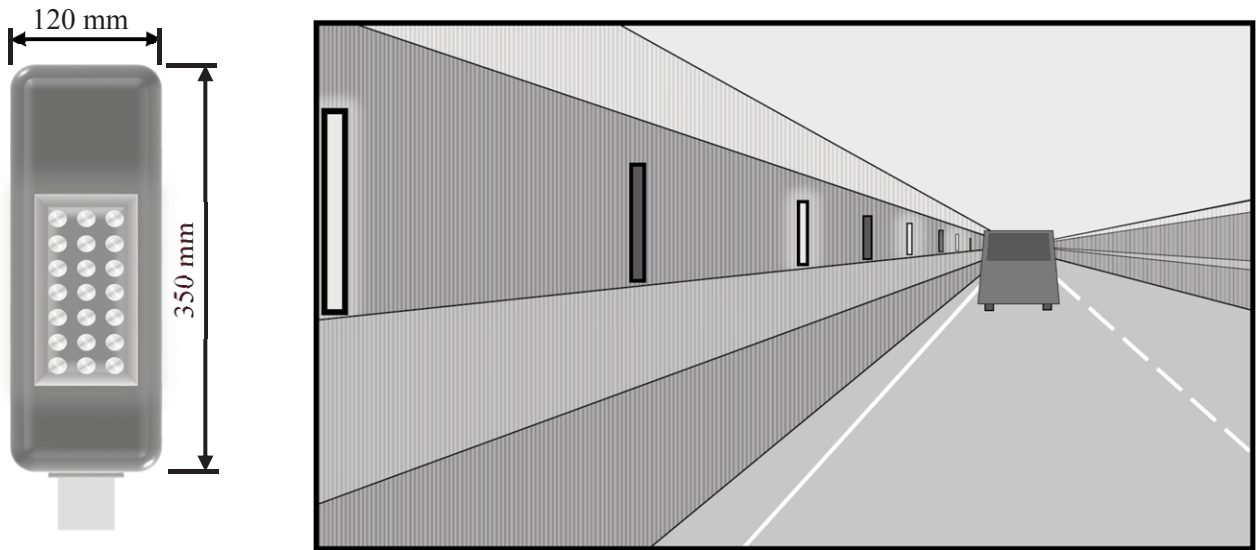


Figure 2 Pace maker lights (illustration).

(2) Research objectives

This study uses time–space diagrams to assess traffic flow and individuals’ driving characteristics on a highway.

2. Micro Traffic Simulation

(1) Examination car following model

To produce a traffic simulation incorporating PML effects, a car-following model for assessment from a micro viewpoint particularly addressing each car's behavior was examined as a basic model. The target intervehicle distance of the driver is incorporated as a parameter in the Koshi model. The formula structure is readily comprehensible. Therefore, the Koshi model⁴⁾ was adopted as the basic formula used for this study. The Koshi model is shown as (1) below. The target intervehicle distance function $f[v(t + T_2)]$ makes it easy to examine the intervehicle distance specifically. Another benefit is that the meanings of terms are easy to understand. However, an important shortcoming is that no desired speed parameter exists, although it is necessary to express the PML speed.

$$\dot{v}(t) = \frac{\alpha \dot{S}(t + T_1)}{S(t + T_1)^l} + \frac{\beta \{S(t + T_2) - f[v(t + T_2)]\}}{S(t + T_2)^m} - \gamma \sin \theta \quad (1)$$

In the equation above, the following variables are used.

- v : Following car speed
- T_1, T_2 : Reaction delay time ($T_1 < T_2$)
- θ : Longitudinal gradient difference
- l, m : Parameters
- S : Intervehicle distance
- $f[v(t + T_2)]$: Target intervehicle distance function of following car driver
- α, β, γ : Constants

Therefore, the modified version of the Koshi model can be expressed as shown below in (2).

$$\frac{dv_1(t + T)}{dt} = a \frac{\min[v_0(t), v^*] - v_1(t)}{|x_0(t) - x_1(t)|^l} + b \frac{(x_0(t) - x_1(t) - s^*)}{|x_0(t) - x_1(t)|^m} - c \sin \theta \quad (2)$$

Therein, the following variables are used.

- v_0, x_0 : Leading car speed [m / s], Leading car position [m]
- v_1, x_1 : Following car speed [m / s], Following car position [m]
- a : Speed difference parameter
- b : Intervehicle distance parameter
- c : Gradient parameter
- l, m : Distance attenuation parameter
- s^* : Desired intervehicle distance [m]
- v^* : Desired speed [m / s]
- T : Reaction delay time [s]
- θ : Longitudinal gradient difference [rad]

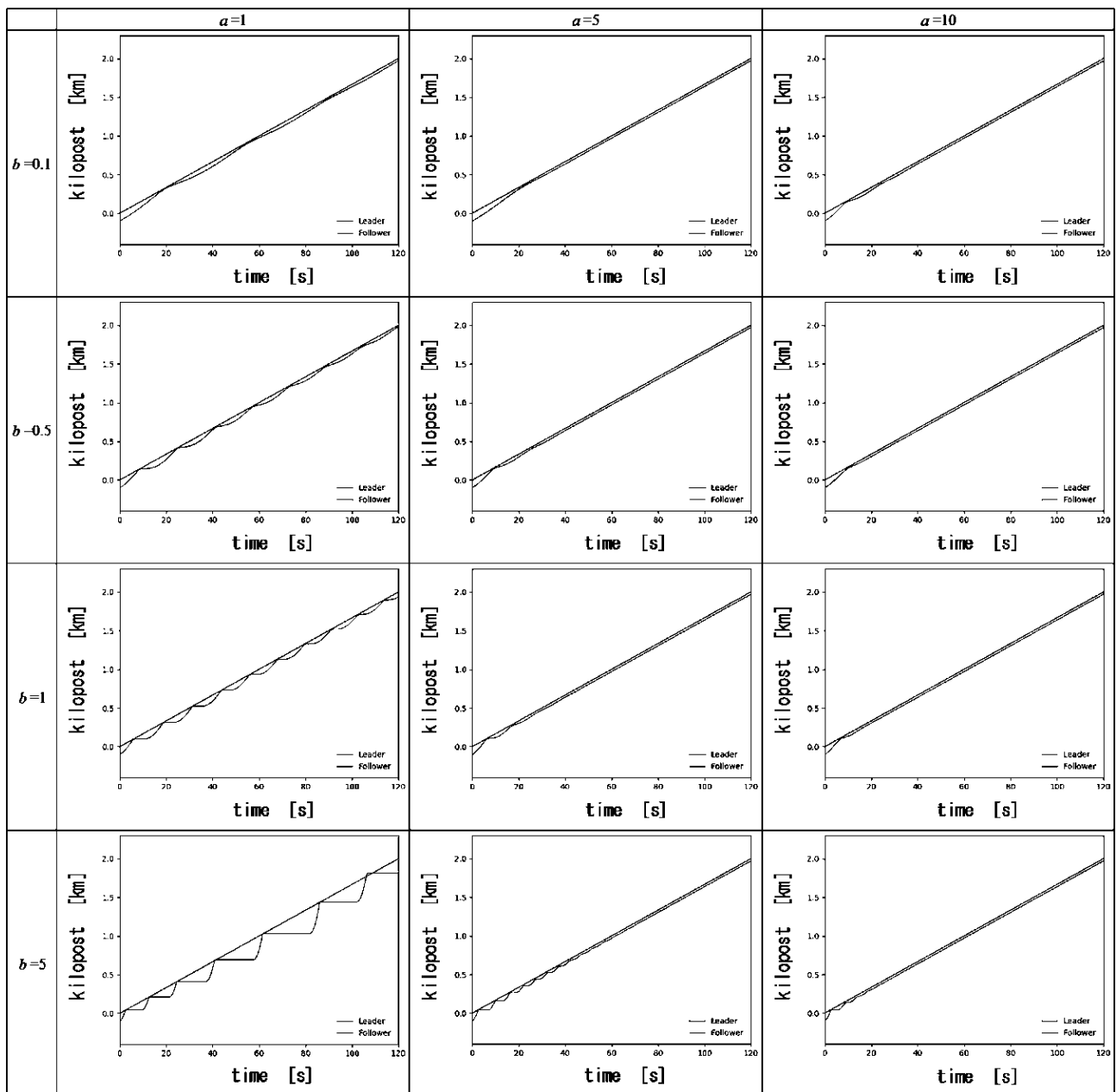
The salient difference from the Koshi model is introduction of the desired speed v^* to the numerator of the first term. Originally, the desired speed is the speed that the driver desires when traveling alone, but in (2), the desired speed is replaced with the setting speed of the PML light flow. This result is based on the assumption that all drivers are influenced by the PML light flow and that they drive at the same speed as the PML setting speed. By combining the desired speed parameter v^* and the speed difference parameter a representing the sensitivity to the speed difference from the leading car, one can set the degree of influence of PML of each driver.

(2) Basic Characteristics of the following car model

To ascertain the influence of the speed difference parameter a and the intervehicle distance parameter b on the following car, simulations were conducted by changing the values of a and b (Table 1). At this time, the longitudinal gradient difference $c = 0$, the desired intervehicle distance $s^* = 30$ m. The desired speed $v^* =$

60 km / h. The larger parameter a becomes, the more sensitive it is to the speed difference from the leading car and the earlier it reaches the same speed as the leading car. The larger parameter b becomes, the more sensitive it becomes to the intervehicle distance. When the intervehicle distance is large, the following car tries to catch up quickly and increases its speed. Results of simulations demonstrate that the larger value a is, the faster the convergence of the expansion and contraction of the intervehicle distance becomes. The larger value b is, the smaller the wavelength of the expansion and contraction of the intervehicle distance becomes. Moreover, the larger the gradient parameter c becomes, the stronger the influence of the longitudinal gradient is, and the slower acceleration becomes. Smaller distance attenuation parameters l and m suggest a greater influence of the preceding vehicle with greater intervehicle distance, the desired speed, and the desired intervehicle distance when trying to approach the distance.

Table 1 Time-space diagrams showing parameter a and b effects on the tracking situation: longitudinal gradient difference $c = 0$, desired intervehicle distance $s^* = 30$ m, and desired speed $v^* = 60$ km / h.



3. Numerical Experiments

(1) Summary

Experiments were conducted to reproduce the sag traffic conditions by characterizing the driver parameters. Using results of the car following experiment for the Hanshin Expressway conducted on 20 subjects shown in Tabira *et al.*³⁾, parameters in the car following model formula are determined. The average and variance of intervehicle distances for respective road segments and respective subjects in a following car were found from experiments conducted without PML, at 60 km / h, and at 80 km / h. Reading the driver characteristics from these data and setting parameters a , b , c , T , s^* , each driving behavior is characterized.

For example, the desired intervehicle distances s^* are 20 m, 30 m, and 40 m because the average intervehicle distance of all drivers was about 11–44 m. For speed difference parameter a and intervehicle distance parameter b , reference was made to the actually observed variances and variances in the simulation. Some extreme cases were also presumed.

Table 2 presents parameters: Nos. 1-1 to 2-3 show susceptibility to PML; Nos. 3 and 4 are set to the intervehicle distance; Nos. 5-1 to 6-3 are set to the gradient; Nos. 7 and 8 are set for the response delay time (Table 2).

Table 2 Driver Parameters

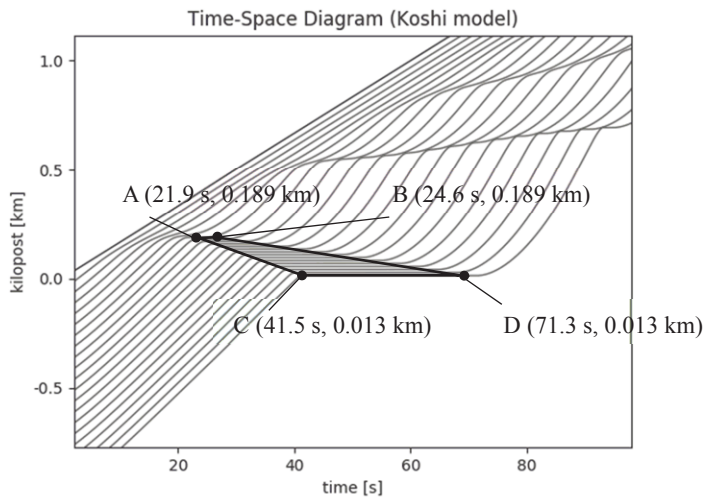
Driver No.	Characteristic	Characteristic Intervehicle	Parameters				
			Speed difference a	Intervehicle distance b	Gradient c	Reaction delay time T [s]	Desired intervehicle distance s^* [m]
0	Standard	Standard	10	0.5	0.5	0.1	30
1-1	Sensitivity to PML: High	Long	15	0.5	0.5	0.1	40
1-2		Standard	15	0.5	0.5	0.1	30
1-3		Short	15	0.5	0.5	0.1	20
2-1	Sensitivity to PML: Low	Long	9	0.5	0.5	0.1	40
2-2		Standard	9	0.5	0.5	0.1	30
2-3		Short	9	0.5	0.5	0.1	20
3	Sensitivity to leading car: High	Standard	10	0.6	0.5	0.1	30
4	Sensitivity to leading car: Low	Standard	10	0.25	0.5	0.1	30
5-1	Effect of gradient: Large	Long	10	0.5	1	0.1	40
5-2		Standard	10	0.5	1	0.1	30
5-3		Short	10	0.5	1	0.1	20
6-1	Effect of gradient: Small	Long	10	0.5	0.1	0.1	40
6-2		Standard	10	0.5	0.1	0.1	30
6-3		Short	10	0.5	0.1	0.1	20
7	Reaction delay time: Large	Standard	10	0.5	0.5	0.2	30
8	Reaction delay time: Small	Standard	10	0.5	0.5	0	30

(2) Method

The experiment was conducted for each driver to produce time–space diagrams. Using those time–space diagrams, one can calculate the congestion amount (congestion duration) and traffic capacity (number of units passing a certain point / unit time). For this study, they were calculated as follows, Figs. 3 and 4. Congestion often refers to a condition in which the speed is 20–30 km / h or less. For simplicity, congestion is defined as the condition of 0 km / h in this study. When several vehicles have a speed of 0 km / h, the time and section appear as a trapezoid on the time–space diagram. The trapezoid area is calculated and is taken as the congestion amount. The traffic capacity was obtained by dividing the number of follower cars (20 units) by time, which took the leading vehicle (0th) to the 20th follower as the distance at which the 20th follower arrived at the simulation end time.

a) Experiment 1

A case in which the same 20 drivers follow in 20 units was simulated. The drivers were classified into four groups by cluster analysis from results of the congestion amount and the traffic capacity. The classification is done hierarchically. The standardized Euclidean distance is used for distance calculation between individuals. The group average method is used to calculate distance between clusters.



Congestion in Figure 3

= Congestion length

× Congestion duration

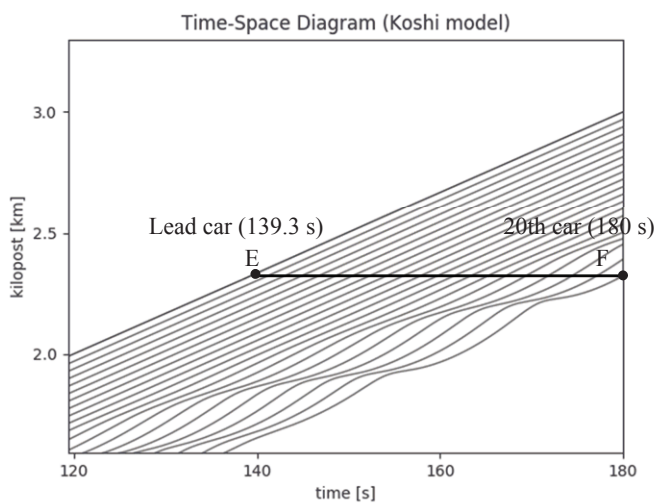
= trapezoid ABCD

$$= \frac{1}{2} \times \{(24.6 - 21.9) + (71.3 - 41.5)\}$$

× (0.189 - 0.013)

$$= 2.86 \text{ [km} \cdot \text{s]}$$

Figure 3 Calculation of congestion.



Traffic capacity in Figure 4

$$= \frac{\text{Number of following cars}}{\text{Length of Line EF}} \times 60$$

$$= \frac{20}{180 - 139.3} \times 60$$

$$= 29.48 \text{ [units/min]}$$

Figure 4 Calculation of the traffic capacity.

b) Experiment 2

Cases were simulated in which 20 drivers belonging to the same group followed in 20 units. We calculated the congestion amount and traffic capacity as in experiment 1. For example, if drivers belonging to the same group are Nos. 1, 2, and 3, the order of following up is 1, 2, 3, 1, ..., 2.

c) Experiment 3

Drivers belonging to different groups were mixed and simulated. For example, for driver Nos. 1, 2, and 3 in Group A and Nos. 4, 5 in Group B, the order of following is 1, 2, 3, 4, 5, ..., 1.

(3) Conditions

The conditions and assumptions of the numerical experiments we conducted are presented as shown below.

- All drivers drive at the PML setting speed.
- The PML set speed is 80 km / h (optimum speed).
- Distance attenuation parameters $l = m = 1$.
- Longitudinal gradient difference is 3.0%.
- Leading car speed is always 60 km / h.
- Simulation time is 180 s.
- Following cars are located every 50 m at the start time.
- Initial speed of the following cars is 60 km / h.

The optimal PML setting speed is expected to be greater than the actual driving speed by 10–20 km / h⁵⁾, so that the PML speed was set to 80 km / h for the Hanshin Expressway, where the speed limit is 60 km / h.

(4) Results

a) Experiment 1

Using the simulation results in the case in which 20 vehicles of the driver with the same characterizing parameter follow the vehicles continuously, the congestion amount and the traffic capacity were calculated. Then, the drivers were classified into four groups using cluster analysis (Tables 3, 4; Fig. 5). Fig. 6 shows some simulation results.

Table 3 Congestion amount and traffic capacity in experiment 1.

Driver No.	Congestion [km · s]	Traffic capacity [unit/min]
0	2.86	29.48
1-1	0.18	24.24
1-2	0.00	32.35
1-3	0.00	48.58
2-1	4.20	14.89
2-2	3.50	25.92
2-3	0.91	48.58
3	3.45	27.97
4	0.00	31.33
5-1	5.57	19.20
5-2	2.89	29.13
5-3	0.66	47.06
6-1	5.59	18.49
6-2	2.78	31.91
6-3	0.57	49.79
7	2.91	28.24
8	2.83	30.38

Table 4 Characteristics of groups using experiment 1.

Group	Congestion	Traffic capacity	Drivers
A	Standard	Standard	0, 2-2, 3, 5-2, 6-2, 7, 8
B	Small	Large	1-3, 2-3, 5-3, 6-3
C	Small	Standard	1-1, 1-2, 4
D	Large	Small	2-1, 5-1, 6-1

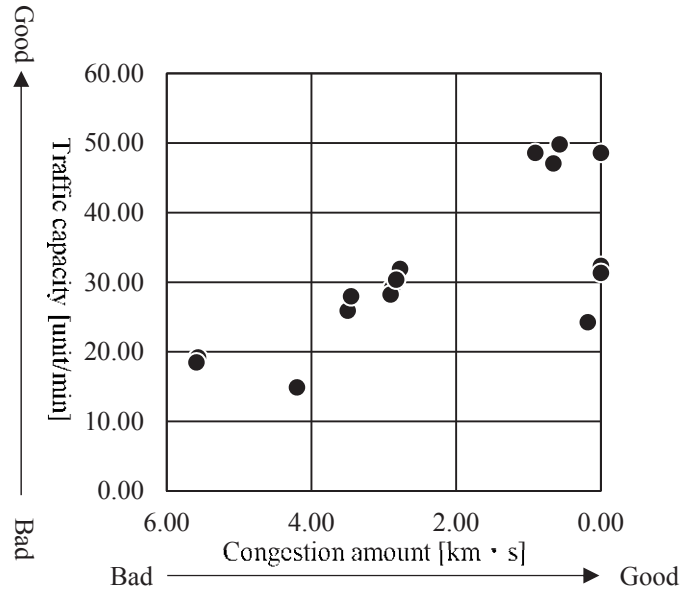


Figure 5 Congestion amount and traffic capacity in experiment 1.

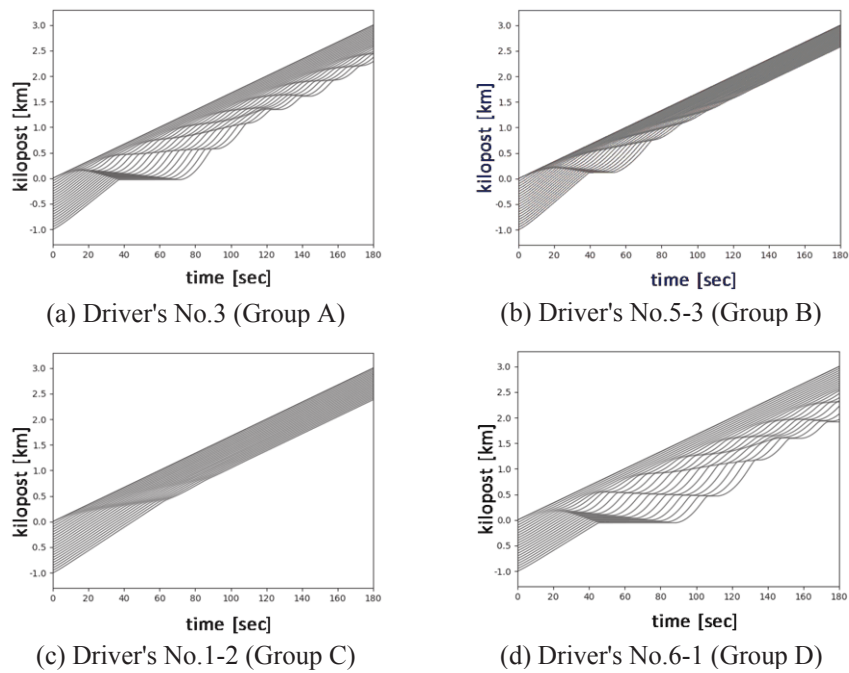


Figure 6 Four time-space diagrams in experiment 1.

We specifically examined the driver numbers of respective groups (Table 4). Group B includes all drivers with small intervehicle distance. Group D includes drivers with large intervehicle distance. It is noteworthy that all drivers with small intervehicle distances belong to group B. These results demonstrate that the desired intervehicle distance of each driver strongly affects the traffic capacity. In addition, there are many drivers who have standard intervehicle distance in groups A and C.

b) Experiment 2

When simulations were conducted in which 20 drivers belonging to the same group were run successively, the congestion amount and traffic capacity were average values within the respective driver groups (Fig. 7, Table 5). Circles designate the values of the respective drivers. Squares represent values of the respective groups.

In Group D, only one driver (No. 2-1) with a small congestion amount as compared with the other two vehicles is mixed, but it apparently does not strongly affect the traffic congestion of the whole group.

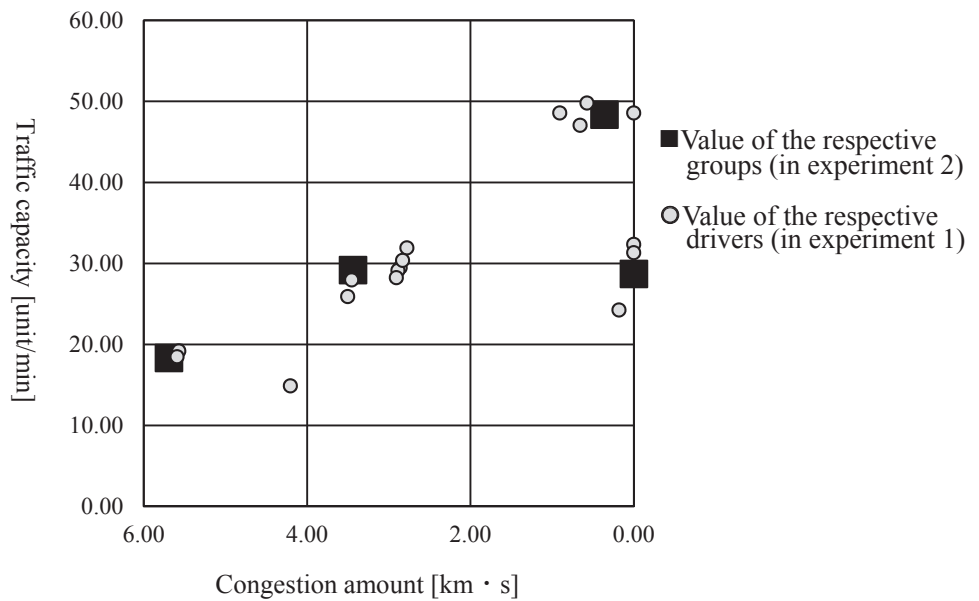


Figure 7 Congestion amount and traffic capacity in experiment 2.

Table 5 Congestion amount and traffic capacity in experiment 2.

Group	Congestion [km · s]	Traffic capacity [unit/min]
A	3.44	29.2
B	0.36	48.39
C	0	28.71
D	5.69	18.35

4. Conclusion

Results of numerical experiments used for this study demonstrated that drivers with a strong influence of PML contributed to a reduction in the congestion amount. Drivers with a small intervehicle distance contributed to an increase in the traffic capacity. Therefore, a good traffic condition (low congestion and high traffic capacity) is achieved when the desired intervehicle distance s^* is small.

Future research should use time–space diagrams and other analytical methods to assess the observed traffic flow, to check reproducibility of these results, and to reexamine the simulation model.

References

- 1) The traffic situation ranking for urban expressway (2016), http://www.mlit.go.jp/road/ir/ir-data/pdf/ranking_6.pdf (in Japanese).
- 2) T. Ueda *et al.*: THE MOVING LIGHT GUIDE SYSTEM ON HANSHIN EXPRESSWAY, *Proceedings of Infrastructure Planning of Japan Society of Civil Engineers*, **53**, 2825–2829, (2016) (in Japanese).
- 3) Y. Tabira and Y. Shiomi: A study on effect of pace maker light on car-following behavior, *Proceedings of Infrastructure Planning of Japan Society of Civil Engineers*, **55**, 16–03 (2017) (in Japanese).
- 4) M. Koshi: CAPACITY OF MOTORWAY BOTTLENECKS, *Journal of Japan Society of Civil Engineers*, No.371/IV-5., pp. 1–7 (1986) (in Japanese).
- 5) M. Endo *et al.*: The measures against traffic congestion in Tokyo Wan Aqua-Line EXPWY, *Proceedings of Conference of the Japan Society of Traffic Engineers*, **34**, 255–261 (2014) (in Japanese).

A Study on the effect of Motorcycle Traffic Safety Workshop using Travel Speed and Vehicle Density in Phnom Penh, Cambodia

Toshiki KOYANAGI* and Nagahiro YOSHIDA**

(Received October 31, 2018)

Synopsis

In Cambodia, motorcycle use has spread rapidly in recent years, and serious accidents involving motorcycles have increased. In particular, many young motorcyclists have been involved in traffic accidents, and various issues in traffic safety are remained. To understand the current situations related to these issues in Phnom Penh, Cambodia, a video observation survey on driving situations of motorcycle users in high school and university were conducted. Based on the results, a traffic safety workshop was held to improve their risk perception ability and basic riding skills. In this study, a statistical analysis was conducted to compare travel speed with vehicle density on arterial roads before and after the workshop. The results showed that travelling speed decreased to be effects of the traffic safety workshop, and the vehicle density could be an explanatory variable to represent various driving conditions of motorcycles including psychological effects.

KEYWORDS: Motorcycles, Hazard perception, Traffic behavior, Traffic safety, Traffic education

1. Introduction

In Cambodia, motorcycle use has spread rapidly in recent years, and the proportion of accidents involving motorcycles has also increased. According to an OECD report, the number of traffic fatality in 2016 was 1852 (11.8 per 100 thousand people), and 73% of these fatalities were riders of "motorized two wheelers" ¹⁾. Motorcycle accidents have accounted for more than 90% in the 15-24 age group, and main factors were identified as excessive speed, drink driving, and dangerous overtaking. In response to these situations, a review of driving license system for motorcycles was underway, while a mandatory helmet law for motorcycle drivers was passed when riding a motorcycle of 49cc or above in 2007, and in 2015, it was made compulsory for motorcycle passengers to wear a helmet and the law regarding traffic violations was toughened. Regarding road infrastructure, the Asian Highway Network including arterial roads in Cambodia are being improved, and traffic signals and a traffic control center are introduced in the capital city, Phnom Penh. With regard to traffic safety education, some activities are supported by NGOs, and the content of the education has been included in the compulsory education curriculum. However, judging from the current situation regarding traffic accidents occurring among young people, both the quantity and the quality of this education are considered insufficient and some advanced knowledge concerning the necessity of additional road safety education and the concrete educational effect are required.

As described above, to understand current situations about driving behaviors and related traffic safety education, the following three activities were described below were carried out. The first, an observation survey using video cameras attached to motorcycles was conducted to understand some insights from actual traffic condition. Next, based on these results, a traffic safety workshop (WS) for the participants in the behavior survey was held. The workshop consisted of two parts: a classroom portion, and a driving portion. In classroom learning, after explaining the situation of traffic accidents in Cambodia, a training aimed at improving hazard prediction ability was carried out using dangerous driving scenarios extracted from the video observation of driving behavior. In driving portion, a basic driving training was given by an instructor. Finally, a video observation of driving behavior was carried out again to examine the impact of the traffic safety workshop. In this study, with the aim of clarifying issues relating to fundamental driving behaviors that contribute to motorcycle traffic safety, such as travel speed. A comparative analysis of driving behavior before

*Student, Master Course of Dept. of Urban Design and Engineering

**Associate Professor, Dept. of Urban Design and Engineering

and after the workshop were conducted by using travel speed and vehicle density. In addition, the motorcycle in this research is an automatic scooter used in Cambodia, not including auto rickshaw.

2. Literature review

Many studies on motorcycle traffic safety examined including analysis of risk behavior in Thailand ²⁾, and various issues have been identified such as helmet use, alcohol, training, daytime running lights, driving licenses, and risk taking behaviors ³⁾.

With regard to driver education, there are many studies on hierarchical models for driving behavior ^{4),5)} and their extension ⁶⁾.

In research on motorcycle use and the effects of education, there are studies on the relationship between education and traffic safety behavior ⁷⁾, educational content and license system ⁸⁾, and educational methods and children's developmental stage ⁹⁾. In particular, to improve traffic safety performance among young people, dealing with risk-taking behavior ¹⁰⁾ and the importance of more advanced driving skill training in addition to the conventional training have been identified ¹¹⁾.

On the other hand, in order to better understand these driving behaviors, the importance of evidence-based traffic safety measures ¹²⁾ such as naturalistic driving observation studies ¹³⁾, have been pointed out.

As mentioned above, there are various research results regarding traffic safety education of motorcycle, but information about current situation of motorcycle driving behavior in young people in Cambodia is limited. In addition, there are rarely evaluated the effects of traffic safety education based on actual driving behavior. So we focused on driver behavioral changes in young people and the possibility of future introduction of more practical traffic safety education and we analyzed traffic safety education and naturalistic driving data in association with each other.

Still more, the content of traffic safety education presented in the project is to improve so-called hazard perception ability, and although there are studies relating to similar objectives ^{14),15)} this study focus on analyzing whether hazard perception education training affects the development of more defensive driving behavior in young people, based on the comparative observation of actual driving behavior.

3. Methodology

3.1 Video observations of actual driving behavior

To confirm the actual situation regarding driving behaviors, video cameras were attached on the motorcycles (50 ~ 125 cc) of students who commute to high school or university within the city of Phnom Penh, and an observation survey was conducted. In the survey, the routine route between their home and school was recorded during two different periods: one from December 2015 to January 2016 and one at the end of July 2017 after the safety workshop described below. The subjects were a total of 27 people who responded to an appeal for cooperation in the survey through a local university. Four of 27 people were common samples before and after the workshop. In the analysis, driving behavior of travelling non-intersection link was compared by separating the 27 people into two groups: one is subjects who had not attended the workshop (before workshop) and another one is subjects who had attended the workshop (after workshop). Individual attributes were summarized in TABLE 1. The equipment used for video observation is the action camera GARMIN VIRB Elite with built-in GPS function. The measured viewing angle was 123°, which is roughly the same as the angle of view of a human being (120°). Using the video data, average speed were measured as driving behaviors indicating driving conditions. As a result, data of for 1014 links totaling 160.5 km was extracted (TABLE 2).

TABLE 1 Individual attributes of subjects fitted with cameras

	Before WS	After WS	Total
Date of observation	Dec. 2015-Jan. 2016	Jul. 2017	
No. of people observed	17	10	27※
Gender	8 males/ 9 females	5 males/ 5 females	13 males/ 14 females
Student category	9 high school students / 8 University students	5 high school students / 5 University students	14 high school students / 13 University students
Driving experience	Less than 1 year:5 people / more than 1 year:12 people	Less than 1 year:0 people / more than 1 year:10 people	Less than 1 year:5 people / more than 1 year:22 people
Motorcycle category	50cc: 4 people / 90-125cc: 13 people	50cc: 3 people / 90-125cc: 7 people	50cc: 7 people / 90-125cc: 20 people
Number of links	584	430	1014
Observation time period	Morning: 327 links /afternoon: 143 links / evening: 114 links	Morning: 129 links /afternoon: 184 links / evening: 117 links	Morning: 456 links /afternoon: 327 links / evening: 231 links
Weather	Clear: 429 links/Cloudy: 155 links	Clear: 192 links/Cloudy: 238 links	Clear: 621 links/Cloudy: 393 links

* Of this total, 4 people participated both before and after the WS

TABLE 2 Overview of video observation result

No. of people observed	27
Observation time	573 min(Average of 24.9 min per Person)
Travel distance (except intersections)	160.5 km (Average of 7.0 km per Person)
No. of links on arterial/non-arterial roads	594/420 (Total 1014)
Average link distance	0.160 km
Average link passage time	29.6 s

3.2 Summary of traffic safety workshop

The traffic safety workshop held at the Royal University of Phnom Penh on July 16, 2017 consisted of 2 hours of classroom learning and 2 hours of driving learning. In classroom learning, after explaining the situation of traffic accidents in Cambodia, hazard prediction training was carried out using dangerous driving scenarios that were extracted from the video observation of driving behavior. Observed cases of near-misses were used as the dangerous driving scenarios, for example, entering the blind spot of a four-wheeled vehicle when weaving between cars, another vehicle suddenly appearing from a blind spot. The training method took the form of stopping the video before the dangerous driving scenario and having the participants anticipate the potential hazards, before explaining the actual dangerous driving scenario. In driving learning, approximately two hours of basic riding skills, such as riding a figure of eight and braking was given by a motorcycle instructor.

3.3 Introduction of average vehicle density around a subject

Although driving behavior on non-intersection links of arterial roads is thought to be influenced by surrounding traffic conditions, measuring the traffic conditions which could be an important factor to describe driver's psychological situations, for each road in different time thought to be difficult. So the observable relationship between average link speed and average vehicle density was employed in this study instead of the relationship between speed and density for each road in traffic flow theory.

First, to define the unit distance of motorcycle use on roads, non-intersection links were defined between intersections. The boundary of intersection was set as the extension of a straight line from the end of the corner cut-off at the intersection. The width and length of the links were measured using Google Earth. Measurement errors may occur in the passage times because the link start and end positions were reliant on visual estimates. As a rough guide, assuming that the error in average link passage time is ± 1 s for both intersections, the error in average link speed will be approximately -1.23 to 1.41 (km/h).

Next, with regard to vehicle density, average vehicle density around the observed vehicle was used. To calculate this, a range with road width in front of the motorcycle was defined using traffic lane markings, and the number of vehicles in the range was counted according to the type of vehicle as shown in FIGURE 1. Area parameters shown in TABLE 3 for each type of vehicle were used to convert the number of vehicles into the total vehicle area in the range. Using Equation (1), the instantaneous vehicle density for every five seconds was averaged over the number of observations within the same link. The coefficients used were a, b, c: number of motorcycles, four-wheeled vehicles, auto rickshaws and others; α , β , γ : area parameters; A: area by which the total vehicle area is divided; n: number of observations within link.

$$\left(\sum_{k=1}^n (\alpha a_{mn} + \beta b_{mn} + \gamma c_{mn})\right) / An \quad (1)$$

Excluding 136 links for which it was not possible to accurately count all of the vehicles inside the angle of view owing to the effect of camera shaking and road congestion, etc., data for a total of 878 links was obtained from the video analysis. The number of observations of instantaneous vehicle density found every five seconds averaged 4.86 per link, with a standard deviation of ± 4.42 .

Using the calculated results, when correlation coefficients of average link speed and average link vehicle density according to road conditions were compared, excluding the small number of one-way links, correlation was highest for “links with median strip, and 2 or more lanes in each direction” (TABLE 4), and the scatter diagram of vehicle density and speed confirmed that, as average link vehicle density increases, average link speed decreases (FIGURES 2, 3). Reasons for different correlation coefficients depending on road conditions include the fact that, in addition to road conditions such as road surface, the situation concerning crossing the centerline, reckless right/left turning, driving in the wrong direction on the road shoulder, etc. also varies according to road conditions. The conditions on “links with median strip, and 2 or more lanes in each direction” are such that driving behavior is less affected by the road and other people, and a detailed analysis of the 542 “links with median strip, and 2 or more lanes in each direction” was conducted.

A: Area by which the total vehicle area is divided

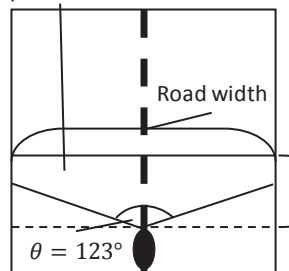


FIGURE 1 Defined range in front of motorcycle

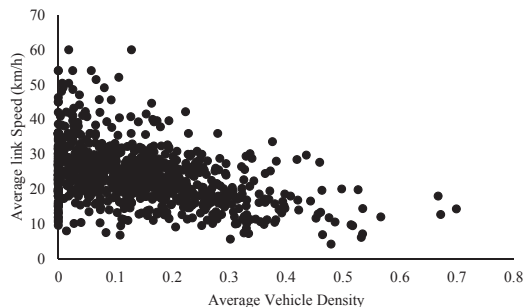


FIGURE 2 Relationship between average vehicle density and average link speed (all links)

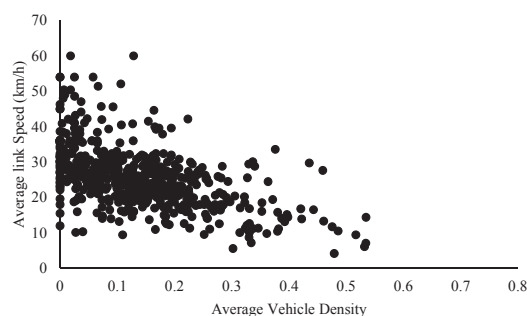


FIGURE 3 Relationship between average vehicle density and average link speed (links with median strip, and 2 or more lanes in each direction)

TABLE 3 Area parameters

	Sample size	Average vehicle area (m ²)	Standard deviation (m ²)
Motorcycle	6	1.22	0.14
Four-wheeler	6	8.51	0.51
Auto rickshaw	10	4.59	0.17

TABLE 4 Correlation between average link speed and average vehicle density for each traffic lane scenario

Traffic lane scenario	No. of links	Correlation coefficient, R
Link without median strip, and 1 or 1.5 lanes in both direction	165	-0.27
Link without median strip, and 2 or more lanes in both direction	126	-0.37
Link with median strip, and 1 or 1.5 lanes in each direction	33	-0.48
Link with median strip, and 2 or more lanes in each direction	542	-0.54
One-way link	12	-0.65
All links	878	-0.43

4. Results

Simple Comparison before/after WS showed that an average traveling speed decreased from 26.67 km/h (267links) to 25.44 km/h (275links). Also, to confirm the effect of the workshop on the travel speed, a multiple regression analysis of the average link speed was carried out using a workshop dummy variable, average link vehicle density, female dummy variable, university student dummy variable, lane line (white line) is drawn dummy variable, right / left turn intersection at the end of link dummy variable, the frequency of passing a motorcycle and being passed by a motorcycle as explanatory variables.

The results (TABLE 5) show that the average link speed decreased approximately 2km/h after participating in the workshop. In term of the overall analysis, the average vehicle density has the greatest influence on the speed reduction and the traffic condition is the dominant factor of the traveling speed. Among individual attributes, the average interval speed is higher in case of male and university student. Furthermore, when lane line (white line) is drawn, average link speed would increase. This result shows excessive speed with overconfidence may become a more serious problem in Cambodia if road surface were improved in the future.

TABLE 5 Multiple regression analysis with the average link speed as the objective variable

	Coefficient	t-value	
Constant term	32.15	45.20	**
Average vehicle density	-39.76	-15.69	**
Female dummy	-3.79	-6.22	**
University student dummy	1.48	2.54	*
WS dummy	-2.16	-3.90	**
Lane line (white line) dummy	1.73	2.98	**
Intersection right / left turn Dummy	-2.70	-3.36	**
Passing a motorcycle / km	0.18	6.86	**
Being passed by a motorcycle / km	-0.10	-5.17	**
Coefficient of determination		0.49	
Number of links		542	

*p < 0.05, **p < 0.01

5. Conclusion

A Study on the effect of Motorcycle Traffic Safety Workshop was conducted based on the video observations of actual driving behavior. Comparing driving behavior on arterial roads before and after the traffic safety workshop which included practical skills and classroom learning aimed at improving hazard prediction ability and acquiring basic driving skills, showed that an average travel speed decreased significantly after the workshop. In the analysis, the variable of average vehicle density had a negative and statistically significant impact on average link speed. This result implied that vehicle density could be an explanatory variable to represent various driving conditions of motorcycles with psychological effects. Furthermore, this result showed that even though average vehicle density was high, some students got average link speed more than the legal limit speed of 30 km/h. These results suggested that many young motorcyclists didn't have sufficient risk awareness and hazard perception skills and the current motorcycle use among young people is not safe due to insufficient educational opportunities. More practical and advanced driver education, such as hazard prediction and knowledge for driving safety can be expected to improve safety performance through motorcycle driving behavior. Hereafter, to clearly demonstrate the relationship between the content of this kind of traffic safety workshop and driving confidence, it is necessary to refine the experimental design, as in a panel study. Regarding the contents of the safety workshop, the development of a traffic safety workshop program that includes advanced driving skills training, such as speed awareness or hazard anticipation would be required for practical implementation.

Acknowledgement

This study is a part of the project supported by the International Association of Traffic and Safety Sciences. The video surveys in this study were conducted with substantial cooperation from the Faculty of Education of the Royal University of Phnom Penh. We would like to take this opportunity to express our gratitude.

REFERENCES

- 1) International Transport Forum: Road Safety Annual Report, OECD Publishing, (2017)
- 2) Prathung Hongsrnagon, Theerachai Khompratya, Surbpong Hongpukdee, Piyalamporn Havanond, Nathawan Deelertyuenyong: Traffic risk behavior and perceptions of Thai motorcyclists: A case study, IATSS Research, Volume 35, Issue 1, Pages 30-33, (2011)
- 3) Mau-Roung Lin, Jess F. Kraus, A review of risk factors and patterns of motorcycle injuries, Accident Analysis & Prevention, Volume 41, Issue 4, Pages 710-722, (2009)
- 4) Michon J.A.: The Mutual Impacts of Transportation and Human Behaviour. In: Stringer P., Wenzel H. (eds) Transportation Planning for a Better Environment. Nato Conference Series, vol 1. Springer, Boston, MA, (1976)
- 5) M. Hatakka, E. Keskinen, N.P. Gregersen, A. Glad, K. Hernetkoski; From control of the vehicle to personal self-control: broadening the perspectives to driver education, Transportation Research Part F: Traffic Psychology and Behaviour, 5, pp. 201-215, (2002)
- 6) Esko Keskinen: Education for older drivers in the future, IATSS Research, Volume 38, Issue 1, Pages 14-21, (2014)
- 7) Patarawan Woratanarat, Atiporn Ingsathit, Pornthip Chatchaipan, Paibul Suriyawongpaisal, Safety riding

- program and motorcycle-related injuries in Thailand, *Accident Analysis & Prevention*, Volume 58, Pages 115-121, (2013)
- 8) Khuat Viet Hung, Le Thu Huyen: Education influence in traffic safety: A case study in Vietnam, *IATSS Research*, Volume 34, Issue 2, Pages 87-93, (2011)
 - 9) Barry Watson, Deborah Tunnicliff, Katy White, Cynthia Schonfeld, Darren Wishart: Psychological and social factors influencing motorcycle rider intentions and behavior, Australian Transport Safety Bureau, (2007)
 - 10) Nina Dragutinovic, Divera Twisk: The effectiveness of road safety education, a literature review, R-2006-6, SWOV Institute for Road Safety Research, (2006)
 - 11) Divera Twisk: Improving Safety of Young Drivers: In Search of Possible Solutions, D-93-2, SWOV Institute for Road Safety Research, (1994)
 - 12) Sudip Barua, Bhazad Sidawi, Shamsul Hoque: Assessment of the Role of Training and Licensing Systems in Changing the Young Driver's Behavior, *International Journal of Transportation Science and Technology*, Volume 3, Issue 1, Pages 63-78, (2014)
 - 13) Fred Wegman, Hans-Yngve Berg, Iain Cameron, Claire Thompson, Stefan Siegrist, Wendy Weijermars: Evidence-based and data-driven road safety management, *IATSS Research*, Volume 39, Issue 1, Pages 19-25, (2015)
 - 14) Stéphane Espié, Abderrahmane Boubezoul, Samuel Aupetit, Samir Bouaziz: Data collection and processing tools for naturalistic study of powered two-wheelers users' behaviours, *Accident Analysis & Prevention*, Volume 58, Pages 330-339, (2013)
 - 15) Atthapol Seedam, Thaned Satiennam, Thana Radpukdee, Wichuda Satiennam: Development of an onboard system to measure the on-road driving pattern for developing motorcycle driving cycle in Khon Kaen city, Thailand, *IATSS Research*, Volume 39, Issue 1, Pages 79-85, (2015)
 - 16) Mark A. Wetton, Andrew Hill, Mark S. Horswill: The development and validation of a hazard perception test for use in driver licensing, *Accident Analysis & Prevention*, Volume 43, Issue 5, Pages 1759-1770, (2011)
 - 17) Tova Rosenbloom, Amotz Perlman, Avihu Pereg: Hazard perception of motorcyclists and car drivers, *Accident Analysis & Prevention*, Volume 43, Issue 3, (2011)

Latent Opportunities for the Use of Two-Rider Bicycles and Associated Challenges by Welfare Service Providers

Takuya KONISHI* and Nagahiro YOSHIDA**

(Received October 31, 2018)

Synopsis

For persons with reduced mobility (PRM), the two-rider bicycle might be a potential, practical means of transportation, and the development of bicycles that meet these needs is in progress. While it revealed that there were many limits imposed on their use as a private use in a previous study, the opportunities for business use or associated challenges remain unclear. Thus, the purpose of this study is to understand the latent opportunities or use of two-rider bicycles by welfare service providers, as well as the associated challenges. A hearing survey was conducted on various type of welfare service providers that operate transportation services for the elderly and people with disabilities. Furthermore, a questionnaire survey was conducted on potential users after providing opportunities to experience two-rider bicycles. The results confirmed that there were different types of latent opportunities for the use of two-rider bicycles by each type of welfare service providers.

KEYWORDS: two-rider-bicycles, elderly or disabled people, welfare serves, hearing survey, questionnaire survey

1. Research Background and Objective

Persons with reduced mobility (PRM) including mothers and young children with disabilities, have expressed an interest in a bicycle that can be ridden by two people, and the development of bicycles that meet these needs is in progress.

According to previous researches, while there were latent opportunities for the use of tandem bicycles especially for people with visual impairment, it revealed that some trainings or experiential sessions were required to reduce subjective fears in some unstable situations¹⁾. Regarding challenges for the use of two-rider bicycles by PRM when they use it in daily life, the result of questionnaire survey showed that they would feel concerned about road conditions, parking spaces, and getting a help for seeking a pilot rider²⁾.

There were many limits imposed on their use as a private use, the opportunities for business use or associated challenges remain unclear. Thus, the purpose of this study was to clarify the latent opportunities or use of two-rider bicycles by potential providers in welfare service sector, as well as the associated challenges.

2. Research Methods

2.1 Method of Hearing Survey

A hearing survey was conducted on various type of welfare service providers (e.g., day care providers, afterschool, visiting long-term care, and guide helper services) that operate transportation services for the elderly and people with disabilities in order to investigate the following topics: first, to research the realities with regard to outings during service provision; and second, to investigate the opportunities of using a two-rider bicycle (Table.1). The hearing survey consisted of five items on organization characteristics, five items on user characteristics, and six items on the presence or absence of current challenges and their details, as well as in the scenarios of bicycle use.

* Student, Master Course of Dept. of Urban Design and Engineering

** Associate Professor, Department of Urban Design and Engineering

Table.1 Subjects of hearing survey

Type of Subject		Day Care Provider	Afterschool	Visiting long-term care	Guide Helpers
Service User		Elderly	Children with Disabilities	Elderly	Disabilities
Place for service		Institution	Institution	Home	Out Side
Observe date		2017/1/20	2017/1/24,26	2016/12/12	2017/1/10
Number		1	2	1	1
Transport service		○	○	×	×
Origin-Destination of Transportation		Institution-Home	Institution-Home/School	No Pick Up	Anywhere based on requests
Mode of Transportation	Vehicle	○	○	×	×
	Wheel Chair	○	○	○	○
	Walk	○	○	○	○
	Public Transportation	×	○	○	○

2.2 Method of Evaluation by Two-Rider-Bicycles Experience

A questionnaire survey was conducted after providing opportunities to experience two-rider bicycles (i.e., tandem bicycles and tricycles with frontal seats) for individuals with limited mobility as a passenger and their families and welfare service providers as a driver. Responses were received from a total of 77 drivers and the passengers, who revealed the latent opportunities of using two-rider bicycles by type of difficulty for going out, as well as the associated challenges (Table.2). The questions included four items on individual characteristics, five questions on daily outing-related behaviors, four questions on bicycle performance, and five questions on intentions of using or owning a bicycle. The questionnaire was designed so that the difficulties of the passenger could be understood from the driver's response in cases where the passenger's disability or other difficulty limited his or her capacity to respond to the questionnaire.

Table.2 Outline of evaluation by two-rider-bicycles experience

Riding Place	Ground, Park and Cycling Stadium (No Vehicle Traffic)	Cycling Road (Less Vehicle Traffic)	Public Road (Much Vehicle Traffic)
Subjects	--Participants of the bicycles experience event --Welfare service providers and its users	--Participants of the bicycles experience event --Welfare service providers and its users	--Participants of the bicycles experience event
Number	27(Difficult to go out:8 (including to answer instead))	44(Difficult to go out:21 (including to answer instead))	5(Difficult to go out:4 (including to answer instead))
Observe Period	2016/10 - 2018/1	2016/11 - 2018/2	2017/3
Two-rider-bicycles	Tandem Bicycles Tricycles with Frontal Seats(2Types)	Tandem Bicycles Tricycles with Frontal Seats(2Types)	Tandem Bicycles

3. Research Results

3.1 Results of Hearing Survey

The results confirmed that there are latent opportunities for the use of two-rider bicycles by welfare service providers, as it can be used for small-scale welfare service businesses that provide transportation as part of their services. The results also confirmed that even welfare service providers that do not offer transportation had needs for recreational purposes for routine outings and other uses as per users' interests. On the other hand, there are many systemic challenges, such as insurance and indemnity liabilities for welfare service providers, as well as challenges associated with the environment of use, such as parking space (Table.3).

Table.3 Opportunities for the use of bicycles by welfare service provider type and associated challenges

Type of provider	(Afterschool) Day services	Visiting long-term care	Guide Helpers
Interests in use by welfare service providers	Transportation, Routine outings	During visits, Routine outings	During accompanied outings
Interests/purpose for use by welfare service users	Recreational purposes	Routine outings Recreational purposes	Routine outings Recreational purposes
Interested purpose for use by welfare service users	Common challenges	[Vehicle] --Poor weather conditions	[Systemic] --Insurance system, indemnity liabilities for transportation [Environment of use] --Parking space
	Individual challenges	Limited number of people who can be transported	Bicycle parking at the visit destination Designation of daily use tools and equipment

3.2 Results of Evaluation by Two-Rider-Bicycles Experience

The study confirmed that there is a level of interest in using two-rider bicycles by people with difficulties for going out. Furthermore, people with inability or difficulty walking tend to be interested in using frontal-seat types for routine outings, and people with visual disabilities tend to be interested in using the tandem type for recreational purposes (Fig.1).

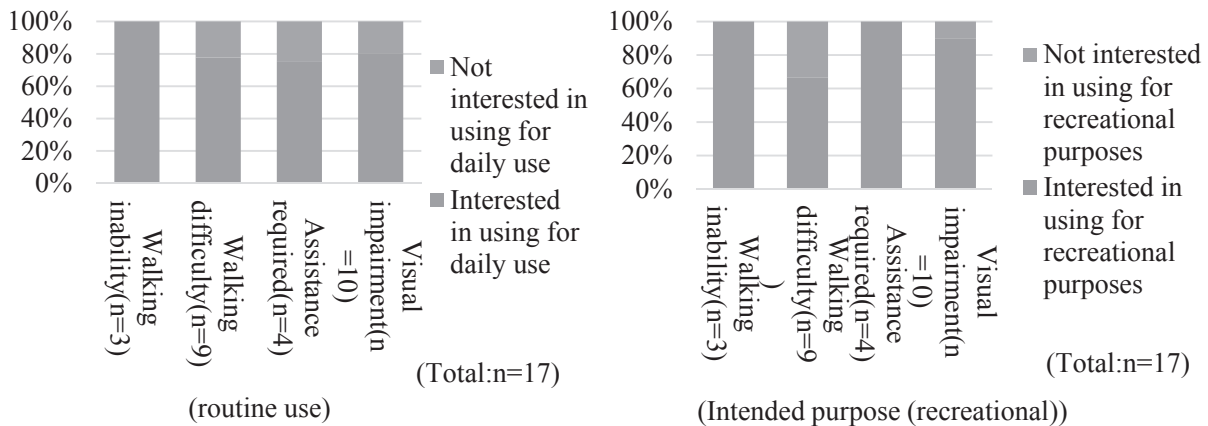


Fig.1 Purposes of the use of bicycles by type of reduced mobility for going out.

4. Conclusion

In this study, the latent opportunities or use of two-rider bicycles were clarified by a hearing survey and a questionnaire survey for potential business users based on an experiential evaluation. We obtained the following results;

- there are latent opportunities for the use of two-rider bicycles by small-scale welfare service businesses that provide transportation as part of their services,

- even welfare service providers that do not offer any transportation service had needs for recreational purposes for routine outings and other uses as per users' interests,
- there are many systemic challenges for welfare service providers, as well as challenges associated with the environment of use, and
- people with inability or difficulty walking tend to be interested in using frontal-seat types for routine outings, and people with visual disabilities tend to be interested in using the tandem type for recreational purposes.

From now on, it will be required to clarify the method of bicycle education for passengers assuming the use of a two-rider bicycle and the benefit in daily use.

5. References

- 1) Y. Yoshida, N. Yoshida, Y. Hino, T. Uchida: A study of availability of Tandem Bicycle for Vision Impaired Persons, Japan Society of Civil Engineers Kansai Branch Annual Scientific Lecture, IV-51, 2013.
- 2) Y. Yariyama, N. Yoshida, I. Fujie: Needs and Tasks for Daily Use of Tandem Bicycles for People Who are Difficult to Move, The City Planning Institute of Japan Kansai Branch, Research Presentation Lecture, Vol. 14, pp. 101-104, 2016.

Abstracts of Papers

Published in Other Journals

Mechanical Engineering

Improvement of Thermal Performance of a Coupling Hot Water-Driven and Gas Fired-Driven Absorption Air Conditioning System by Both Using Solar Energy and Gas Engine Cooling Water

Nobuya NISHIMURA, Ryusuke MATSUDA, Norio UEDONO, Toru SHIBA and Tomohisa MEKATA
Proceedings of Grand Renewable Energy 2018 (GRE2018) International Conference, Yokohama, June 17-22, P-St-8 (on CD-ROM) (2018).

This paper presents the thermal evaluation results on a solar-assisted coupling hot water-driven and gas fired-driven absorption air conditioning system at experimental apartment housing NEXT21. The coupling air conditioning system consist of hot water driven single effect absorption refrigerator of 31.3 kW rated cooling capacity and gas-fired double effect absorption chiller of 105 kW rated cooling capacity. Performances of both each two types of absorption refrigerator and whole absorption air conditioning system were evaluated by COP and compared each other.

Characteristics and Mechanism of Bubble Formation in Plastic Packaging for Food

T. INOUE (Toyo College of Food Technology), T. SHIONO (Toyo College of Food Technology), H. IYOTA
Japan J. of Food Eng., Vol.16, No.3, pp.145-150 (2018). DOI: 10.11301/jsfe.17507

Heat-sealing technology, which is used for plastic packaging, entails laminating multiple kinds of films together to form a barrier with varying permeability and stiffness. Creating a heat seal consists of heating the heat-seal material and then immediately cooling it down. However, overheating the heat-seal material can introduce defects such as bubble formation. This study examined the effect of the moisture content on bubble formation by using retort pouches as the sample material. The material is composed of polyester, nylon, and polypropylene as the outermost layer, barrier layer, and heat seal material, respectively. A mechanism of bubble formation is proposed on the basis of the moisture adsorption characteristics, viscous elasticity, and barrier characteristics of the sample material.

Measurement of Constant Drying Rate of Wet Material Placed in a Fluidized Bed of Inert Particles under Reduced Pressure

Y. TATEMOTO (Shizuoka Univ.), R. OGAWA (Shizuoka Univ.), H. IYOTA
Drying Technology, Vol.36, No.11, pp.1380-1386 (2017). DOI: 10.1080/07373937.2017.1403926

The objective of this study is to estimate the drying characteristics of a relatively large material immersed in a fluidized bed under reduced pressure by measuring the constant drying rate. The constant drying-rate period in a fluidized bed under reduced pressure is difficult to measure because it is extremely short. To maintain the constant drying-rate period, distilled water is directly supplied to the drying material. Through our experiment, the heat transfer coefficient of the material surface was also determined. The results were compared with data on hot air drying. The constant drying rate is higher for fluidized bed drying than for hot air drying. It suggests that the heat transfer coefficient on the surface of the drying material is much larger for fluidized bed drying than for hot air drying. For fluidized bed drying, the effect of pressure in the drying chamber on the heat transfer coefficient is slight at the same normalized mass velocity of dry air (G/Gmf). The temperature difference between the inside of the drying chamber and the drying material is much smaller for fluidized bed drying than for hot air drying. The constant drying rate increases as the pressure in the drying chamber decreases.

Residual Bubble Volume Formed behind a Sphere Plunging into Liquid Bath (Meniscus Breakdown with Finite Velocity of Sphere Penetration)

Kenji KATOH , Tatsuro WAKIMOTO, Yoshiaki UEDA (Setsunan Univ.) and Manabu IGUCHI
Physics of Fluids, Vol.30, No.8, 082106, 11 pages (2018).

The residual bubble formed from spherical particles plunging into a liquid bath has an important effect on the performance of CaO particles used for the desulfurization of melted iron. Previous work has theoretically estimated the residual bubble volume resulting from quasi-static sphere immersion by applying the energy minimization principle to the gas-liquid interface meniscus at its rupture [Katoh et al., "Residual bubble formed behind a sphere plunging into liquid bath (in Japanese)," *Jpn. J. Multiphase Flow* 28, 547-553 (2015)]. Here, we propose a method to theoretically estimate the residual bubble volume for sphere penetration with a finite velocity from 0.05 to 30 mm/s into a liquid bath. To do so, the meniscus rupture at the sphere's critical depth was

calculated via a dynamic equation in which the energy gradient along the sphere surface was considered as the driving force to move the triple-phase contact line. The bubble volume was then estimated by calculating the system energy at the meniscus breakpoint and by using the principle of minimum energy. The model results were verified experimentally for a variety of liquids, showing that the proposed model can be used for estimation of the residual bubble volume.

Control of Droplet Movement on an Inclined Wall with Sawtoothed Wettability Pattern by Applying Ultrasonic Vibration

Kenji KATOH, Hiroki TAMURA, Eriko SATO and Tatsuro WAKIMOTO

Experiments in Fluids, Vol.59, No.9, 141, 10 pages (2018).

This study deals with the control of the movement of liquid droplets rolling down an inclined plate based on the differences in the wettability of the plate. We used a photoreactive polymer poly(7-methacryloyloxy coumarin) (PMC) whose molecular structure can be changed reversibly to realize different wettabilities by ultraviolet irradiation. We proposed employing sawtooth patterns at boundaries between areas with different contact angles to control the droplet trajectory. Furthermore, we experimentally observed that the droplet moves along a line inclined to the direction of gravity. The droplet behavior can be analyzed using a theoretical model based on the droplet dynamics wherein the surface tension acting on the contact line and the gravitational force are considered. The theoretical results suggest that inclination from the gravitational direction can be increased if the advancing contact angle is reduced. In the experiments conducted herein, ultrasonic vibration was applied to the inclined plate to reduce the contact angle hysteresis. The results showed that the advancing contact angle actually decreased and that the droplet trajectory was controlled to realize motion along a line with inclination angle almost twice of that realized without vibration.

Wetting Behavior of Falling Liquid Film Flowing on a Plate with a Side Wall

Kenji KATOH, Changing XU, Yoshiaki ISO (IHI Corp.), Ryosuke IKEDA (IHI Corp.) and Tatsuro WAKIMOTO

Japanese Journal of Multiphase Flow, Vol.32, No.1, pp.35-42 (2018) (in Japanese).

The wettability of liquid film flowing on an inclined plate is extremely deteriorated if there is a vertical wall on the channel side. In this study, an experimental study was conducted to investigate the influence of the side wall on the dryout of liquid film flow. The film surface forms a meniscus having a minimum film thickness near the side wall. The thin film thickness causes the dryout of film flow at lower flow rate. To avoid the appearance of the minimum thickness, the test channels of SUS-304 plate having circular side walls with various curvature radii R_S were manufactured and the surface profiles of liquid film were measured experimentally for three kinds of test liquids. The meniscus profile was flattened at appropriate radius of curvature, i.e., $R_S \sim 6$ mm for $\theta_R = 20 \sim 30^\circ$ (θ_R : receding contact angle) in this experiment. The critical Weber number at which dryout disappears is lowered remarkably and is recovered to the value those experienced for the flat plate without side walls.

Simultaneous Determination of Micellar Structure and Drag Reduction in a Surfactant Solution Flow Using the Fluorescence Probe Method

Tatsuro WAKIMOTO, Koichi ARAGA and Kenji KATOH

Physics of Fluids, Vol.30, No.3, No. 033103, 11 pages (2018).

As widely known, the addition of a specific type of surfactant to water reduces drag in a pipe flow. This effect is considered to be a result of the suppression of turbulent transition caused by the ordered structure of rod-like micelles that is referred to as a shear-induced structure (SIS). However, it is typically difficult to determine the SIS since it is necessary to noninvasively detect the SIS with several hundred nanometers in the actual moving flow. In this study, we used the fluorescence probe method to locally determine the SIS in a pipe flow. When hydrophobic fluorescence molecules are added to the surfactant solution, the fluorescence molecules are trapped in micelles. Thus, fluorescence intensity varies based on the change in the micellar structure. We verified the applicability of the fluorescence probe method to the SIS detection and determined the relationship between the micellar structure and the drag reduction in the pipe flow by simultaneously measuring the fluorescence intensity and pipe friction factor. The experimental result demonstrates that the SIS formation in the near-wall region is closely correlated with the drag reduction and suggests that the near-wall SIS suppresses the turbulent transition.

Development of a Wave Power Generation System Using a Slit Type Breakwater (Performance of Bending Plate Type Generator in 1/5 Scale Experiment)

Tatsuro WAKIMOTO, Kenji KATOH, Takaaki SHIGEMATSU and Shin'ya YOSHIOKA

Advanced Experimental Mechanics, Vol.3, pp.98-103 (2018).

A new wave power generation system is proposed to be installed in a vertical slit type breakwater. The merits of the system are as follows: (i) no occupation of sea surface, (ii) low cost maintenance, and (iii) high energy efficiency by using accelerated flow from the slit of breakwater. In this study, a new, higher efficiency generator is proposed. An elastic rectangular plate connected to a wheel and axle via a wire is set in the water chamber. When the wave drag bends the plate, tension appears in a wire causes rotation of a wheel connected to a generator. To estimate the power of the proposed system at full scale, the wave energy flowing into the breakwater was simulated numerically. The results show that more than 60% of the wave energy is collected in the water chamber behind the slit with a small opening ratio. Although the output power of the bending plate is rather small, the power per unit of occupied sea area is somewhat superior to that of existing systems.

Evaluation of Gas-Lift Effect by Bubbles Rising in a Vertical Circular Pipe

Tomonori SUWA, Tatsuro WAKIMOTO, Kenji KATOH and Manabu IGUCHI

Transactions of the JSME, Vol.84, No.860, 17-00591, 12 pages (2018) (in Japanese).

The gas-lift effect appears in various types of gas-liquid two-phase flows. Information on the effect in a still liquid however is very limited compared to that in a moving liquid. Experiments were carried out in this study on the case that air bubbles rose in still water contained in a vertical circular pipe made of transparent acrylic resin. The flow pattern covered bubbly and slug flow regimes. The effect is composed of bath surface elevation effect and liquid flow induction effect. The latter effect was quantitatively evaluated in terms of the pipe friction loss in the pipe. An empirical equation on an apparent frictional coefficient was proposed for predicting the loss. The experimental results reveal that the liquid flow induction effect is weak in the bubbly flow regime, while prevails significantly in the slug flow regime.

Effect of Air Injection Method on the Efficiency of Oxygen Dissolution into a Cylindrical Water Bath

Tomonori SUWA, Tatsuro WAKIMOTO, Kenji KATOH and Manabu IGUCHI

Journal of JSEM, Vol.18, No.2, pp.116-123 (2018) (in Japanese).

Experimental investigations were carried out to find out an efficient method of oxygen dissolution into water. Air injection through a single-hole nozzle was chosen in this model study because of its good handling performance and low running cost. First, basic three types were mentioned; bottom, top, and side gas injection into a cylindrical water bath. The air flow rate and the height of bubble dispersion region were kept constant. The dissolved oxygen was measured with a membrane electrode sensor. The history of dissolved oxygen concentration obeyed the first order reaction law. The dissolution efficiency therefore was evaluated in terms of the volumetric mass transfer coefficient. The side gas injection was found to be most effective among the three methods under the experimental conditions considered.

Numerical and Theoretical Analyses of the Dynamics of Droplets Driven by Electrowetting on Dielectric in a Hele-Shaw Cell

Yasufumi YAMAMOTO (Kansai Univ.), Takahiro ITO (Nagoya Univ.), Tatsuro WAKIMOTO and Kenji KATOH

Journal of Fluid Mechanics, Vol.839, pp.468-488 (2018).

Droplet movement by electrowetting on dielectric (EWOD) in a Hele-Shaw cell is analysed theoretically and numerically. We propose a simple theoretical model for the motion, which describes well the voltage dependency of droplet speed below the saturation voltage as measured experimentally. The simulation method for numerical analyses is constructed by using the Young-Lippmann equation to represent EWOD and the generalised Navier boundary condition to represent the moving contact line in the context of the front-tracking method. With an adjusted slip parameter, the present full three-dimensional numerical simulation reproduces well the shape evolution and movement speed of droplets as observed experimentally. We verify the proposed theoretical model in numerical experiments with various shapes and voltages. Furthermore, we analyse theoretically the behaviour of the contact line at the onset of droplet motion as observed in the simulation and experiment, and we are able to estimate very well the time scale on which the contact angle changes.

Removal of Fine Particles on a Wall by High-Speed Impinging Air Jet with Enhanced Turbulence (A Study on Optimal Nozzle Shape)

Tatsuro WAKIMOTO, Atsushi NAKAGAWA, Katsuki CHINO, Kazuhiko SOEMOTO (Shinco Co. Ltd.) and Kenji KATOH

Proc. of the 6th International Conference on Jets, Wakes and Separated Flows, USB-memory, 4 pages (2017).

In this study, a cleaning device to remove micron-sized particles on a solid surface by an air jet is developed. This device has a special nozzle containing a triangular cavity to add high intensity turbulence to the air jet, and the air

jet impinges on the solid surface removing the particles. Assuming that the spherical particles are removed by rotational movement, we estimated the rotational moment induced by drag force and local pressure gradient from calculated flow field by numerical simulation. From the moment estimation for various nozzle shapes, it is clarified that the addition of a rectangular interspace to the cavity increases the removal moment and the inlet width of the cavity has an optimal value. Under the experimental conditions in this study, the inlet width of 1mm gives the best removal performance.

Visualization of Viscoelastic Behavior in vivo Skin using Optical Coherence Tomography-based Straingraphy combined with Suction Device

Yusuke HARA, Daisuke FURUKAWA and Souichi SAEKI

Mechanical Engineering Letters, Vol.4, 17-00656 (2018).

Although various apparatuses have been developed to assess the skin mechanical function, the spatial viscoelastic behavior of each skin layer including the epidermis and dermis is yet unclear. To resolve that lack of clarity, we built a handmade system combining a suction device with optical coherence tomography (OCT). OCT can visualize the vertical section of the skin with high spatial resolution and high acquisition speed. In addition, we developed an algorithm for time-dependent strain tomography, named Dynamic Optical Coherence Straingraphy (D-OCSA), which can analyze the changes in strain distributions over time in sequential OCT images. Using the system, successive OCT images of volar forearm skin were obtained after the suction release, followed by calculation of spatial distribution of creep recovery time as an index of viscoelastic behavior. As a result, we revealed that the creep recovery time in the dermis was significantly larger than that of the epidermis. This is the first report to provide evidence that there is a spatial difference in the viscoelastic behavior in the skin. Future application of our method would be beneficial to the diagnosis of skin mechanical function and the validation of cosmetic and medical applications.

Visualization of Visco-elastic Behavior in Skin Equivalent using Optical Coherence Tomography Straingraphy

Yusuke HARA, Yuki OGURA, Toyonobu YAMASHITA, Daisuke FURUKAWA and Souichi SAEKI

Skin Research and Technology, Vol.24, pp.334-339, 10.1111/srt.12435 (2018).

Background/Purpose: The relationships between the skin components and these mechanical roles are still unclear. To clarify these relationships, we investigated spatial mapping of the mechanical behavior of cultured skin equivalents (SEs) using optical coherence tomography (OCT)-based strainingraphy. Methods: We built a strain relaxation test system combined with OCT and developed an algorithm that could visualize a time-dependent strain distribution, named dynamic-optical coherence strainingraphy (D-OCSA). Using this system, we analyzed how the spatial mechanical changes in the SEs depended on the culture duration. For quantitative analysis of viscoelastic behavior, we defined a relaxation attenuation coefficient of strain rate, which indicates the ratio of viscosity and elasticity in the Klevin-Voight model. Results: By culturing for 4 days in comparison to culturing for 1 day, the strain relaxation attenuation coefficient of the whole skin, especially at the region of the dermal-epidermal junction (DEJ), significantly increased in the negative direction. In tissue slices taken for microscopy, several cracks were observed in the SEs cultured for 4 days. Conclusion: This study is the first to provide quantified evidence that the DEJ is a dynamically specialized region. An OCT-based strainingraphy system (D-OCSA) would be beneficial for evaluating the quality of SEs, as well as functional analysis of their mechanics.

Visualization of Age-related Vascular Alterations in Facial Skin using Optical Coherence Tomography-based Angiography

Yusuke HARA, Toyonobu YAMASHITA, Kumiko KIKUCHI, Yoshihide KUBO, Chika KATAGIRI, Kentaro KAJIYA and Souichi SAEKI

Journal of Dermatological Science, Vol.8, S0923-1811(18) (2018).

The assessment of dermal vasculature is crucial for understanding skin homeostasis, inflammation and disease. Various methods have been used to investigate structural alterations of the dermal vasculature. Histological approaches have revealed vascular alterations in aged skin, for example decreasing vessel density, and irregular and disorganized vessels. However, the complex three-dimensional arrangement of vascular plexuses cannot be seen and investigated by the examination of conventional histological tissue sections. In general, the different horizontal vascular plexuses, which are interconnected by vertically oriented vessels, are well developed at a specific depth, for example in the sub-epidermal and sub-dermal regions. A stereographic study of venous plexuses, following injection of a contrast medium, showed that venous plexuses extend continuously over neighboring venous polygons in the sub-epidermal plane [3]. Non-invasive angiography is a technique for vascular imaging that has been developed recently and continues to evolve. It allows non-invasive visualization of

dermal vascular anastomoses, not only vertically, but also horizontally [4–6]. In particular, angiography based on optical coherent tomography (OCT) can be used to analyze vascular plexuses at the micron level [5,6]. The principle of OCT angiography is to identify dynamic structural changes in the skin through a time-series of OCT tomograms, based on the idea that movement within the skin in the absence of an external force reflects blood flow, and so provides a good approximation of vascular plexus structure. Here, we performed a pilot study to evaluate the potential of OCT angiography for non-invasively investigating age-related vascular alterations in facial skin. This study was conducted according to the Declaration of Helsinki Principles and approved by the Ethics Committee of Shiseido Ltd. We enrolled 61 female Japanese subjects aged 21–69 years (19, 21 and 21 subjects in the 20s, 40 s and 60 s age groups, respectively), who gave their informed consent. Dermal vascular images were acquired by OCT angiography of their right cheeks, after a 15-min acclimatization period at 24 degree C.

In vivo Micro-tomographic Visualization of Capillary Angio-Dynamics around upper dermis under mechanical stimuli using Low Coherence Interferometer, “Optical Coherence Doppler Velocigraphy”

Daisuke FURUKAWA, Souichi SAEKI, Takafumi ITO and Yoshiaki NISHINO

American Journal of Physics and Applications, Vol.6, Issue 4, pp.89-96, (2018).

The skin aging process, e.g. wrinkles and sagging, caused by not only aging but also ultraviolet irradiation, could be related to the depression of metabolic function. Therefore, an *in vivo* quantitative measurement of capillary blood flow velocity governing skin metabolism functionally, i.e. microcirculation, is crucial to clarify the skin aging and to create skincare products. The purpose of this study is to visualize the tomographic velocity of red blood cell in capillaries just below human epidermal skin using Optical Coherence Doppler Velocigraphy, namely OCDV. This was constructed on a low coherence interferometer, which could provide tomographic distribution of flow-modulated Doppler frequency by developing OCDV algorithm of Hilbert transform and adjacent autocorrelation. In order to validate OCDV system, this was *in vivo* applied to human forearm skin under respective mechanically stimulated conditions of control and avascularization. As a result, a cross-sectional imaging of blood flow velocity was found to display not only morphological OCT images but also networks of capillary vasculature inside dermal tissue. It was confirmed that blood flow velocity further decreased in upper dermis under avascularization than control condition. Additionally, OCDV could provide a velocity map of blood flow having sensitivity to mechanical stimulus, so has strong efficacy to diagnose “*Capillary Angio-Dynamics*” of skin tissue. In conclusions, OCDV system could be quite useful for a micro-tomographic imaging of blood flow velocity of capillaries inside skin.

Vascular Morphology in Facial Solar Lentigo assessed by Optical Coherence Tomographic Angiography

Yusuke HARA, Toyonobu YAMASHITA, Kumiko KIKUCHI, Takako SHIBATA, Masato NINOMIYA, Chika KATAGIRI, Kentaro KAJIYA, Souichi SAEKI and Hajime IIZUKA

The 42nd Annual Meeting of the Japanese Society for Investigative Dermatology, JSID2018 (2017).

The histological features of solar lentigo (SL), including epidermal thickening and hyperpigmentation, suggest that altered dermal vasculature affects epidermal regulation. SLs show a significant increase in vessel density and increased levels of vascular endothelial growth factor expression. It is known that the horizontal vascular plexuses are well developed in the sub-epidermal region, which affects epidermal regulation. However, little is known about the dermal vascular plexuses underlying pigmented lesions such as SL. We investigated vascular morphology in facial solar lentigo, focusing on the horizontal vascular plexuses of the sub-epidermal region. Eleven Japanese women aged 43–59 years with a clinical diagnosis of facial SL were enrolled. For visual assessment, we used newly-developed high-speed optical coherence tomographic (OCT) angiography, which can acquire *en-face* optical sections at high resolution. As a consequence of image analysis, OCT revealed that the epidermis in SL is thicker than that of surrounding normal skin. OCT angiography allowed clear visualization of the depth-resolved vascular plexuses image. In addition, we confirmed that there was a significant increase in the density of dermal blood vessels in SL. This finding extended from the papillary dermis to the upper reticular dermis at a depth of 200 μm . In conclusion, our results suggest that SL vascularity can be characterized using OCT angiography. Future applications of OCT angiography may be beneficial in the diagnosis of hyperpigmentary disorders.

Application Study on Micro-tomographic Visualization of Spatio-Temporal Mechanical Characteristics of Biological Tissue

Souichi SAEKI, Daisuke FURUKAWA and Takeshi NAGASAKI

The 4th International Symposium on Multidisciplinary Computational Anatomy, A02-KB111 (2018).

Authors have developed Dynamic OCSA, which provide tomographic distribution of deformation velocity

dynamically based on cross-correlation technique using OCT images. In this study, the present method was *in vivo* applied to forearm skin tissue to evaluate viscoelastic behavior related with complicated micro-biomechanics of superficial skin structures as tomographic distribution of creep recovery time. As a result, creep recovery time around capillary vessels was observed to be larger, where there is fine and soft collagen and viscous effect of microcirculation. So, it was confirmed that Dynamic OCSA can non-invasively visualize space-dependent and time-dependent biomechanical properties as creep recovery time.

Characterization of Facial Solar Lentigo using Optical Coherence Tomographic Angiography

Yusuke HARA, Toyonobu YAMASHITA, Kumiko KIKUCHI, Takako SHIBATA, Masato NINOMIYA, Chika KATAGIRI, Kentaro KAJIYA, Hajime IIZUKA, Daisuke FURUKAWA and Souichi SAEKI

SPIE Photonics West BIOS, 10467-35; The 4th International Symposium on Multidisciplinary Computational Anatomy, on CD-rom (2018).

Chronic sun exposure causes cutaneous vascular and pigmentary changes, leading to photoaging. A solar lentigo (SL) is one of the major signs of photoaging on the face. Histological approach in SL biopsies showed a significant increase in vessel density and increased levels of vascular endothelial growth factor expression. As a dermal-vascular morphology, it is known that the horizontal vascular plexuses are well developed in the sub-epidermal region which affects epidermal regulation. However, little is known about the alteration of superficial vascular plexuses underlying SL. To clarify the superficial vascular features of SL, we developed two types of angiographies using optical coherence tomography (OCT), customized correlation-mapping OCT (cmOCT) and optical coherence doppler velocimetry (OCDV). Our cmOCT allows clearly visualization of depth-resolved vasculature by noise removal algorithm which detected body motion in epidermal region. OCDV could detect depth-profile of phase change in axial-scanned interference signals by the collaboration of Hilbert transform and adjacent autocorrelation. Using these techniques, we investigated vascular morphology in facial SL, focusing on the horizontal vascular plexuses in the sub-epidermal region. Eleven Japanese women aged 43–59 years with a clinical diagnosis of facial SL were enrolled. As a consequence of OCT angiographies, there was a significant increase in the density of dermal blood vessels in SL, comparing to that of surrounding SL. This tendency was confirmed from the papillary dermis to the upper reticular dermis at a depth of 200 μm . Proposed methodology can be a useful method for the examination of vascular characteristics in cutaneous pigmentary disorders.

Micro-tomographic Diagnosis of Skin, Cartilage, Atherosclerosis, Tumor and Regenerative Tissue using Multi-functional OCT

Souichi SAEKI

9th OCARINA International Symposium, O-4, p.14 (2018).

Water has significant influence on human body due to physiological carrier media. In addition, rheological behavior of interstitial fluid in epidermal and dermal tissue, including blood micro-circulation, can vary skin mechanics in micro scale, i.e. *vis*. Therefore, an *in vivo* measurement of moisture content and capillary blood flow velocity is necessary to clarify skin mechanics. This paper presents 2C-OCM (2-Color Optical Coherence Moisturegraphy), which was composed of two-band light sources having different optical absorption properties of water respectively. These are capable of tomographically *in vivo* diagnosing the moisture content. Furthermore, OCDV (Optical Coherence Doppler Velocigraphy) algorithm can visualize the tomographic flow velocity of red blood cell in capillaries of human epidermal skin. In this experiment, 2C-OCM & OCDV were *in vivo* applied to human skin and regenerative tissue. Consequently, it was concluded that 2C-OCM & OCDV can provide micro tomography of moisture content and capillary blood velocity inside skin tissue, which can be attributed to biomechanical properties.

Study on *in vivo* 3D Micro-Tomographic Visualization of Vascular Plexuses and Capillary Blood Flow Using Optical Coherence Doppler Velocigraphy

Daisuke FURUKAWA, Ryohei NISHINO, Naoya KUSUMOTO, Souichi SAEKI, Yusuke HARA, Masatsugu SHIBA, Susumu AOKI, Takafumi ITO and Yoshiaki NISHINO

9th OCARINA International Symposium, P-36, (2018).

The skin aging process, e.g. wrinkles and saggings, caused by not only aging but also ultraviolet irradiation, could be related to the depression of metabolic function. The microcirculation system should be an important guideline of skin care for the anti/smart-aging. Rheological behavior of interstitial in epidermal and dermal tissue, including blood micro-circulation, can vary skin mechanics in micro scale, i.e. visco-elasticity. Therefore, an *in vivo* quantitative measurement of capillary blood flow velocity is crucial to clarify their properties. The purpose of this study is to visualize the tomographic flow velocity of red blood cell in capillaries below human epidermal skin

using Optical Coherence Doppler Velocigraphy, i.e. OCDV [1]. This is constructed on a low coherence interferometer [2], which is based on Hilbert transform and adjacent auto-correlation. In order to validate OCDV system, this was *in vivo* applied to human cheek skin under the condition of control. As a result of skin tomography obtained by OCDV, *en face* cross-sectional imaging of doppler velocity was found to display networks of capillary blood vessels in upper dermal tissue around hair follicles, as well as morphological skin structure. It was confirmed that capillary vasculature and blood velocity can be visualized tomographically even in the upper subpapillary layer. In summary, OCDV system could be quite useful for a micro-tomographic imaging of blood flow velocity of capillary vessels inside skin.

Wall Inspection Robot with Maneuvering Assist Control System Against Crosswind

Yogo TAKADA, Yuhei TOKURA, Yodai MATSUMURA, Takahiro TANAKA and Tatsuki KANADA
Journal of Robotics and Mechatronics, Vol.30, No.3, pp.416-425 (2018). DOI:10.20965/jrm.2018.p0416

Many social infrastructures and buildings are aging. Therefore, inspections to find deteriorated parts to prevent accidents are important. However, significant costs and inspection time are required for the current technologies. Therefore, inspection methods using robots are attracting attention. As the most appropriate option to traverse freely on concrete bridges and building walls is by traversing with lift force from propellers, a robot called HORNET has been developed that can run along a wall with two rotors. However, the floating-type robot with propellers could drop from a wall if hit by strong wind. Therefore, a gyro sensor was installed in the robot to detect its posture and adopted a simple maneuvering assist control to reduce the above-mentioned issue. In this study, the motion of HORNET was analyzed and a simple control system was designed to realize the maneuvering assist control. It was confirmed that the resistance of HORNET to the crosswind was improved by adding the control system.

Development of Small Robotic Fish Equipped with FPGA and CMOS Camera for Tracking Live Fish

Takuya ARITANI, Naoki KAWASAKI, and Yogo TAKADA

Proceedings of 7th International Symposium on Aero Aqua Bio-mechanisms (ISABMEC), 4 pages on USB Memory (2018).

A robotic fish used to investigate live fish needs the ability to recognize and track the observation target. We have developed an image processing system with the FPGA that processes signals from a CMOS camera to recognize an investigation target and to locate its position. Besides, high turning ability is required to keep capturing the target by a camera. Therefore, we improved the turning ability by bending the body of a robotic fish greatly with multiple joints. In this study, we have confirmed that the robot can recognize the investigation target and it has desirable turning ability.

Investigation of Rotors Imitating Bird Wings for Reducing Electricity Consumption of Structure Inspection Robot HORNET

Yogo TAKADA, Takahiro TANAKA, Tatsuki KANADA and Yodai MATSUMURA

Proceedings of 7th International Symposium on Aero Aqua Bio-mechanisms (ISABMEC), 5 pages on USB Memory (2018).

As bridges and buildings have been deteriorating, we have developed a robot, HORNET to inspect the wall. This robot travels on the wall surface with lift of propellers with contacting the wheels to the wall. Since the running duration is short on the smooth surface, the cross-sectional shape of a rotor was obtained to reduce the power consumption by optimizing with two-dimensional numerical analysis with genetic algorithm. Besides, we manufactured several kinds of rotors imitating birds and experimented to confirm a good shape concerning electricity consumption. Furthermore, we made HORNET's dynamic model, and simulated to confirm the reduction of the electricity consumption.

Effect of Surface Roughness on Antibacterial Properties of Copper and Cupronickel

Hisashi KATO, Yoshihiro SATO, Hiroshi KAWAKAMI and Yasushi KIKUCHI

Journal of Japan Institute of Copper, 57, pp.304-306 (2018) (in Japanese).

Copper is known as an antibacterial metal. Introducing antibacterial metals into environment surface in hospitals will decrease the number of viable bacteria on the environmental surface, and contribute to prevent hospital acquired infection. One of well known antibacterial mechanism of copper is that copper ions inactivate respiratory enzymes by oxidizing thiol groups, leading cell to be damaged. The amount of copper ion eluting from copper is hence an important factor in antibacterial property of copper. Increase in surface roughness will increase surface area and, as a results, the amount of copper ion eluting from copper, resulting in higher antibacterial properties of copper. In this research, we investigated effects of surface roughness on antibacterial properties of oxygen-free

copper (OFC) and cupronickel against Escherichia coli and on copper and nickel ions eluting from the surfaces. The surface of specimens was finished by buff polishing with aluminum oxide or wet-grinding with emery papers. The range of surface roughness of OFC was $R_a = 0.05$ (for buff polishing) ~ 0.93 (μm) and that of cupronickel was $R_a = 0.06$ (for buff polishing) ~ 0.50 (μm). Antibacterial property was evaluated in accordance with JIS Z 2801 except that the exposure time was set to 15 minutes. The amount of copper ion and nickel ion eluting from specimens was measured using inductively coupled plasma-mass spectrometry (ICP-MS). For OFC, the surface roughness had no effect on antibacterial properties. The buff polished OFC released more copper ion than the wet grinded OFC. For cupronickel, surface roughness had no effect on antibacterial properties nor on the amount of copper ion and nickel ion eluting.

Effects of Protein Surface Contamination on Antibacterial Activities of Copper Alloys

Yuzo TODA, Yuta TAKASHIMA, Hiroshi KAWAKAMI, Yoshihiro SATO and Yasushi KIKUCHI

Journal of Japan Institute of Copper, **57**, pp.307-312 (2018) (in Japanese).

Copper alloys are known as antibacterial metallic materials. Introducing such copper alloys into frequently hand-touched places has been considered to reduce risks of outbreaks of illnesses caused by pathogens on environmental surfaces. When copper alloys are used in environmental surfaces, surfaces of copper alloys are exposed to the surrounding environment and become contaminated by various substances in the surroundings. As surface contamination can reduce the antibacterial activity of copper alloys, cleaning henceforth must be carried out periodically on the contaminated surfaces. In this study, the antibacterial activities of copper alloys contaminated with protein were evaluated using bovine serum albumin (BSA) as a model protein contaminant. Also, in this study, we prepared specimens which were firstly contaminated with $0.80 \mu\text{g}/\text{mm}^2$ of BSA and then subjected to wipe-cleaning loaded with the sodium hypochlorite aqueous solution. For those specimens, we carried out antibacterial tests and measurements of the amount of BSA remaining of the cleaned surfaces. The antibacterial activities of the copper alloys was equal to the antibacterial activities of the clean copper alloys. The antibacterial activities of the copper alloys decreased with the increase in the amount of surface contaminant. However, when the amount of the BSA surface contaminant was $0.016 \mu\text{g}/\text{mm}^2$ and $0.16 \mu\text{g}/\text{mm}^2$, in those cases the surface of the specimen was completely covered with BSA molecules, the bacterial counts recovered from the copper alloys were one to two orders lower than those from the stainless steel specimens. The bacterial counts recovered from specimens contaminated with $0.80 \mu\text{g}/\text{mm}^2$ of BSA were not different from those from stainless steel specimens which don't have antibacterial activities. The bacterial counts recovered from the copper alloys after wipe-cleaning was more than the bacterial counts recovered from the clean copper alloys. When the amount of residual surface contaminants was reduced to $0.0016 \mu\text{g}/\text{mm}^2$, the surfaces of the copper alloys regained antibacterial activities to the same level as those in a clean surface condition. Hence, it is necessary to find cleaning conditions such that the amount of BSA decreases to $0.0016 \mu\text{g}/\text{mm}^2$ or less.

First-Principles Calculations of Ionic Conduction in Olivine-Type Li_xFePO_4

Ippei KISHIDA, Shota KOYAMA and Yoshiyuki YOKOGAWA

Materials Transactions, **59** (7), pp.1062-1067 (2018).

Super ionic conductors are required for all solid Li ion batteries. Conduction mechanism of Li_xFePO_4 has been revealed by first-principles calculations using plane-wave basis. Crystal structures were constructed using a unit cell and a $1 \times 2 \times 1$ super cell. Transition of Li site occupation with the smallest energy fluctuation was searched through graph theory. Trajectories of Li ions and migration energies were obtained by Nudged Elastic Band Method. Results show the migrating atoms pass through faces of O polyhedra. At dilute limit of Li, a single ion migrated and had very low migration energy of 0.14 eV. Increasing the carrier concentration resulted in pairing of Li atoms and raised the migration energy. At higher concentration region, cooperative ionic conduction mechanisms of two Li ions occurred. Low migration energies were obtained to be 0.20 and 0.22 eV for $x = 0.25$ and 0.5 of Li_xFePO_4 , respectively. Considering the migration energy and carrier concentration, Li_xFePO_4 with the concentration region $0.25 \leq x \leq 0.5$ should have high ionic conductivity. These mechanisms would be applied to develop new superionic conductors.

First-Principles Study of Silicon-Embedded Ni(110)

Tsuneo FUKUDA and Ippei KISHIDA

E-Journal of Surface Science and Nanotechnology, **15**, pp.96-101 (2017).

First-principles total energy calculations were performed to investigate stable atomic structures for the displacive adsorption of silicon on the Ni(110) surface. Gibbs free energies were compared for 0-4 silicon atoms embedded into the top layer in a 2×2 unit for the Ni(110) surface. When a half monolayer of Si was embedded, the $p(1 \times 2)$ structure had the lowest energy, and the $c(2 \times 2)$ structure had only 13 meV/ 1×1 higher energy than the $p(1 \times 2)$

structure. By extending to a 4×2 unit, the $c(4 \times 2)$ structures had almost the same energy with the $p(1 \times 2)$ structure. Alternating Si-Ni chains along the close-packed [1-10] row play an essential role to stabilize these structures. Si and Ni are alternatively aligned in separate [1-10] rows forming a $p(2 \times 1)$ structure, which had 276 meV/ 1×1 higher energy than the $p(1 \times 2)$ structure. For the $p(2 \times 1)$ structure, unique one-dimensional electronic bands derived by the Si-3s states were formed along the [1-10] direction. (This is identical to the abstract that will appear in the section of Applied Physics and Electronics Engineering).

Initial surface silicidation on Ni(110)

Tsuneo FUKUDA, Ippei KISHIDA and Kenji UMEZAWA

Surface Science, 659, pp.1-4 (2017).

Initial silicide formation on a Ni(110) surface was studied by scanning tunneling microscopy (STM) in an ultrahigh vacuum. Less than 0.5 ML of Si deposition initiated a Si-Ni mixed layer by displacing substrate Ni, and dark sites were formed in the STM images. A 0.5 ML-Si deposited surface showed that Si and Ni were alternately aligned in a close-packed row whereas Si pairs aligned along the $\langle 110 \rangle$ direction forming $p(1 \times 2)$, obliquely aligned forming $c(2 \times 2)$, or even straightly-and-obliquely aligned forming $c(4 \times 2)$ superstructures. A first-principles total energy calculation showed that the $p(1 \times 2)$ and $c(4 \times 2)$ structures had almost the same energy while the $c(2 \times 2)$ structure gave 13 meV/ 1×1 higher energy. Because a Si-Si bond in the close-packed row is energetically unfavorable, Si deposition of more than 0.5 ML did not further replace the substrate Ni, but silicide islands were nucleated along with a trench structure. (This is identical to the abstract that will appear in the section of Applied Physics and Electronics Engineering).

Effects of Ultrasonic Waves during Resin Impregnation on the Mechanical Properties of Unidirectional Composite Materials

Yasunari KURATANI, Aya MIKI, Norimichi NANAMI, Hayato NAKATANI and Hiroyuki HAMADA

Open Journal of Composite Materials, Vol.8, No.1, pp.1-10 (2018).

Effects of ultrasonic vibrations on mechanical properties of fiber reinforced plastics were investigated during molding resin impregnation process in vacuum assisted resin transfer molding. The vacuum bag including the preformed each non-crimp fabrics (carbon and glass fibers) was placed in a water bath of an ultrasonic wave generator during resin impregnation. The mechanical properties of the laminates were evaluated through the mechanical strength tests and scanning electron microscope (SEM) observation. The results revealed that ultrasonic waves improved transverse tensile, flexural, interlaminar shear, and compressive strengths of the carbon fiber (CF) laminates and interlaminar shear and compressive strengths of the glass fiber (GF) laminates. It was found from SEM observation that the fracture modes of the CF and GF laminates processed using ultrasonic waves were resin fracture. Accordingly, the adhesion of the fiber/resin interface was improved by oscillating ultrasonic vibration during resin impregnation, leading to an increase of the interface strength.

Evaluation of Flexural Properties of the U-shape Composite Spring

Katsuyuki HARA, Toshikazu UCHIDA, Yosuke WATANABE, Norimichi NANAMI, Hayato NAKATANI and Hiroyuki HAMADA

Procedia Manufacturing, Vol.26, pp.530-536 (2018).

CFRP (carbon fiber reinforced plastics) which provides high specific strength/stiffness is adopted in assistive products such as orthosis for relieving the physical burden of patients. The orthosis needs the flexible configuration of articulations like walking of normal subjects. Since the CFRP autoclave method is suitable for molding complex shape parts, a structural component containing a partially curved region such as U-shape can be integrally molded by the method. Flexibility characteristics are added to a structural component without an increase in the number of parts. In this study, the flexibility of CFRP was evaluated for embedded light and durable springs into orthosis. First, three-point bending tests of the flat laminate were performed to assess the advantage of CFRP used as spring materials. Second, the flexural properties and fracture mechanism of a U-shape spring were investigated in comparison with the results of the flat laminate. The study confirmed the advantage of CFRP employed as a spring material.

Large Deformation Behavior of Angle-Plied CFRP Laminates by inserting PA Mesh as Interlayer

Kazuki UEDA, Hayato NAKATANI and Katsuhiko OSAKA

Proc. 12th Canada-Japan Workshop on Composites, Takayama, Japan, July 4-7, paper ID: 024 (2018).

When angle-plied CFRP laminates which do not contain 0° fibers are loaded in tension, intralaminar matrix cracks are developed in all plies and followed by interlaminar delamination, and then this leads to rupture of laminates at relatively low strain. Some studies found that greater fracture strain can be achieved by using thin plies since

matrix crack is suppressed by the constraint effect. However using thin plies is costly because stacking number increases. The present study applies polyamide (PA) mesh which can improve interlaminar fracture toughness by inserting them between plies. This study aims greater fracture strain in angle-ply laminates by suppressing interlaminar delamination between plies by inserting PA mesh. Damage behavior in two kinds of angle-ply CFRP laminates such as $[45_2/-45_2]_S$ and $[45_2/PA/-45_2]_S$ are evaluated by tensile tests. It is found that by inserting PA mesh strength and maximum strain improved compared to the laminates without PA mesh. An X-ray observation for the specimen just before tensile rupture reveals that interlaminar delamination is not induced though there are many intralaminar matrix cracks in the laminates with PA mesh. From these experimental results, it is assumed that even if matrix cracking occurred, it does not progress to interlaminar delamination by inserting PA mesh and these phenomena lead to greater fracture strain due to accumulation of damage.

Estimation of R-curve for Mode II Interlaminar Fracture Toughness by using CFRP Laminates with Fibre Discontinuities

Takaaki WARABINO, Hayato NAKATANI and Katsuhiko OSAKA

Proc. 12th Canada-Japan Workshop on Composites, Takayama, Japan, July 4-7, paper ID: 025 (2018).

When CFRP plates of structures with complicated geometry are fabricated by using prepregs, fiber discontinuities remain in the laminates since some slits or cuts are introduced in prepregs before lamination. The CFRP laminates with fibre discontinuities show tensile failure at much lower stress due to crack originated from the discontinuities. Previous studies have shown that the stress at which crack propagation from fiber discontinuity occurs can be predicted by using mode II interlaminar fracture toughness G_{II} . The present study aims to reverse this methodology in order to estimate the R curve of mode II interlaminar fracture toughness G_{II} from tensile test of CFRP laminates with fiber discontinuity. In the technique we suggest here there is no need to perform stabilized ENF tests that require a variety of controls. Tensile tests for CFRP laminates that contain fiber discontinuous dispersed at an arbitrary interval are carried out. Relations between the obtained fracture stress and the interval are converted into that between critical energy release rate (CERR) in mode II and crack extension that can be compared with R-curve obtained by ENF tests. As a result, although mismatch are found in the initial region of R-curve a.k.a. G_{IIC} , CERR matched with R-curve during crack propagation, which is the region where the change of G_{II} converges as G_{IIR} .

Electroless Copper Plating Process by Applying Alternating One-Side Air Stirring Method for High-Aspect-Ratio Through-Holes

H. KANEMOTO, T. KAWAMURA, H. SUZUKI, T. MIYAZAKI, H. MOZUMI and Y. KANEKO

J. Electrochem. Soc., 164 (12), pp.D771-D777 (2017).

A new electroless copper plating process, namely, an alternating one-side air stirring method, was studied to improve the throwing power of high-aspect-ratio through-holes in multilayer printed wiring boards. The throwing power can even be improved for through-holes of a 40-aspect ratio under an appropriate flow velocity of the solution because the generation of differential-pressure between the front and the back of the board enhances supplying the solution into the through-holes. The necessary flow velocity can be estimated by considering the consumption rate of copper ions in a through-hole and calculating it on the basis of Bernoulli's and Hagen-Poiseuille's equation.

Evaluation of Microscopically Anisotropic Deformation Fields of Polycrystalline Pure Copper using Digital Image Correlation Method

M. UCHIDA, A. TANIGUCHI and Y. KANEKO

Proc. ISEMI2, Paper No. 035, 5pages (2017).

Microscopic deformation of the polycrystalline metal is characterized by anisotropic deformation depending on the crystalline orientation of grains and the interaction with adjacent grain. The estimation of the slip deformation under the complex stress state in the polycrystalline structure can provide an important information to understand the deformation mechanisms of crystalline material. In the present study, the evaluation method of slip deformation in the microscopic local region is proposed by coupling the Digital Image Correlation (DIC) Method and the crystalline plasticity theory. Microscopic strain field and slip deformation of the polycrystalline pure copper under uniaxial tension were evaluated using the proposed method. The nonuniform deformation in the crystal grain was firstly evaluated by DIC. Then, the slip deformation for all grains and all slip systems were estimated using proposed method. Series of the experimental result clarified that the multiple slip deformation occurred for almost crystal grain regardless of the degree of the total slip in FCC metal.

Evaluation of Deformation Behavior of Hydrogel on Uniaxial Tensile Test using Digital Image Correlation

K. SUZUKI, M. UCHIDA, Y. KANEKO, D. OKUMURA, H. TANAKA and S. IDA
Proc. ISEM12, Paper No. 059, 5pages (2017).

Hydrogel materials, which have been employed for a wide range of biomedical applications, contain water within a three-dimensional network of polymer chains. Since this material is extremely soft as compared with other engineering materials, it is necessary to establish a mechanical test method suitable to accurately evaluate the deformation behavior of such soft materials. In this study, we evaluated the development of strain field and the relationships between true stress and true strain using digital image correlation (DIC) method. It was confirmed that tensile strain was uniformly distributed, and tensile strength and elongation of hydrogel specimens decrease with increasing the amount of cross-linking.

Basic Verification of an Extended Flory-Rehner Model using Polyacrylamide Hydrogels

D. OKUMURA, S. SHIMIZU, S. IDA, M. UCHIDA and H. TANAKA

J. JSCME, 17, pp.53-58 (2017) (in Japanese).

In this study, we perform the basic verification of an extended Flory-Rehner (F-R) model using experimental data of polyacrylamide hydrogels. The equilibrium free swelling and subsequent uniaxial tensile tests are experimentally performed to determine two scaling exponents characterizing the extended F-R free energy function for polymeric gels. To show the ability of the two scaling exponents, the Ogden model is compared as the different strain energy in the F-R model. The parameter set in the Ogden model cannot uniquely be determined to represent the swelling effects on stress-stretch responses while the extended F-R model can predict them well only with one scaling exponent. In addition, the other scaling exponent has a strong interaction with the Flory-Huggins interaction parameter.

Experimental Modeling of Nonuniform Deformation in Finite Volume Evaluation Region of Heterogeneous Material

M. UCHIDA and Y. KANEKO

Heliyon, 4, e00578, 21pp., (2018).

The objective of the present study is to establish the experimental modeling process of the nonuniform deformation behavior of heterogeneous materials. For this purpose, the constant stress moment, which is the work conjugate quantity of the constant strain gradient for the finite volume evaluation region, is introduced. The proposed stress moment can be evaluated from the stress field. The extended constitutive equation that relates the strain, stress, strain gradient, and stress moment is then formulated to predict the nonuniform deformation behavior of heterogeneous materials. In order to confirm that the proposed method is appropriate to represent the nonuniform deformation, finite element method (FEM) simulations of bending of macroscopically and microscopically heterogeneous materials were performed. The proposed method could predict the bending deformation of macroscopically heterogeneous material as precisely as the homogeneous case because the distribution of the heterogeneity is introduced in the extended constitutive equation. A bending simulation of a laminated cantilever was then performed using the extended constitutive equation for the microscopically heterogeneous material. The proposed method was capable of representing the analytically verified size-dependent bending deformation of the laminated cantilever.

Estimation of Slip Deformation of Polycrystalline Pure Copper using Digital Image Correlation Method and Crystalline Plasticity Theory

M. UCHIDA, A. TANIGUCHI and Y. KANEKO

Advanced Experimental Mechanics, 3, pp.135-140, (2018).

The estimation of the slip deformation under the multiaxial stress state in the polycrystalline structure, which is caused by highly anisotropic deformation in microscopic scale of material, can provide an important information to understand the deformation mechanisms of crystalline material. In the present study, an evaluation method of slip deformation in the microscopic local region is proposed by coupling the Digital Image Correlation (DIC) Method and the crystalline plasticity theory. Microscopic strain field and slip deformation of the polycrystalline pure copper under uniaxial tension were evaluated using the proposed method. The nonuniform deformation in the crystal grain was firstly evaluated by DIC. Then, the slip deformation for all grains and all slip systems were estimated using the proposed method. Although the initial crystalline orientations were similar for different grains, the active slip systems for the grains did not coincide due to the interaction with surrounding grains. The multiple slip deformation occurred for almost crystal grain regardless of the degree of the total slip in the FCC metal.

Effects of Two Scaling Exponents on Biaxial Deformation and Mass Transport of Swollen Elastomers

D. OKUMURA, M. MIZUTANI, H. TANAKA and M. UCHIDA

Int. J. Mech. Sci., 146-147, pp.507-516, (2018).

In this study, we investigate the effects of two scaling exponents on the biaxial deformation and mass transport of swollen elastomers. Two scaling exponents are included in an extended version of the Flory–Rehner model (Okumura et al., *J. Mech. Phys. Solids*, 2016); two scaling exponents are used to adjust the swelling effects on the Young's modulus and osmotic pressure of swollen elastomers, resulting in the ability to predict swelling-induced strain softening under uniaxial tensile loading. It is found that when biaxial tensile loading is given under stress control, strain softening is accelerated by increasing the biaxial stress ratio, while under strain control, the responses become more complicated, which can be interpreted by considering that Poisson's ratio at equilibrium free swelling can take negative values depending on the two scaling exponents. Further, the effect of the two scaling exponents on mass transport is discussed by analyzing the swelling kinetics of a gel layer constrained on a rigid substrate.

Transient Mechanical Relaxation Behavior of Glassy Polymers Subjected to A Stepwise Change of Compression Rate

Shin'ya YOSHIOKA and Ryuki MASUDA

Nihon Reoroji Gakkaishi (J. Soc. Rheol., Jpn), Vol.45, pp.235-241 (2017) (in Japanese).

Transient single relaxation time τ_{SS} of glassy polymers was evaluated by using a nonlinear single relaxation model during uniaxial compression processes in which the compression rate changed stepwise from $\dot{\epsilon}_{n1}$ to $\dot{\epsilon}_{n2}$. After the change of compression rate, stress showed an undershoot ($\dot{\epsilon}_{n1} > \dot{\epsilon}_{n2}$) or an overshoot ($\dot{\epsilon}_{n1} < \dot{\epsilon}_{n2}$) before reaching the same value as the constant-rate compression at $\dot{\epsilon}_{n2}$. After a decrease of compression rate, τ_{SS} increased monotonously to the steady value at $\dot{\epsilon}_{n2}$. When the compression rate increased, τ_{SS} showed a discontinuous increase right after the acceleration, then steeply decreased to the steady value at $\dot{\epsilon}_{n2}$. Transient values of τ_{SS} after a decrease of compression rate as a function of the nonlinear flow rate $\dot{\epsilon}_{\dot{\eta}}$ of the dashpot in the model were almost the same function as the steady value of τ_{SS} , which was almost inversely proportional to $\dot{\epsilon}_{\dot{\eta}}$. After an increase of compression rate and also in the transient state under the constant rate compression, $\tau_{SS}(\dot{\epsilon}_{\dot{\eta}})$ showed a higher value than those in the steady flow state. This observation indicates that, when glassy structures are getting unstable due to deformation, the nonlinear flow requires larger stress than the steady flow.

Transient Variation of Dynamic Viscoelasticity of Uniaxially Stretched Glassy Poly(methyl methacrylate) after Abrupt Change of Tensile Rate

Shin'ya YOSHIOKA and Hiroaki MATSUMOTO

Nihon Reoroji Gakkaishi (J. Soc. Rheol., Jpn), Vol.46, pp.185-187 (2018) (in Japanese).

Variation of dynamic shear modulus, $G^* = G' + iG''$, was measured for glassy poly(methyl methacrylate) (PMMA) during uniaxial stretching processes where the tensile rate changed stepwise. Under the condition of constant-rate stretching, it is known that G' and G'' gradually change to their steady values in the post-yield range of strain, and that the change occurs strongly at a higher tensile rate, indicating strain-induced changes in glassy structures. After a change of tensile rate, G' as well as G'' varied monotonously from their values at the initial tensile rate to those at the final rate in a strain range where the uniaxial stress σ exhibited transient responses to the tensile rate change. The observed variation of G' and G'' simply indicates that, after an abrupt change of tensile rate, structures of the glass successively change from those corresponding to initial tensile rate to final rate.

Applied Physics and Electronics

Ultrafast Dynamics of Coherent Optical Phonon Correlated with the Antiferromagnetic Transition in a Hexagonal YMnO₃ Epitaxial Film

Takayuki HASEGAWA, Norifumi FUJIMURA and Masaaki NAKAYAMA

Applied Physics Letters, Vol. 111, 192901 (5 pages) (2017)

We report on the observation of the coherent optical phonon in a hexagonal YMnO₃ epitaxial film using a reflection-type pump-probe technique at various temperatures, excitation powers, and energies. We detected an oscillatory structure with a frequency of ~5.1 THz, which is assigned to the coherent optical phonon with A₁ symmetry, in a time-domain signal. It was found that the coherent optical phonon can be observed at temperatures from 10 K to room temperature, while the oscillation amplitude markedly decreases with an increase in temperature around ~70 K corresponding to the Néel temperature. The temperature dependence of the oscillation amplitude indicates that the coherent optical phonon is sensitive to the spin-lattice coupling connected with the antiferromagnetic transition.

DOI: 10.1063/1.5003269

Screening Effects of Photogenerated Carriers on Terahertz Radiation from Coherent GaAs-like Longitudinal Optical Phonons in (11 \bar{n})-Oriented GaAs/In_{0.1}Al_{0.9}As Strained Multiple Quantum Wells

Hideo TAKEUCHI, Souta ASAI and Masaaki NAKAYAMA

Journal of Physics: Conference Series, Vol. 906, 012020 (4 pages) (2017)

We investigated terahertz radiation from coherent GaAs-like longitudinal optical (LO) phonons in (11 \bar{n})-oriented GaAs/In_{0.1}Al_{0.9}As strained multiple quantum wells for clarifying the screening effects of photogenerated carriers. We observed the intense quasi-monochromatic terahertz wave from the coherent GaAs-like LO phonon, which originates from the initial polarization enhanced by the strong piezoelectric field. The intensity of the coherent GaAs-like LO-phonon band exhibited a saturation behavior as the pump power was increased. We evaluated the saturation behavior in terms of excitation efficiency of the terahertz wave from the coherent GaAs-like LO phonon using the parameter of unit-power intensity. From the pump-power dependence of the unit-power intensity, we conclude that the screening effect of high density photogenerated carriers on the piezoelectric field causes saturation of the terahertz-wave intensity from the coherent GaAs-like LO phonon.

DOI: 10.1088/1742-6596/906/1/012020

Bayesian Spectroscopy of Admixed Photoluminescence Spectra with Exciton, Biexciton and Electron Hole Droplet States in a GaAs/AlAs Type-II Superlattice

Kazanori IWAMITSUA, Yoshiaki FURUKAWA, Masaaki NAKAYAMA, Masato OKADA and Ichiro AKAI

Journal of Luminescence, Vol. 197, pp. 18-22 (2018)

We have analyzed a photoluminescence (PL) spectrum in a GaAs/AlAs type-II superlattice and have statistically confirmed stable existence of an electron-hole droplet (EHD) state. Although the PL spectrum consists of spectral components of the EHD, exciton and biexciton states, we have succeeded in decomposing the admixed spectrum into the respective components. In addition, posterior probability distributions of spectral parameters have been obtained in all spectral components from 30,000 times samplings through a replica exchange Monte Carlo method. By using mean values of their posterior probabilities, the PL spectrum can be completely reproduced by the sum of these spectral components. The stability energy of the EHD state has a sharp distribution in its posterior probability and has been confirmed to be enough larger than the ambient thermal energy. This fact is a strong evidence for the stable formation of the EHD state in the GaAs/AlAs type-II superlattice.

DOI: 10.1016/j.jlum.2018.01.002

Quantitative Evaluation of Light-Matter Interaction Parameters in Organic Single-Crystal Microcavities

Takumi NISHIMURA, Kenichi YAMASHITA, Shun TAKAHASHI, Takeshi YAMAO, Shu HOTTA, Hisao YANAGI and Masaaki NAKAYAMA

Optics Letters, Vol. 43, pp. 1047-1050 (2018)

Investigation of physics on light-matter interaction and strong coupling formation in organic microcavities is important to characterize the device structure enabling efficient room-temperature polariton condensation. In this study, we evaluate quantitatively the light-matter interaction parameters for three types of organic single-crystal microcavities and discuss the effects of microcavity structures on the strong coupling formation. We found that

improvement in cavity quality factor causes a reduction in the photon damping constant, which results in an increase in the Rabi splitting energy. Moreover, when we used a metal thin film as the cavity mirror, it was revealed that the exciton damping became 30 times stronger than that in a dielectric mirror cavity. These experimental findings are very intriguing to achieve low-threshold or electrically pumped organic polariton devices.

DOI: 10.1364/OL.43.001047

Temperature Effect on the Dispersion Relation of Nonequilibrium Exciton-Polariton Condensates in a CuBr Microcavity

Masaaki NAKAYAMA and Kazuki TAMURA

Journal of the Physical Society of Japan, Vol. 87, 053701 (4 pages) (2018)

We observed the dispersion relation of nonequilibrium exciton-polariton condensates at 10 and 80 K in a CuBr microcavity using angle-resolved photoluminescence spectroscopy. The dispersion relation consists of dispersionless and dispersive parts in small and large in-plane wave vector regions, respectively. It was found that the cutoff wave vector of the dispersionless region at 80 K is larger than that at 10 K. From quantitative analysis of the dispersion relation based on a theory for nonequilibrium condensation, we show that the larger cutoff wave vector results from an increase in the effective relaxation rate of the Bogoliubov mode in equilibrium condensation; namely, a degree of nonequilibrium at 80 K is higher than that at 10 K.

DOI: 10.7566/JPSJ.87.053701

Biexciton Relaxation Associated with Dissociation into a Surface Polariton Pair in Semiconductor Films

Yasuyoshi MITSUMORI, Shimpei MATSUURA, Shoichi UCHIYAMA, Kentarao SAITO, Keiichi EDAMATSU, Masaaki NAKAYAMA and Hiroshi AJIKI

Physical Review B, Vol. 97, 155303 (6 pages) (2018)

We study the biexciton relaxation process in CuCl films ranging from 6 to 200 nm. The relaxation time is measured as the dephasing time and the lifetime. We observe a unique thickness dependence of the biexciton relaxation time and also obtain an ultrafast relaxation time with a timescale as short as 100 fs, while the exciton lifetime monotonically decreases with increasing thickness. By analyzing the exciton-photon coupling energy for a surface polariton, we theoretically calculate the biexciton relaxation time as a function of the thickness. The calculated dependence qualitatively reproduces the observed relaxation time, indicating that the biexciton dissociation into a surface polariton pair is one of the major biexciton relaxation processes.

DOI: 10.1103/PhysRevB.97.155303

Ultrafast Dynamics of Polariton Cooling and Renormalization in an Organic Single-Crystal Microcavity under Nonresonant Pumping

Kenichi YAMASHITA, Uyen HUYNH, Johannes RICHTER, Lissa EYRE, Felix DESCHLER, Akshay RAO, Kaname GOTO, Takumi NISHIMURA, Takeshi YAMAOKA, Shu HOTTA, Hisao YANAGI, Masaaki NAKAYAMA and Richard H. FRIEND

ACS Photonics, Vol. 5, pp. 2182-2188 (2018)

Microcavity systems with organic luminescent materials have a hot prospect for room-temperature cavity-polariton devices. The polariton dispersion relation of organic microcavities is significantly different from that of inorganic microcavities due to the strong localization of Frenkel excitons. Also photoexcited particles will undergo a different cooling mechanism until they reach the polariton ground state. In the characterization of efficient polariton condensates, therefore, the polariton cooling dynamics as well as the kinetics of the polariton eigenstate should be measured. Here we present experimental studies on ultrafast dynamics of cavity polaritons in an organic single-crystal microcavity under nonresonant pumping. In time-resolved photoluminescence measurements we observed, for the first time, an ultrafast dynamics of stimulated cooling of the organic cavity polariton. Transient transmission measurement enabled us to investigate the detailed renormalization dynamics of the polariton eigenstate. The results clearly demonstrated the prospect of organic microcavities for room-temperature polaritonic devices.

DOI: 10.1021/acsp Photonics.8b00041

Evidence for Spatial Propagation of Photon-like Polaritons Generated by Exciton-Exciton Scattering in a GaAs/AlAs Multiple-Quantum-Well Structure

Yoshiaki FURUKAWA and Masaaki NAKAYAMA

Journal of the Physical Society of Japan, Vol. 87, 094718 (6 pages) (2018)

We have investigated the polariton characteristics of the photoluminescence (PL) due to exciton-exciton

scattering at 10 K in a GaAs/AlAs multiple-quantum-well structure with the use of spatially-resolved PL spectroscopy. We found that the PL band from the exciton–exciton scattering, the so-called P emission, is detected only at spots along a sample edge which is spatially separated from an excitation spot. In contrast, the PL bands attributed to the exciton and biexciton were observed only at the excitation spot. Because the exciton–exciton scattering occurs at the excitation spot, the appearance of the spatially-separated P-emission spot demonstrates that the photon-like lower polariton, which is the final state of the exciton–exciton scattering process, propagates along the interface, leading to conversion to a photon. The spectral shape of the P-PL band detected at the spatially-separated spot exhibits a fringe pattern, which is quantitatively explained by the Fabry–Pérot interference originating from the spatial separation of the P-emission and excitation spots.

DOI: 10.7566/JPSJ.87.094718

Quick Synthesis of Water-Soluble, Luminescent ZnTe Nanoparticles by Hydrothermal Technique

Hang-Beom BU and DaeGwi KIM

Chem. Lett. Vol. 47, pp. 152–155 (2018).

We first report the successful quick synthesis of water-soluble ZnTe nanoparticles (NPs) by a hydrothermal technique. The use of *N*-acetyl-L-cysteine as a ligand and adjustment of the precursor solution's pH to 10.3 ± 0.2 are believed to play key roles in the quick synthesis of ZnTe NPs with a high photoluminescence quantum efficiency of 15%. The reaction time is at least 140-fold quicker than the previous works.

DOI:10.1246/cl.170917

Experimental Verification of Förster Energy Transfer and Quantum Resonance Between Semiconductor Quantum Dots

DaeGwi Kim, TaeGi Lee, Yong-Shin Lee, and Taichi Watanabe

Current Appl. Phys. Vol. 18, pp. S14-S20 (2018).

Quantum dot (QD) superlattices have the potential to provide new optical properties and functions based on interactions between adjacent QDs. Two types of interactions occur between the QDs: energy transfer (ET) from small-sized QDs to large QDs and resonant coupling between QDs with equal eigenenergies. Since ET and resonant coupling strongly depend on the distance between QDs, it is critical to precisely control the distance to understand the interaction mechanism. In this review, we describe that the distance between QDs can be controlled with an accuracy of 1 nm by a layer-by-layer method and further explain the mechanisms of ET and resonant coupling between adjacent QDs.

DOI:10.1016/j.cap.2017.11.012

Surface Modification Effects on Defect-Related Photoluminescence in Colloidal CdS Quantum Dots

TaeGi Lee, Kunio SHIMURA, and DaeGwi KIM

Phys. Chem. Chem Phys. Vol. 20, pp. 11954-11958 (2018).

We investigated the effects of surface modification on the defect-related photoluminescence (PL) band in colloidal CdS quantum dots (QDs). A size-selective photoetching process and a surface modification technique with a Cd(OH)₂ layer enabled the preparation of size-controlled CdS QDs with high PL efficiency. The Stokes shift of the defect-related PL band before and after the surface modification was ~ 1.0 eV and ~ 0.63 eV, respectively. This difference in the Stokes shifts suggests that the origin of the defect-related PL band was changed by the surface modification. Analysis by X-ray photoelectron spectroscopy revealed that the surface of the CdS QDs before and after the surface modification was S rich and Cd rich, respectively. These results suggest that Cd-vacancy acceptors and S-vacancy donors affect PL processes in CdS QDs before and after the surface modification, respectively.

DOI:10.1039/C7CP07812A

Linear stability of periodic three-body orbits with zero angular momentum and topological dependence of Kepler's third law: a numerical test

Veljko DMITRASINOVIC, Ana HUDOMAL, Mitsuru SHIBAYAMA and Ayumu SUGITA

Journal of Physics A: Mathematical and Theoretical, 51, 315101 (2018)

We test numerically the recently proposed linear relationship between the scale-invariant period $T_{s.i.} = T|E|^{3/2}$, and the topology of an orbit, on several hundred planar Newtonian periodic three-body orbits. Here T is the period of an orbit, E is its energy, so that $T_{s.i.}$ is the scale-invariant period, or, equivalently, the period at unit energy $|E|=1$. All of these orbits have vanishing angular momentum and pass through a linear, equidistant configuration at least once. Such orbits are classified in ten algebraically well-defined sequences. Orbits in each sequence follow an approximate linear dependence of $T_{s.i.}$, albeit with slightly different slopes and intercepts. The orbit with the

shortest period in its sequence is called the 'progenitor': six distinct orbits are the progenitors of these ten sequences. We have studied linear stability of these orbits, with the result that 21 orbits are linearly stable, which includes all of the progenitors. This is consistent with the Birkhoff–Lewis theorem, which implies existence of infinitely many periodic orbits for each stable progenitor, and in this way explains the existence and ensures infinite extension of each sequence.

Electrical Characteristics of Solder-Free SiC Die/Metal Foil/AlN Plate Junctions Fabricated Using Surface Activated Bonding

Sho MORITA, Jianbo LIANG, and Naoteru SHIGEKAWA

Extended Abstracts of Americas International Meeting on Electrochemistry and Solid State Science (AiMES), 961 (2018).

Atomistic Structure of Low-Resistance Si/GaAs Heterointerfaces Fabricated By Surface-Activated Bonding at Room Temperature

Yutaka OHNO (Univ. of Tohoku), Hideto YOSHIDA (Univ. of Osaka), Seiji TAKEDA (Univ. of Osaka), Liang JIANBO, and Naoteru SHIGEKAWA

Extended Abstracts of Americas International Meeting on Electrochemistry and Solid State Science (AiMES), 968 (2018).

Investigation of Residual Strain in 4H-SiC/Si Heterostructures Fabricated By Surface Activated Bonding

Jianbo LIANG, Yan ZHOU (Univ. of Bristol), Shoji YAMAJO, Martin KUBALL (Univ. of Bristol), Manabu ARAI (New Japan Radio Co. Ltd.), and Naoteru SHIGEKAWA

Extended Abstracts of Americas International Meeting on Electrochemistry and Solid State Science (AiMES), 975 (2018).

Room-temperature Direct Bonding of Diamond and Al

Jianbo LIANG, Shoji YAMAJO, Martin KUBALL (Univ. of Bristol), and Naoteru SHIGEKAWA

Scripta Materialia 159, 58 [4 pages] (2018)

The direct bonding of diamond and Al substrates was achieved by surface activated bonding at room temperature. The interfacial structure of the diamond/Al bonding interface with annealing at different temperatures was investigated under in-situ annealing in a transmission electron microscope (TEM). An amorphous layer with a thickness of about 4 nm was present at the bonding interface without annealing, the thickness of the amorphous layer decreased with increasing annealing temperature, the amorphous layer vanished after annealing at 600 °C. No structural defects were observed at the bonding interface with annealing at different temperatures. The sp²/(sp² + sp³) ratio in the diamond near the interface estimated from the X-ray photoemission spectra increased from 3.4 % to 26.6 % after the irradiation of Ar fast beam that is an essential process to activate the surface of the bonding materials, and decreased from 26.6 % to 1.2 % after annealing at 600 °C, which should be predominantly attributable to the diamond-graphite conversion.

The combination of Diamond devices with Si LSI by surface activated bonding

Jianbo LIANG, Satoshi Masuya (Univ. of Saga), Makoto Kasu (Univ. of Saga), and Naoteru SHIGEKAWA

Extended Abstracts of 12th New Diamond and Nano Carbons Conference, pp. 36 (2018).

Room-temperature direct bonding of diamond to aluminum

Jianbo LIANG, Shoji YAMAJO, Martin KUBALL (Univ. of Bristol), and Naoteru SHIGEKAWA

Extended Abstracts of 29th International Conference on Diamond and Carbon Materials, O4.1 (2018).

GaAs/indium tin oxide/Si bonding junctions for III-V-on-Si hybrid multijunction cells with low series resistance

Naoteru SHIGEKAWA, Tomoya HARA, Tomoki OGAWA, Jianbo LIANG, Takefumi KAMIOKA (Toyota Technological Institute), Kenji ARAKI (Toyota Technological Institute), and Masafumi YAMAGUCHI (Toyota Technological Institute)

IEEE J. Photovoltaics 8, 579 [8 pages] (2018)

Effects of GaAs/indium tin oxide (ITO)/Si junctions on III-V-on-Si multijunction solar cells are examined by fabricating and characterizing InGaP/GaAs/ITO/Si triple-junction (3J) solar cells. The 3J cells are fabricated by evaporating ≈100-nm-thick ITO films on the surfaces of Si bottom cells and bonding the InGaP/GaAs double-junction (2J) subcells and the ITO films using surface activated bonding technologies at room temperature.

The current-voltage characteristics of 3J cells with p^+ -GaAs/ITO/ n^+ -Si and n^+ -GaAs/ITO/ n^+ -Si junctions are compared with those of an InGaP/GaAs/Si 3J cell. The parasitic resistance of the respective 3J cells is estimated by analyzing their characteristics in the dark. We find that the 3J cell with an n^+ -GaAs/ITO/ n^+ -Si junction shows the lowest parasitic resistance, which is the origin of its lowest differential resistance at the open-circuit voltage and highest fill factor. This means that n^+ -GaAs/ITO/ n^+ -Si junctions are promising for improving the performances of III-V-on-Si hybrid multijunction cells. The spectral response characteristics of these cells indicate that the thickness of the ITO films must be optimized.

Electrical properties of Al foil/n-4H-SiC Schottky junctions fabricated by surface-activated bonding

Sho MORITA, Jianbo LIANG, Moeko MATSUBARA (Toyo Aluminum K. K.), Marwan DHAMRIN (Toyo Aluminum K. K.), Yosataka NISHIO (Toyo Aluminum K. K.), and Naoteru SHIGEKAWA

Jpn. J. Appl. Phys. 57, 02BE01 [5 pages] (2018)

We fabricate 17- μm -thick Al foil/n-4H-SiC Schottky junctions by surface-activated bonding. Their current-voltage and capacitance-voltage characteristics are compared with those of Schottky junctions fabricated by evaporating Al layers on n-4H-SiC epilayers. We find that the ideality factor of Al foil/SiC junctions is larger than that of conventional junctions, which is due to the irradiation of the fast atom beam (FAB) of Ar. The ideality factor of Al foil/SiC junctions is improved by annealing at 400 °C. We also find that the Schottky barrier height is increased by FAB irradiation, which is likely to be due to the negative charges formed at SiC surfaces.

Electrical properties of GaAs//indium tin oxide/Si junctions for III-V-on-Si hybrid multijunction cells

Tomoya HARA, Tomoki OGAWA, Jianbo LIANG, Kenji ARAKI (Toyota Technological Institute), Takefumi KAMIOKA (Toyota Technological Institute), and Naoteru SHIGEKAWA

Jpn. J. Appl. Phys. 57, 08RD05 [6 pages] (2018)

The electrical properties of GaAs//indium tin oxide (ITO)/Si junctions fabricated by surface-activated bonding (SAB) are investigated with emphasis on their dependence on the temperature of postbonding annealing. The current-voltage (I-V) characteristics of n^+ -GaAs//ITO/ p^+ -Si and n^+ -GaAs//ITO/ n^+ -Si junctions without annealing are linear. Those of p^+ -GaAs//ITO/ p^+ -Si and p^+ -GaAs//ITO/ n^+ -Si junctions without annealing are nonlinear. Although the interface resistance of all the junctions increases with increasing annealing temperature, the resistances of the respective junctions after the annealing at 400 °C are still smaller than the series resistance of the actual SAB-based InGaP/GaAs//Si hybrid triple-junction cells ($\sim 4\Omega\text{cm}^2$). The n^+ -GaAs//ITO/ n^+ -Si junction reveals the lowest resistance among the investigated junctions after annealing. These results demonstrate that GaAs//ITO/Si junctions with an ITO intermediate layer could be effective for reducing series resistance in hybrid multijunction cells.

Intrinsic microstructure of Si/GaAs heterointerfaces fabricated by surface-activated bonding at room temperature

Yutaka OHNO (Univ. of Tohoku), Hideto YOSHIDA (Univ. of Osaka), Seiji TAKEDA (Univ. of Osaka), Liang JIANBO, and Naoteru SHIGEKAWA

Jpn. J. Appl. Phys. 57, 02BA01 [3 pages] (2018)

The intrinsic microstructure of Si/GaAs heterointerfaces fabricated by surface-activated bonding at room temperature is examined by plane-view transmission electron microscopy (TEM) and cross-sectional scanning TEM using damage-free TEM specimens prepared only by mechanochemical etching. The bonded heterointerfaces include an As-deficient crystalline GaAs layer with a thickness of less than 1 nm and an amorphous Si layer with a thickness of approximately 3 nm, introduced by the irradiation of an Ar atom beam for surface activation before bonding. It is speculated that the interface resistance mainly originates from the As-deficient defects in the former layer.

Analysis of effects of interface-state charges on the electrical characteristics in GaAs/GaN heterojunctions

Shoji Yamajo, Jianbo LIANG, and Naoteru SHIGEKAWA

Jpn. J. Appl. Phys. 57, 02BE02 [5 pages] (2018)

Electrical properties of p^+ -GaAs/n-GaN and n^+ -GaAs/n-GaN junctions fabricated by surface-activated bonding are investigated by measuring their capacitance-voltage (C-V) and current-voltage (I-V) characteristics. The difference between their flat-band voltages (0.17 eV), which are extracted from C-V measurements, disagrees with the ideal value (1.52 V), suggesting that the Fermi level should be pinned at the bonding interface. The C-V characteristics of the two junctions are calculated by assuming that the Fermi level is pinned at the interface. The measured C-V characteristics quantitatively agree with modeled ones obtained by assuming that the interface

state density and conduction band discontinuity are $1.5 \times 10^{14} \text{cm}^{-2} \text{eV}^{-1}$ and 0.63 eV, respectively. The effective heights of barriers at interfaces, which we estimate by analyzing dependences of I–V characteristics on the ambient temperature, are $\sim 10\text{--}20$ meV for the two junctions at room temperature. This suggests that the transport of carriers is dominated by tunneling through interface states.

Transport characteristics of minority electrons across surface-activated-bonding based p-Si/n-4H-SiC heterointerfaces

Naoteru SHIGEKAWA, Sae SHIMIZU, Jianbo LIANG, Masato SHINGO (Univ. of Fukui), Kenji SHIOJIMA (Univ. of Fukui), and Manabu ARAI (New Japan Radio Co. Ltd.)

Jpn. J. Appl. Phys. 57, 02BA04 [5 pages] (2018)

We investigate the transport properties of minority electrons across p-Si/n-4H-SiC interfaces fabricated using surface activated bonding. The transport properties along each direction are examined by measuring the photoresponse (PR) of p-Si/n-4H-SiC heterojunctions and characterizing 4H-SiC/Si heterojunction bipolar transistors (HBTs). The photoyield obtained in PR measurements is sensitive to the concentration of acceptors in p-Si and reverse-bias voltages, which indicates that the energy of optically excited electrons in p-Si is first relaxed and then they are driven to n-SiC through the tunneling process. By the postprocess annealing of HBTs, the properties of emitter/base interfaces are improved so that the current gain is drastically increased, which means that the Si/4H-SiC interfaces are in metastable states when the device process is completed. A maximum current gain of >10 is demonstrated.

Electrical conduction of Si/indium thin oxide/Si junctions fabricated by surface activated bonding

Jianbo LIANG, Tomoki OGAWA, Kenji ARAKI (Toyota Technological Institute), Takefumi KAMIOKA (Toyota Technological Institute), and Naoteru SHIGEKAWA

Jpn. J. Appl. Phys. 57, 02BA03 [5 pages] (2018)

The electrical properties of n⁺-Si/indium tin oxide (ITO)/n⁺-Si, n⁺-Si//ITO/p⁺-Si, and p⁺-Si//ITO/n⁺-Si junctions fabricated by surface activated bonding (SAB) were investigated. The current–voltage (I–V) characteristics of n⁺-Si//ITO/n⁺-Si, n⁺-Si//ITO/p⁺-Si, and p⁺-Si//ITO/n⁺-Si junctions showed excellent linear properties. The interface resistances of n⁺-Si//ITO/n⁺-Si, n⁺-Si//ITO/p⁺-Si, and p⁺-Si//ITO/n⁺-Si junctions were found to be 0.030, 0.025, and $0.029 \Omega \cdot \text{cm}^2$, respectively, which are lower than required for concentrator photovoltaics. The interface resistances of all the junctions increased with increasing annealing temperature. The degradation of the interface resistance is lower in n⁺-Si//ITO/n⁺-Si junctions than in n⁺-Si//ITO/p⁺-Si and p⁺-Si//ITO/n⁺-Si junctions, when the annealing temperature is higher than 100 °C. These results demonstrate that the ITO thin film as an intermediate layer has high potential application for the connection of subcells in the fabrication of tandem solar cells.

Semi-analytical Model for a Static Sheath Including a Weakly Collisional Presheath

Tatsuru SHIRAFUJI and Kazuki DENPO (Tokyo Electron Technology Solutions Ltd.)

Jpn. J. Appl. Phys., Vol. 57, 06JG02 (8 pages) (2018)

A semi-analytical static sheath (SASS) model can provide a spatial potential profile on a biased surface with microstructures, which can be used for predicting ion trajectories on the surface. However, two- or three-dimensional SASS models require a search procedure for a sheath edge equipotential profile, at which ions have the Bohm velocity, as the starting positions for calculating ion trajectories. This procedure can be troublesome when surface microstructures have complex structures. This difficulty is due to the fact that the SASS model cannot handle a presheath region. In this work, we propose a modified SASS model that can handle a presheath region. By using the modified SASS model, ion trajectories can be calculated from edges with arbitrary geometry without searching for the equipotential profile corresponding to sheath edges.

DOI: 10.7567/JJAP.57.06JG02

Effects of Ambient Air on the Characteristics of an Atmospheric-pressure Plasma Jet of a Gas Mixture of Highly N₂-diluted O₂ on a Sliding Substrate

Tatsuru SHIRAFUJI and Yasushi SAWADA (Air Water R&D Co., Ltd.)

Jpn. J. Appl. Phys., Vol. 57, 01AA06 (10 pages) (2018)

We have performed numerical simulations of reaction kinetics and flow dynamics of an atmospheric-pressure plasma jet (APPJ) of a gas mixture of 99.9% N₂ and 0.1% O₂ in a two-dimensional flow channel with a height of 5 mm and investigated the effects of a sliding substrate and the substitution of the ambient gas. The sliding substrate in the flow channel produces the gas-drag effect, which results in not only the bending of the APPJ

trajectory but also significant loss of atomic oxygen when the ambient gas is air. The flux of atomic oxygen integrated on the substrate is reduced to 19% of that integrated on the fixed substrate. We discuss the mechanisms of the reduction in the atomic oxygen flux through the analysis of spatial distributions of atomic oxygen loss reactions and show that the reduction in the atomic oxygen flux can be suppressed by substituting the ambient gas (air) with N₂.

DOI: 10.7567/JJAP.57.01AA06

Au-nanoparticle-embedded Cross-linked Gelatin Films Synthesized on Aqueous Solution in Contact with Dielectric Barrier Discharge

Tatsuru SHIRAFUJI, Yusuke NAKAMURA, Shiori AZUMA, Naoya SOTODA and Toshiyuki ISSHIKI (Kyoto Inst. Technol.)

Jpn. J. Appl. Phys., Vol. 57, 0102BE (8 pages) (2018)

A wine-red free-standing thin film has been formed by irradiating dielectric barrier discharge plasma on an aqueous solution containing H₂AuCl₄ and gelatin. The film has a fibrous structure with an inhomogeneous thickness profile and is composed of cross-linked gelatin, as confirmed by optical microscopy and infrared absorption spectroscopy. The film has embedded Au nanoparticles (GNPs), as confirmed by transmission electron microscopy. In the region with a relatively small film thickness, the number density of GNPs is relatively low, and the sizes of GNPs range from 5.3 to 34.3 nm. In the region with a relatively large film thickness, on the other hand, GNPs are highly accumulated, and the sizes of GNPs range from 10.0 to 26.7 nm. The aqueous solution remains transparent even after the film growth process, which indicates that the plasma-induced processes involving GNP formation and film growth are confined near the surface of the aqueous solution. A possible film growth mechanism is discussed on the basis of the experimental results of this study.

DOI: 10.7567/JJAP.57.0102BE

Simultaneous Generation of Acidic and Alkaline Water Using Atmospheric Air Plasma Formed in Water

Shin-ichi IMAI (Panasonic Corp.), Yoshihiro SAKAGUCHI (Panasonic Corp.) and Tatsuru SHIRAFUJI

Jpn. J. Appl. Phys., Vol. 57, 0102BC (6 pages) (2018)

Plasmas on water surfaces and in water can be generated at atmosphere pressure using several kinds of gases, including helium, argon, oxygen, and air. Nitrates are generated in water through the interaction between water and atmospheric plasma that uses ambient air. Water that has been made acidic by the generation of nitric acid and the acidic water can be used for the sterilization of medical instruments, toilet bowls, and washing machines. Dishwashers are another potential application, as alkaline water is needed to remove grease from tableware. To investigate the production of alkaline water and its mechanism, gas component analysis was performed using an atmospheric quadrupole mass spectrometer. It was found that hydrogen gas evolves from the water surrounding both the positive and negative electrodes. The gas and water analyses carried out in this study revealed that acidic water of pH 2.5 and alkaline water of pH 10 can be simultaneously generated by our ambient air plasma device, which has been altered from our original model. The alternative plasma device has a partition wall, which is made of conductive resin, between the positive and negative electrodes.

DOI: 10.7567/JJAP.57.0102BC

Plasma Materials Processing Involving Liquid

Tatsuru SHIRAFUJI

Vac. Surf. Sci., Vol. 61, 119-130 (2018) (in Japanese)

In materials processing using plasma in contact with liquid, plasma plays an important role as a trigger to promote primary processes at the plasma/liquid interface. However, direct effects such as radicals from plasma vanish after traveling a few or a few 10 nm from the plasma/liquid interface. The rest of the processes in liquid proceed only deep inside the liquid where the direct effects of plasma are no longer expected. This situation can be regarded as robustness in the process. However, at the same time, it has a negative aspect of poor controllability by plasma. In other words, the factor of “the unique to plasma” governs only the limited part of a whole process. In this paper, we survey recent research activities on materials processing using plasma in contact with liquid from the view point mentioned above and discuss why we use plasma.

DOI: 10.1380/vss.61.119

Retinal projection type super multi-view 3D head-mounted display using the time division projection optical system

Tadayuki KONDA, Katsuhisa TANAKA, Kayo YOSHIMOTO, and Hideya TAKAHASHI

Proc.SPIE Advanced in Display Technologies VIII, San Francisco, Feb. 19, Vol.10556, CD-ROM (2018).

We have previously proposed the see-through retinal projection type super multi-view head-mounted display (HMD). The smooth motion parallax provided by the super multi-view technique enables a precise superposition of virtual 3D images on real scene. Moreover, if a viewer focuses one's eyes on the displayed 3D image, the stimulus for the accommodation of human eye is reproduced naturally. To realize the super multi-view condition, multiple parallax images must be projected onto the retina. However, in the previous proposed HMD, since the respective parallax images were spatially divided and were projected onto the retina, the image resolution was low and the optical system was complicated. In order to overcome these problems, we propose the improved see-through retinal projection type super multi-view HMD by using the time division projection optical system. The proposed HMD consists of a multiple exposure holographic lens with multi-convergence points, a high frame rate display device, and a high-speed optical shutter. Multiple parallax images are displayed by time division and are converged on respective points by the holographic lens. The optical shutter which synchronized to the display device passes only one convergence light corresponding to the right parallax image. Therefore, proposed HMD realizes the pseudo super multi-view condition and displays the virtual image at the distance within ability for focusing on the human eye. To verify the effectiveness of the proposed HMD, we confirmed the depth range of the 3D image by the prototype of the proposed HMD was more than 250 mm in front of the pupil.

3D registration method for assessing the gastrointestinal motility using spectral reflectance estimation

Kazuki NOBE, Kayo YOSHIMOTO, Kenji YAMADA (Osaka University), and Hideya TAKAHASHI

Proc.SPIE Advanced Biomedical and Clinical Diagnostic and Surgical Guidance Systems XVI, San Francisco, Feb. 12, Vol.10484, CD-ROM (2018).

Functional gastrointestinal disorders (FGID) are the most common gastrointestinal disorders. The term "functional" is generally applied to disorders where there are no structural abnormalities. One of the major factors for FGID is abnormal gastrointestinal motility. We have proposed a system for assessing the function of gastric motility using a 3D endoscope. In this previous study, we established a method for estimating characteristics of contraction wave extracted from a 3D shape include contraction wave obtained from stereo endoscope. Because it is difficult to fix the tip position of the endoscope during the examination, estimation of the 3D position between the endoscope and the gastric wall is necessary for the accurate assessment. Then, we have proposed a motion compensation method using 3D scene flow. However, since mucosa has few feature points, it is difficult to obtain 3D scene flow from RGB images. So, we focused on spectral imaging that can enhance visualization of mucosal structure. Spectral image can be obtained without switching optical filters by using technique to estimate spectral reflectance by image processing. In this paper, we propose registration method of measured 3D shape in time series using estimated spectral image. The spectral image is estimated from the RGB image for each frame. 3D scene flow of feature points, that is, enhanced mucosal structure calculated by spectral images in a time series. The position change between the endoscope and gastric wall is estimated by 3D scene flow. We experimented to confirm the validity of the proposed method using papers with a grid of colors close to the background color.

Development of pulse wave sensing textile using conductive fiber

Kayo YOSHIMOTO, Katsuhisa TANAKA, Hideya TAKAHASHI, and Atsuji MASUDA (Industrial Technology Center of Fukui Prefecture)

Journal of Fiber Science and Technology, vol.73, no.11, pp.294-299 (2017).

This paper describes a pulse wave sensing textile to measure pulse wave continuously without stress. Due to aging population, the attention is focused on measurement of vital signs during daily life. Blood pressure (BP) is widely used as an index representing the state of the circulatory system. BP can be estimated from electrocardiogram (ECG) and photoplethysmogram (PPG). PPG can be obtained by a combination of a light emitting diode (LED) and a phototransistor (PT). The textile measured PPG has not been realized although there are fabric electrodes for measuring ECG. Therefore we developed the pulse wave sensing textile for

using underwear aiming to continuously BP estimation. By using conductive fibers woven into the textile as wiring, the pulse wave sensing textile is realized. In order to improve the stability of pulse wave measurement, LEDs and PTs were arranged in array on the textile. We designed the textile circuit under the consideration that circuit lines on the textile must be straight. We showed that arranging LEDs and PTs in an array improve the stability of pulse detection and evaluated that the proposed sensing textile can be measured pulse wave on the waist even if a person attached the proposed sensing textile is moving. These results suggest that the proposed sensing textile could be built into underwear and used as a part of BP estimation system. Unconscious continuous BP monitoring underwear could be realized by combining the proposed textile with fabric electrodes.

Dynamic hand gesture recognition on 3D virtual cultural heritage ancient collection objects using k-nearest neighbor

Adri Gabriel Sooai (ITS), Khamid (ITS), Kayo YOSHIMOTO, Hideya TAKAHASHI, Surya Sumpeno (ITS), and Mauridhi Hery Purnomo (ITS)

Engineering Letters, vol.26, no.3, EL_26_3_09 (2017).

This paper discusses on how to prepare a specific dynamic hand gesture, modeling and testing it to interact with 3D virtual objects of cultural heritage ancient collection. Those virtual objects prepared to avoid damage on the original one. Several kinds of research work for recreation or reactivating ancient heritage for educational purposes can take place using it. The dynamic hand gesture detected using hand movement sensor. We recorded ten specific dynamic hand gesture that stands for the interaction between museum visitors and the ancient collection chosen for the test. All ten gestures consist of fingers tips coordinates, palm, and wrist movement. A total of 14474 rows in 30 features forming fingers and palm movements information. Those gestures namely: pickup , sweep from right to left, sweep from left to right, grab from above, grab from the right side, pinch from above, pointing, scooping, push and picking. We train ten dynamic hand gestures using K-NN classifier and using different distance metric namely Cosine, Euclidean and Cubic. The best result of trained model reaches 99.3% accuracy. Later, we use the new hand gesture to test the trained model. It consists of 15000 rows of fingers coordinates in 30 features. The results show that from all ten gestures, there are four gestures reach recognition accuracy more than 92%. One gesture reaches 100%, two gestures on 82% and 89% and three gestures below 64%. The gesture which reaches high accuracy in training and testing consider selected for default model.

Application of online supervisory control of discrete-event systems to multi-robot warehouse automation

Yuta TATSUMOTO, Masahiro SHIRAISHI, Kai CAI, and Zhiyun LIN (Hangzhou Dianzi University)

Control Engineering Practice, vol. 81, pp. 97-104 (2018).

In this paper we present an online supervisory control approach, based on limited lookahead policy, that is amenable for the control of multi-agent discrete-event systems. We then apply this online control scheme to model and control a warehouse automation system served by multiple mobile robots; the effectiveness of this scheme is demonstrated through a case study. Moreover, we build an experiment testbed for testing the validity of our proposed method with implementation on real robots.

Application of supervisory control theory with warehouse automation case study

Yuta TATSUMOTO, Masahiro SHIRAISHI, and Kai CAI

Transactions of the Institute of Systems, Control and Information Engineers, vol. 62, pp. 203-208 (2018).

In this paper we provide a tutorial on supervisory control theory, and introduce a new application on warehouse automation using mobile robots. In presenting supervisory control theory, we demonstrate the procedure of supervisory control design by using an easy-to-use software package TCT. Our purpose is for control scientists and engineers who may not be familiar with the theory to still carry out the design of supervisory controllers step-by-step in TCT.

On algebraic connectivity of directed scale-free networks

Takanobu IMAE and Kai CAI

Journal of the Franklin Institute, vol. 355, pp. 8065–807 (2018).

In this paper, we study the algebraic connectivity of directed complex networks with scale-free property.

Algebraic connectivity of a directed graph is the eigenvalue of its Laplacian matrix whose real part is the second smallest. This is known as an important measure for the diffusion speed of many diffusion processes over networks (e.g. consensus, information spreading, epidemics). We propose an algorithm, extending that of Barabasi and Albert, to generate directed scale-free networks, and show by simulations the relations between algebraic connectivity and network size, exponents of in/out-degree distributions, and minimum in/out degrees. The results are moreover compared to directed small-world networks, and demonstrated on a specific diffusion process, reaching consensus.

Supervisory control of discrete-event systems: a brief history

W.Murray WONHAM (University of Toronto), Kai CAI, and Karen RUDIE (Queen’s University)

Annual Reviews in Control, vol. 45, pp. 250-256 (2018).

This brief history summarizes the ‘supervisory control of discrete-event systems’ as it has evolved in the period 1980–2017. Overall, the trend has been from centralized or ‘monolithic’ control to more structured architectures, and from ‘naive’ to symbolic computation. Like any ‘history’ this one represents the perspective of the authors; in consequence some important contributions may have been overlooked or short-changed.

Quantitative Analysis of Large Voltage Hysteresis of Lithium Excess Materials by “Backstitch Charge and Discharge” Method

Kingo ARIYOSHI, Takayuki INOUE, Yusuke YAMADA

J. Electrochem. Soc., Vol. 165, pp. A2675-A2681 (2018)

Lithium-excess (LEX) materials ($\text{LiMO}_2 \cdot \text{Li}_2\text{MnO}_3$; $\text{M} = \text{Co}, \text{Ni}, \text{etc.}$) are attractive as potential positive electrodes of high-capacity lithium-ion batteries, however, large voltage hysteresis of LEX materials in charge and discharge disturbs real application. Thus, the large voltage hysteresis was investigated by a novel electrochemical method termed as a “backstitch charge and discharge” (backstitch CD) method, in which unsymmetrical charge and discharge with a small capacity were continuously repeated. The backstitch CD method was applied to $\text{Li}[\text{Li}_{1/5}\text{Co}_{2/5}\text{Mn}_{2/5}]\text{O}_2(0.5\text{LiCoO}_2 \cdot 0.5\text{Li}_2\text{MnO}_3)$ known as an LEX material for the first time. $\text{Li}[\text{Li}_{1/5}\text{Co}_{2/5}\text{Mn}_{2/5}]\text{O}_2$ showed different reversible potentials during the backstitch CD processes in spite of symmetrical polarization behavior at each process. The voltage hysteresis in $\text{Li}[\text{Li}_{1/5}\text{Co}_{2/5}\text{Mn}_{2/5}]\text{O}_2$ resulted from electrochemically reversible but different reactions occurring during charging and discharging processes. Contributions of overpotential and difference in reversible potential to the voltage hysteresis can be evaluated quantitatively by the backstitch CD method.

Effect of Surface Acidity of Cyano-bridged Polynuclear Metal Complexes on Catalytic Activity for Hydrolysis of Organophosphates

Hiroyasu TABE, Chihiro TERASHIMA, Yusuke YAMADA

Catal. Sci. Technol., Vol. 8, pp. 4747-4756 (2018)

Heterogeneous catalysis of cyano-bridged polynuclear metal complexes, which were prepared by systematic replacement of C-bound metal ions (M^{C}) and/or N-bound metal ions (M^{N}) of Prussian blue ($[\text{M}^{\text{N}}(\text{H}_2\text{O})_x]_y[\text{Fe}^{\text{II/III}}(\text{CN})_6]$; $\text{M}^{\text{N}} = \text{Fe}^{\text{III}}, \text{Ga}^{\text{III}}, \text{Mn}^{\text{II}}, \text{Zn}^{\text{II}}$ or Co^{II} ; $[\text{Fe}^{\text{II/III}}(\text{H}_2\text{O})_x]_y[\text{M}^{\text{C}}(\text{CN})_6]$; $\text{M}^{\text{C}} = \text{Fe}^{\text{II}}, \text{Pt}^{\text{IV}}, \text{Co}^{\text{III}}, \text{Ir}^{\text{III}}$ or Ru^{II}), was examined for the hydrolysis of *p*-nitrophenol phosphate (*p*-NPP) as a model compound of insecticides. The catalytic activity of the complexes was enhanced by employing metal ions in higher oxidation states at the C- and N-bound sites, although only N-bound metal ions act as active sites. The dependence of the initial reaction rates for the hydrolysis on the initial concentration of *p*-NPP suggested that the rate determining step is the adsorption of *p*-NPP onto catalyst surfaces. The surface acidity of each complex estimated by the heat of pyridine desorption is strongly correlated with catalytic activity.

Photocatalytic Hydrogen Evolution Systems Constructed in Cross-linked Porous Protein Crystals

Hiroyasu TABE, Hikaru TAKAHASHI, Takuya SHIMOI, Satoshi ABE, Takafumi UENO, Yusuke YAMADA

Appl. Catal. B, Vol. 237, pp. 1124-1129 (2018)

Cross-linked hen egg white lysozyme crystals (CL-HEWL) have been employed as supports to construct heterogeneous catalysts for photocatalytic hydrogen (H_2) evolution, where rose bengal (RB) and Pt nanoparticles (PtNPs) acted as a photosensitizer and H_2 -evolution catalysts, respectively. Single-crystal X-ray structure analyses of the CL-HEWL immobilizing a precursor for PtNPs suggested that a coordination site of the precursor locates in immediate proximity to potential adsorption sites for RB. The accumulation of the components facilitated photo-induced electron transfer, resulting in efficient H_2 evolution. These results suggest that porous protein crystals are promising platforms to periodically and rationally accumulate catalytic components by using molecular interactions.

High Dimensional Stability of LiCoMnO_4 as Positive Electrodes Operating at High Voltage for Lithium-ion Batteries with a Long Cycle Life

Kingo ARIYOSHI, Hiroya YAMAMOTO, Yusuke YAMADA

Electrochim. Acta, Vol. 260, pp. 498-503 (2018)

Dimensionally stable LiCoMnO₄ having a spinel-framework structure was developed as a positive electrode of lithium-ion batteries with a long cycle life. Well-crystallized LiCoMnO₄ prepared by a two-step solid-state reaction shows large rechargeable capacity of 120 mAh g⁻¹ at high operating voltage of 5 V. Ex-situ XRD measurements of the LiCoMnO₄ revealed small change in the cubic lattice parameter (*ca.* 0.7%) during charge and discharge. Change in electrode thickness of LiCoMnO₄ measured by using a precision dilatometer is accordance with the change in the cubic lattice parameter. The LiCoMnO₄ electrode showed high dimensional stability compared with other LiMn₂O₄-based materials having a spinel-framework structure.

Cobalt-copper Nanoparticles Catalyzed Selective Oxidation Reactions: Efficient Catalysis at Room Temperature

Biraj Jyoti BORAH, Abhijit MAHANTA, Manoj MNDAL, Hemen GOGOI, Yusuke YAMADA, Pankaj BHARALI

Chem. Select, Vol. 3, pp. 9826-9832 (2018)

Bimetallic nanoparticles (NPs) play a pivotal role in promoting high activity and selectivity towards various industrially important reactions in comparison to single metal NPs due to their modulated electronic and surface properties. Herein, we report the synthesis of non-precious CoCu NPs, which serve as an excellent catalyst for the selective oxidation of a wide range of electronically diverse benzyl alcohols to benzaldehydes, in the presence of *tert*-butyl hydroperoxide (TBHP) as an oxidant at room temperature. The excellent catalytic activity of CoCu NPs is ascribed to a two-fold synergistic effect arising from the combination of enhanced peroxide decomposition, active Co²⁺ catalyst regeneration driven by the faster redox processes (between Co³⁺ and Cu⁺), and a feasible cobalt dimerisation-regeneration process. The recoverability and reusability of CoCu NPs are also demonstrated. With the merits of low-cost and recyclable catalysis under mild conditions, the present catalyst represents an efficient and potential alternative to precious metal catalysts.

Construction of Assemblies for Photocatalytic Hydrogen Evolution Using Various Supports

Yusuke YAMADA, Hiroyasu TABE

JXTG Technical Review, Vol. 60, pp. 8-14 (2018) (in Japanese)

The review discloses how to construct photocatalytic assemblies for hydrogen evolution on various supports. The assemblies involve a photosensitizer and a hydrogen evolution catalyst in the presence of a sacrificial electron donor. The supports are chosen from conventional mesoporous silica-alumina, assembly of silica-alumina nanoparticles, porous protein crystals, and a layered metal oxide semiconductor.

Electrocatalysts for Hydrogen Peroxide Reduction Used in Fuel Cells

Yusuke YAMADA

Anion Exchange Membrane Fuel Cells, Principles, Materials and Systems (Eds. Liang AN, T. S. ZHAO), pp. 141-168, Springer (ISBN: 978-3-319-71370-0)

Hydrogen peroxide is a strong oxidant, which enables to enhance the output power of fuel cells. Thus, electrocatalysts for hydrogen peroxide reduction have been investigated with various materials such as metals, metal oxides and metal complexes. This review focuses on cathode materials utilized in hydrogen peroxide fuel cells.

X-Ray Technology

Kouichi TSUJI

Encyclopedia of Analytical Chemistry., *Kirk-Othmer Encyclopedia of Chemical Technology*, John Wiley & Sons, Inc.(2018) DOI: 10.1002/0471238961.2418012519160118.pub3

Analytical X-ray instruments are used to characterize materials in several ways. There are analytical instruments that can produce images of the internal structure of objects that are opaque to visible light. There are instruments used to determine chemical composition of an object, the crystalline phases of solids, and the complete atomic and

molecular structure of a single crystal. The determination of particle size, structural information for fibers and polymers and the study of stress, texture, and thin films are applications that are growing in importance and can be examined with X-ray instruments. This article gives information on the characterization, generation, and properties of X-Rays, and principles of X-ray diffraction. Small molecule and macromolecule single-crystal structure determinations are discussed. These techniques are compared with powder diffraction. X-ray reflectometers, position sensitive detectors, and area detectors are some of the special instruments designed to measure properties of the new and exotic materials being manufactured. Details on X-ray fluorescence spectrometry and X-ray radiography are also given.

X-Ray Spectrometry

Kouichi TSUJI, Yasuji MURAMATSU

Kodansha Ltd., total page 352 (2018) (in Japanese)

Fundamentals and applications of X-ray fluorescence (XRF), Electron microprobe analysis (EPMA), x-ray absorption (XAS) including EXAFS and XANES, total reflection XRF (TXRF), soft x-ray XRF, XRF imaging, and scanning transmission x-ray microscope (STXM) are described in details. In chapter 2, x-ray tube, synchrotron radiation, x-ray detectors are explained. In chapter 3, quantitative XRF analysis using fundamental parameter (FP) method and principle of XRF technique are explained. In chapter 4, EPMA are introduced with introduction of wavelength dispersive spectrometer. In chapter 5, fundamental of XAS and applications are shown. Finally, in chapter 6, applications of x-ray techniques to metals, inorganic materials, plastic materials, soils, aerosol particles, catalyst materials, battery materials, and biological and food samples are shown as well as sample preparation techniques.

Large-area Imaging by WD-XRF Analysis and Elemental Monitoring of the Dissolution Process of a Solid Sample

Shota AIDA, Yuki TAKIMOTO, Takuto SAKUMURA, Kazuyuki MATSUSHITA, Takashi SHOJI, Naoki KAWAHARA

Bunseki Kagaku, Vol. 66, pp. 885-892 (2017) (in Japanese)

A wavelength-dispersive X-ray fluorescence (WD-XRF) imaging spectrometer gives XRF images more rapidly than energy-dispersive X-ray fluorescence (ED-XRF). The analyzing area by this method is dependent on the diameter of the used 2D collimator. We considered large-area imaging while scanning a sample, to enlarge the analyzing area. Then, the analyzing object was measured at each segment, and obtained XRF images were combined. As the result, Cu and Br elemental whole images were constructed for an electronic circuit card (30 mm × 54 mm), with a total exposure time of 54 s. In addition, WD-XRF imaging rapidly provides specific elemental images. Therefore, this method was applied for the monitoring of chemical reactions in liquid samples. WD-XRF imaging was repeated in an exposure time of 60 s/frame for observing the dissolution process of metals in solutions. Consequently, the dissolution process of a Zn piece in hydrochloric acid was visualized from Zn K_{α} intensity distributions.

Fundamental Study on Quantitative Full Field XRF Imaging with X-ray CCD Camera

Masaki YAMANASHI, Aoi YAMAUCHI, Kouichi TSUJI

Bunseki Kagaku, Vol. 66, pp. 901-907 (2017) (in Japanese)

A full field energy-dispersive X-ray imaging apparatus (FF-EDXRF) using photon counting technique was proposed by our group and confirmed its performance. The energy resolution was 142 eV for Fe K_{α} line, the spatial resolution was 52 μm . These values are equally of the energy-dispersive X-ray detector and micro-XRF imaging apparatus. X-ray fluorescence images of multi elements was obtained at the same time for the print color board sample. The quantitative method of full field X-ray imaging apparatus has not established. The calibration curve created by Ni standard materials (FXS 326 - 331) are evaluated by R^2 value. The accuracy of calibration

curve and R^2 value was satisfied and one calibration curve created by summarized all calibration curve are applied for all effective pixels.

Cross Sectional Elemental Mapping of Under Film Corrosion of Galvanized Steel Sheets by Confocal XRF Analysis

Koji AKIOKA, Takashi DOI, Ryota YAGI, Tsuyoshi MATSUNO, Kouichi TSUJI

Proc. of the 11th Int. Conf. on Zinc and Zinc Alloy Coated Steel Sheet Galvatech2017, Tokyo, Japan, ISIJ, pp. 161-168 (2017)

For the understanding of the under film corrosion behavior of the painting steel sheet, grasp of the element behavior in the solid - liquid interface is important. Because the XRF analysis technique using fluorescence X-rays can get element distribution information in nondestructiveness, it is thought that it is effective analysis technique. Above all, as for the micro-XRF technique using the confocal optical system, the section observation of test specimens is possible in nondestructiveness. This time, the process of under film corrosion of painted galvanized steel sheet was investigated by confocal micro-XRF method. To reduce the attenuation of fluorescent x-ray by air, the area of analysis was placed in a vacuum chamber. L-line of Rh target of X-ray was used to measure the signal from light element sensitively. Painted galvanized steel sheet was prepared by electro-deposition coating with zinc phosphate conversion coating. Moving test specimens to depth direction with confocal optical placement, the cross sectional element map was measured. The depth profiles of light element were broad compare to those of heavy element. The thickness of each layer was estimated by comparing the peak distance of the profile of each element.

To investigate the under film corrosion process, the dipping type acceleration corrosion test was applied. The painted galvanized steel sheet was scratched to reach Fe substrate, and then, it was immersed to a 5 mass % sodium chloride solution at 55 °centigrade. The cross section maps of the same field of vision were observed every 48 hours to make use of the merit of the non-destructive analysis. The obtained element map of Ti revealed that blister type corrosion around the scratch. From the depth maps of P and Zn, these were observed that the cross sectional elemental maps were changed and the intensity of P and Zn signal were decreased near the blister. It was suggested that some Zn and P atoms in the zinc phosphate coating layer dissolved into the NaCl solution. After 240 hours, the cross sectional elemental maps obtained by this XRF non-destructive method were compare to the cross sectional SEM/EDS images obtained by destructive method.

The 17th International Conference on Total Reflection X-Ray Fluorescence Analysis and Related Methods (TXRF2017)

Kouichi TSUJI

Adv. X-Ray. Chem. Anal., Japan, Vol. 49, pp. 71-76 (2018) (in Japanese)

The 17th International Conference on Total Reflection X-Ray Fluorescence Analysis and Related Methods (TXRF2017) was held in the period from 19 Sept. to 22 Sept. 2017 at “Centro Pastorale Paolo VI” Conference Centre in Brescia Italy. Details of this international conference were reported as well as VAMAS (Versailles Project on Advanced Materials and Standards) course, which was held during TXRF2017. In addition, ISO TC201/ SC10 meeting was held before TXRF2017. The activity of SC10 was also described.

Elemental Distribution Analysis in the Hair by Confocal Micro XRF

Naoya YOMOGITA, Kouichi TSUJI

Adv. X-Ray. Chem. Anal., Japan, Vol. 49, pp. 209-218 (2018) (in Japanese)

Confocal micro X-ray fluorescence is an effective method for obtaining information about elemental distribution inside the sample. A hair has trace elements such as Ca and Zn, so it is possible to examine deficiency of these elements and whether we take harmful metal by scanning one's hair. Then, we tried obtaining elemental map at any position and revealing information about elemental distribution from the hair root to top by applying confocal micro XRF. We also investigated the possibility about invasion of element from outside by analyzing fluorescent

X-ray intensity of hair on surface and at center in specific cross section. In the hair applied a permanent wave, it became clear that it receives strong contamination from the outside.

Elemental Analysis of Teas, Herbs and Their Infusions by Means of Total Reflection X-Ray Fluorescence

Rogerta DALIPI, Laura BORGESSE, Kouichi TSUJI, Elza BONTEMPI, Laura E. DEPERO

Journal of Food Composition and Analysis, Vol. 67, pp. 128-134 (2018)

This work shows that total reflection X-ray fluorescence (TXRF) is a suitable tool for multi-elemental analysis of teas, herbs and their infusion. A low power benchtop TXRF spectrometer was used. Safety of infusion consumption was evaluated. Many commercially available teas, herbs and roots samples were analyzed. Total concentrations of thirteen elements K, Ca, Ti, Cr, Mn, Fe, Ni, Cu, Zn, Rb, Sr, Ba and Pb as well as their extraction efficiencies into infusion were determined. The content of Pb is highlighted in all teas and herbs, in the concentration range between 0.5 and 4.8 mg/g, but only in infusions of herbs. Chemometry was applied for classification purposes. Elemental daily intakes with respect to infusion drinking was calculated and compared with dietary reference intake values. Results show that TXRF is a fast and simple technique for safety check of tea and herb infusions on a routine basis.

Corrosion Process Analysis of Steel Samples by Confocal Micro 3D X-Ray Fluorescence Analysis

Kouichi TSUJI

NSST Communication Bulletin, Vol. 99, pp. 2-3 (2018) (in Japanese)

Fundamental of confocal micro-XRF technique was introduced. A few applications of this technique to steel samples were introduced.

X-Ray Fluorescence Elemental Imaging of Liquid Samples Near Solid Surface.

Kouichi TSUJI

Transactions of The Research Institute of Ocean Chemistry, Vol. 31, No. 1, Apr., pp. 27-30 (2018) (in Japanese)

Fundamental of confocal micro-XRF technique was introduced. A few applications of this technique to solid-liquid interface analysis were shown.

Sample Preparation for Total Reflection X-ray Fluorescence Analysis Using Resist Pattern Technique

Kouichi TSUJI, Naoya YOMOGITA, Yuji KONYUBA

Spectrochim. Acta Part B, Vol. 144, pp. 68-74 (2018)

A circular resist pattern layer with a diameter of 9 mm was prepared on a glass substrate (26 mm × 76 mm; 1.5 mm thick) for total reflection X-ray fluorescence (TXRF) analysis. The parallel cross pattern was designed with a wall thickness of 10 μm, an interval of 20 μm, and a height of 1.4 or 0.8 μm. This additional resist layer did not significantly increase background intensity on the XRF peaks in TXRF spectra. Dotted residue was obtained from a standard solution (10 μL) containing Ti, Cr, Ni, Pb, and Ga, each at a final concentration of 10 ppm, on a normal glass substrate with a silicone coating layer. The height of the residue was more than 100 μm, where self-absorption in the large residue affected TXRF quantification (intensity relative standard deviation (RSD): 12–20%). In contrast, from a droplet composed of a small volume of solution dropped and cast on the resist pattern structure, the obtained residue was not completely film but a film-like residue with a thickness less than 1 μm, where self-absorption was not a serious problem. In the end, this sample preparation was demonstrated to improve TXRF quantification (intensity RSD: 2–4%).

Comparison of Multiple X-Ray Fluorescence Techniques for Elemental Analysis of Particulate Matter Collected on Air Filters

Fabjola BILO, Laura BORGESSE, Anne WAMBUI, Ahmad ASSI, Annalisa ZACCO, Stefania FEDERICI, Diane EICHERT, Kouichi TSUJI, Roberto LUCCHINI, Donatella PLACIDI, Elza BONTEMPI, Laura Eleonora DEPERO

Journal of Aerosol Science, Vol. 122, pp. 1-10 (2018)

This work reports on qualitative and semi-quantitative elemental analysis of particulate matter (PM) collected on PTFE membrane filters, for a source apportionment study conducted in Brescia (Italy). Sampling was undertaken in a residential area where an increase in Mn emissions has been highlighted by previous studies. Filters are measured by means of X-ray Fluorescence (XRF) based techniques such as micro-XRF and grazing incidence XRF using synchrotron radiation, Mo or W excitation sources, after applying an automatized sample preparation method. A heterogeneous distribution in PM shape, size and composition was observed, with features typical of anthropogenic sources. XRF measurements performed at various incidence angle, on large areas and different experimental setup were reproducible. The results demonstrate a successful comparison of the various XRF instrumentation, and the decrease in Mn content with the distance away from the identified emission source. This work highlights the potentialities of the presented approach to provide a full quantitative analysis, and ascertain its suitability for providing a direct, fast, simple and sensitive elemental analysis of filters in source apportionment studies and screening purposes.

Wavelength-Dispersive XRF Imaging Using Soller Slits and 2D Detector

Shota AIDA, Masaki YAMANASHI, Takuko SAKUMURA, Kazuyuki MATSUSHITA, Takashi SHOJI, Naoki KAWAHARA, Kouichi TSUJI

Advances in X-ray Analysis, Vol. 61, pp. 180-187 (2018)

A new wavelength-dispersive X-ray fluorescence (WD-XRF) imaging spectrometer equipped with a highly sensitive two-dimensional detector was developed in our laboratory. In this spectrometer, a straight type polycapillary optic was applied instead of a Soller slit which is used in conventional WD-XRF spectrometers. The straight type polycapillary optic worked as a 2D collimator for fluorescent X-rays to keep the information of the elemental distribution in the sample. However, the analyzing area of this technique is limited by the outer diameter of the polycapillary optic, because it is practically difficult to make a polycapillary with a large diameter. Therefore, we attempted the use the Soller slits for 2D collimator. Two Soller slits were orthogonally arranged between the sample and the analyzing crystal (LiF). Elemental images of Cu and Pb were clearly obtained with improved spatial resolution compared to the elemental images with the polycapillary optic.

Photocatalytic Reduction of CO₂ by Pt-Loaded TiO₂ in the Mixture of Sub- and Supercritical Water and CO₂

Noritsugu KOMETANI, Shoutarou HIRATA, Masaaki CHIKADA

Journal of Supercritical Fluids, Vol. 120, pp. 443-447 (2017)

Photocatalytic reduction of CO₂ by Pt-loaded TiO₂ in the mixture of CO₂ and water has been examined as a function of temperature and pressure up to 400 °C and 30 MPa. The abrupt increase in the yields of CO, CH₄, HCOOH and HCHO was observed as temperature was elevated from 300 to 400 °C at a constant pressure of 30 MPa. This is attributed to the formation of uniform single phase mixture of water and CO₂ under supercritical condition, leading to the enhanced efficiency of CO₂ reduction. In contrast, the yield of H₂ produced by water reduction showed a monotonous increase with temperature because of the thermal acceleration of photocatalytic reaction. It is suggested that the control of the phase state of reaction medium has a key role in the determination of conversion efficiency for the photocatalytic reduction of CO₂ with water.

Development of Cu/Ni Binary Catalyst for Hydrothermal Oxidation of Refractory Compounds

Noritsugu KOMETANI, Masaaki NARITA

Proceedings of 12th International Symposium on Supercritical Fluids, Paper ID: OI04 (2018)

We have reported that Cu-based materials show a remarkable catalytic effect for the treatment of refractory organic compounds such as chlorophenol and trichloroethylene by catalytic hydrothermal oxidation, because of enhanced generation of hydroxyl radicals through Fenton-like reaction catalyzed by Cu(I) ion under hydrothermal condition. Here, we report that Cu/Ni binary catalyst exhibits a higher activity than Cu for the hydrothermal

oxidation of 3,4-dichlorophenol. It is indicated by EXAFS data that the atomic interaction between Cu and zero-valent Ni may accelerate Fenton-like reaction, resulting in enhanced degradation and mineralization of 3,4-dichlorophenol.

Development of Dissolution Inhibitor in Chemically Amplified Positive Tone Thick Film Resist

Yusuke SOTOKAWA, Takashi NISHIYAMA, Eriko SATO, Hideo HORIBE

J. Photopolym. Sci. Technol., Vol. 31(3), pp. 399-402 (2018)

Thick film resist is applied to a template for microelectrode used in semiconductor device integration. Utilization of positive type resist in chemically amplified system for thick film is expected to improve production efficiency of semiconductor device integration, but improvement of resolution is required. In order to improve the resolution of chemically amplified positive tone thick film resist, chemical structure of the dissolution inhibitor (DI) was designed for the control of solubility in resist polymer. The increase of molecular size in DI improved the dissolution inhibiting ability for the resist polymer in the unexposed area and the high acidity of the deprotected DI having carboxyl group improved dissolution promoting ability for the resist polymer in the exposed area. The resist containing DI possessing a large molecular size and high acidity improved its sensitivity and resolution.

Time-Resolved Analysis of Resist Stripping Phenomenon Using Laser Irradiation

Tomosumi KAMIMURA, Yuji UMEDA, Hiroyuki KURAMAE, Kosuke NUNO, Ryosuke NAKAMURA, Hideo HORIBE

J. Photopolym. Sci. Technol., Vol. 31(3), pp. 413-418 (2018)

Resist stripping phenomenon with laser irradiation was observed by using a time-resolved analysis. The time change of the resist stripping phenomenon by a probe laser irradiation was observed from the viewpoint of the intensity change of the probe laser. As for the laser irradiation in the water, the probe laser intensity arrived at the maximum after around 40 μ s. During the pump laser irradiation of 8 ns, a large compressive stress of -10 MPa was confirmed inside the resist from the FE analysis results. The generation of this compression stress is important for starting the resist stripping process, and is thought to improve the resist removal efficiency.

Fabrication of Mesoscopic Structure on PMMA Surface by Atomic Hydrogen and Evaluation of the Surface Functionality

Akari MATSUO, Seiji TAKAGI, Takashi NISHIYAMA, Masashi YAMAMOTO, Eriko SATO, Hideo HORIBE

J. Photopolym. Sci. Technol., Vol. 31(3), pp. 369-372 (2018)

Surface properties of polymers such as wettability and adhesiveness play an important role in industrial applications. The properties can be enhanced by fabricating a mesoscopic structure to the surface. In this study, we examined a chemical etching which is a simple and direct technique for the surface profile control, using atomic hydrogen generated by hot-wire catalytic method. Several tens of nanoscale structures were fabricated on poly(methyl methacrylate) (PMMA) surface by atomic hydrogen irradiation, and the size and pitch of the structure could be controlled by reaction temperature and time. The wettability of PMMA film surface changed from hydrophilicity to hydrophobicity by formation of mesoscopic structures.

Degradation of Poly(acrylic acid) in Aqueous Solution by Using O₃ Microbubble

Terumi MIYAZAKI, Takashi NISHIYAMA, Eriko SATO, Hideo HORIBE

J. Photopolym. Sci. Technol., Vol. 31(3), pp. 409-412 (2018)

Polyacrylic acid (PAA) aqueous solution was treated with O₃ microbubbles and O₃ water, there was no difference in decrease in molecular weight of PAA due to the presence or absence of microbubbles. Regardless of dissolved O₃ concentration, O₃ microbubbles alone did not cause reduction in TOC and mineralization did not proceed. In the advanced oxidation processes with hydrogen peroxide added, the molecular weight and TOC decreased. It is considered that active oxygen is generated from hydrogen peroxide by advanced oxidation and PAA is

decomposed. From these results, it is no considered generation of reactive oxygen species by microbubbles in the decomposition of PAA.

Removal of Polymers for KrF and ArF Photoresist Using Hydrogen Radicals Containing a Small Amount of Oxidizing Radicals

Masashi YAMAMOTO, Tomohiro TAKI, Takuto SUNADA, Tomokazu SHIKAMA, Shiro NAGAOKA, Hironobu UMEMOTO, Hideo HORIBE

J. Photopolym. Sci. Technol., Vol. 31(3), pp. 419-424 (2018)

Photoresist removal method using hydrogen radicals, which are produced on a tungsten hot-wire catalyst, is effective to resolve some environmental and industrial problems in conventional methods for the fabrication of electronic devices. However, its removal rate is not as good as that of the conventional ones. We have previously described that the removal rate of a positive-tone novolac photoresist is enhanced by the addition of a small amount of oxygen gas to the atmosphere, in which hydrogen radicals are produced. Oxidizing radicals, such as OH and O radicals, can be produced together with H radicals. In present study, we examined the effects of oxygen addition on base polymers of KrF and ArF photoresists: the former is poly(vinyl phenol) (PVP), and the latter is poly(methyl methacrylate) (PMMA). Effects of oxygen addition on PVP was confirmed, as was found for the novolac photoresist. On the other hand, the effects on PMMA were different from the cases of the novolac photoresist and PVP. Results were ascribed to the presence or absence of benzene rings, the properties of polymers and the reactivity of oxidizing radicals.

Chemical Structure of the Ion Beam Irradiated Polymer

Hideo HORIBE

RADIOISOTOPES, Vol. 66(11), pp. 567-577 (2017) (in Japanese)

We investigated the chemical structure of positive-tone novolac photoresists into which B, P, and As ions were implanted with doses of 5×10^{12} to 5×10^{15} atoms/cm². The thickness of the surface-hardened layer of ion-implanted photoresists increased in the order As–P–B. The energy supplied from the ions to the photoresist concentrated on the surface side in the increasing order of B–P–As. The photoresists are exhibiting carbonization and/or crosslinkage attributable to the decrease in OH, CH, and O1s and the increase in C=C, C1s, and π -conjugated systems.

Material Design of the Chemically Amplified Positive Type Electron Beam Resist

Hideo HORIBE

RADIOISOTOPES, Vol. 66(11), pp. 557-566 (2017) (in Japanese)

The dissolution characteristics of a chemically amplified electron beam (EB) resist composed of partially tert-butoxycarbonyl group (tBOC) protected poly(p-vinylphenol) (PVP), a dissolution inhibitor, and an acid generator were investigated. The resist sensitivity was improved with decreasing tBOC ratio of the matrix resin. As the tBOC ratio increased, the resolution of the resist was better. SEM observation of the pattern profile was carried out to investigate the sensitivity and the resolution of the resist. The optimum tBOC ratio was 23.8%. As dissolution inhibitors, hydroquinone protected by a tert-butoxycarbonyl group (B-HQ) and isophthalic acid protected by a tert-butyl group (B-IP) are used. Dissolution inhibitors (B-HQ and B-IP) become dissolution promoters (HQ and IP) after exposure. The dissolution rate of the resist consisting of B-IP was faster than that of B-HQ in the exposed area. pK_a of IP is smaller than that of HQ, and the acidity of IP is higher than that of HQ. Therefore IP enhances the solubility of the matrix resin in the alkaline developer. We evaluated the dependence of sensitivity of the resist upon acid generators. Triphenylsulfonium triflate, Diphenyliodonium triflate, Triphenylsulfonium antimonate, and Diphenyliodonium antimonite were used. When iodonium ion was used as cation, the sensitivity of the resist was better. When antimonate ion as anion was used, the sensitivity of the resist was better.

Effect of Glass Transition Temperature on Heat-Responsive Gas Bubbles Formation from Polymers Containing *tert*-Butoxycarbonyl Moiety

Masashi ISEKI, Yuta HIRAOKA, Chu JING, Haruyuki OKAMURA, Eriko SATO and Akikazu MATSUMOTO
J. Appl. Polym. Sci., Vol. 135(19), Article No. 46252 (7 pages) (2018)

Various types of polymers containing *tert*-butoxycarbonyl (BOC) moiety as the typical protecting group of functional moieties have been used for the design of stimuli-responsive polymer materials. In this study, we investigated the heat-responsive deprotection behavior of BOC-containing polymers obtained by radical polymerization of 4-(*tert*-butoxycarbonyloxy)styrene (BSt) and copolymerizations of BSt with styrene and methyl acrylate. The deprotection of BOC groups accompanying the evolution of isobutene and carbon dioxide as gaseous products was monitored by thermogravimetric analyses at different temperature circumstances; that is, on heating at a rate of 10 °C/min and under isothermal conditions at various temperatures. The deprotection resulted in a significant decrease in the transmittance of visible light due to the formation of a large number of gas bubbles, that is, foaming, in the polymer films when a heating temperature was close to the glass transition temperature of the used polymer. The potential of BOC-containing polymers was also evaluated as the heat-responsive adhesive polymers for dismantlable adhesion.

Cross-Linked Polyperoxides for Photoremovable Adhesives

Eriko SATO, Chisato OMORI, Takashi NISHIYAMA and Hideo HORIBE
J. Photopolym. Sci. Technol., Vol. 31(4), pp. 511-515 (2018)

Photoremovability of cross-linked polyperoxides was investigated considering the application to dismantlable adhesives. Applying lap-shear stress on the glass joints bonded by the cross-linked polyperoxides, i.e., the alternating copolymer of 2-hydroxyethyl sorbate and oxygen cross-linked by tolylene 2,4-diisocyanate, resulted in the failure of the glass adherend. UV irradiation on the bonded glass joints more than 19 J/cm² resulted in a significant decrease in the lap-shear adhesion strength due to the photodegradation of the cross-linked polyperoxides, and the bonded glass joints were successfully debonded without breaking the glass adherends. The failure mode was the cohesive failure of the adhesive and the residue of the cross-linked polyperoxides heavily adhered on the both debonded glass adherends. The additional photoirradiation on the debonded glass adherends in tetrahydrofuran resulted in the significant removal of the adhered cross-linked polyperoxide due to the further photodegradation. After 150 J/cm² irradiation, the adhesive residues were completely wiped off from the glass adherends.

Control of Droplet Movement on an Inclined Wall with Saw-Toothed Wettability Pattern by Adding Ultrasonic Vibration

Kenji KATO, Hiroki TAMURA, Eriko SATO and Tatsuro WAKIMOTO
Exp. Fluid., Vol. 59(9), Article ID. 141 (10 pages) (2018)

This study deals with the control of the movement of liquid droplets rolling down an inclined plate based on the differences in the wettability of the plate. We used a photoreactive polymer poly(7-methacryloyloxy coumarin) (PMC) whose molecular structure can be changed reversibly to realize different wettabilities by ultraviolet irradiation. We proposed employing sawtooth patterns at boundaries between areas with different contact angles to control the droplet trajectory. Furthermore, we experimentally observed that the droplet moves along a line inclined to the direction of gravity. The droplet behavior can be analyzed using a theoretical model based on the droplet dynamics wherein the surface tension acting on the contact line and the gravitational force are considered. The theoretical results suggest that inclination from the gravitational direction can be increased if the advancing contact angle is reduced. In the experiments conducted herein, ultrasonic vibration was applied to the inclined plate to reduce the contact angle hysteresis. The results showed that the advancing contact angle actually decreased and that the droplet trajectory was controlled to realize motion along a line with inclination angle almost twice of that realized without vibration.

(This is identical to the abstract that appeared in the section of Mechanical and Physical Engineering)

Design of Pressure-Sensitive Dismantlable Adhesives Utilizing Living Radical Polymerization

Eriko SATO

In *Living Radical Polymerization: Recent Development of Synthesis and Application of Functional Polymers*, Edited by Akikazu MATSUMOTO, CMC Publishing, pp. 261-267 (323 pages in total) (2018) (in Japanese)

Reactive Polymers for the Design of Dismantlable Adhesives: From the Perspective of Dismantling Mechanisms

Eriko SATO and Akikazu MATSUMOTO

Kagaku To Kogyo, Vol. 92(1), pp. 7-12 (2018) (in Japanese)

Dismantlable Adhesives Using Light Irradiation

Eriko SATO

The Technical Association of Photopolymers, Japan, Newsletter, Vol. 82, pp. 5-7 (2018) (in Japanese)

Synthesis of Well-Defined Reactive Polymers and Their Application to Dismantlable Adhesives

Eriko SATO

Function & Materials (Kinou Zairyuu), Vol. 38(9), pp. 37-44 (2018) (in Japanese)

Development of Thermal Latent Reductants and Their Application to Accelerated Degradation of Polyperoxides (Hot Topics)

Chisato OMORI, Michihiro YURI, Eriko SATO, Takashi NISHIYAMA and Hideo HORIBE, *Kobunshi (High Polymers, Japan)*, Vol. 61(4), p. 180 (2018)

Cycloreversion Reaction of a Diarylethene Derivative at Higher Excited States Attained by Two-color Two-photon Femtosecond Pulsed Excitation

Hikaru SOTOME, Tatsuhiko NAGASAKA, Kanako UNE, Soichiro MORIKAWA, Tetsuro KATAYAMA, Seiya KOBATAKE, Masahiro IRIE, Hiroshi MIYASAKA

J. Am. Chem. Soc., Vol. 139(47), pp. 17159-17167 (2017)

Two-color, two-pulse femtosecond pulsed excitation was applied to the elucidation of the dynamics and mechanism of cycloreversion reaction of a diarylethene derivative in the higher excited states. Transient absorption spectroscopy under one-photon visible excitation revealed that the 1B state produced by the excitation undergoes the internal conversion into the 2A state with a time constant of 200 fs. Geometrical rearrangement of the 2A state takes place concomitantly with the vibrational cooling with a time constant of 3 ps. The resultant 2A state undergoes the transition into the conical intersection point in competition with nonradiative as well as radiative deactivation into the ground state with a time constant of 12 ps. The second pulse excitation of the 2A state, especially the geometrically relaxed 2A state, led to the significant enhancement of the cycloreversion reaction through the large reaction quantum yield of ca. 50–90% in the higher excited state (S_n state), while the excitation of the 1B state, leading to the S_n' state, did not induce such enhancement. By integrating with the excitation wavelength dependence of the second pump laser pulse, we discussed the chemical reactivity of diarylethene derivatives in terms of the symmetry of the electronic states.

Solid-state Fluorescence Behavior Induced by Photochemical Ring-opening Reaction of 1,2-Bis(3-methyl-5-phenyl-2-thienyl)perfluorocyclopentene

Tatsumoto NAKAHAMA, Daichi KITAGAWA, Hikaru SOTOME, Syoji ITO, Hiroshi MIYASAKA, Seiya KOBATAKE

Bull. Chem. Soc. Jpn., Vol. 91(2), pp. 153-157 (2018)

Crystals consisting of the closed-ring form of 1,2-bis(3-methyl-5-phenyl-2-thienyl)perfluorocyclopentene underwent a photochemical ring-opening reaction accompanying crystal fragmentation upon irradiation with visible light. The open-ring form crystal produced by the ring-opening reaction exhibited green fluorescence, whereas open-ring form crystals produced by recrystallization exhibit orange or yellow fluorescence depending on the polymorphic forms. The fluorescence quantum yield of the photogenerated open-ring form crystal was larger than that in *n*-hexane. The open-ring form exhibits different fluorescence colors depending on the intermolecular interaction in different states.

Photomechanical Motion of Diarylethene Molecular Crystal Nanowires

Fei TONG, Daichi KITAGAWA, Xinning DONG, Seiya KOBATAKE, Christopher J. BARDEEN
Nanoscale, Vol. 10(7), pp. 3393-3398 (2018)

Crystalline nanowires composed of the photochromic diarylethene derivative 1,2-bis(2,4-dimethyl-5-phenyl-3-thienyl)perfluorocyclopentene are prepared and characterized. 200 nanometer diameter wires with a length of 60 microns are grown by slow solvent annealing in a porous anodic aluminum oxide template. The nanowires are oriented crystals, as determined by X-ray diffraction measurements, and can be liberated by dissolving the template in acid. They exhibit pronounced bending when exposed to ultraviolet light that can be reversed by visible light irradiation. The bending–unbending sequence can be repeated for more than 10 cycles without fatigue. This robustness results from the ability of the nanowires to maintain their crystallinity during the forward and reverse reactions. The small diameter of these nanowires allows them to achieve curvatures that are at least 40 times greater (200 mm^{-1} versus 5 mm^{-1}) than those observed for micron-thick diarylethene needles. This first demonstration of photomechanical nanostructures based on diarylethene photochromism opens up the possibility of making more complicated structures composed of this high-performance photochrome.

Fluorescence On/Off Switching in Nanoparticles Consisting of Two Types of Diarylethenes

Tatsumoto NAKAHAMA, Daichi KITAGAWA, Hikaru SOTOME, Tuyoshi FUKAMINATO, Syoji ITO, Hiroshi MIYASAKA, Seiya KOBATAKE
ACS Omega, Vol. 3(2), pp. 2374-2382 (2018)

Single- and double-component nanoparticles consisting of two types of diarylethenes, 1,2-bis(3-methyl-5-phenyl-2-thienyl)perfluorocyclopentene (**1a**) and 1,2-bis(2-methyl-5-phenyl-3-thienyl)perfluorocyclopentene (**2a**), were fabricated by a reprecipitation method. Nanoparticles consisting of **1a** exhibited orange or green fluorescence depending on the fabrication condition and did not undergo any photocyclization reaction. In contrast, nanoparticles consisting of **2a** underwent photoreversible photochromic reactions upon alternating irradiation with ultraviolet and visible light. Nanoparticles composed of **1a** and **2a** exhibited fluorescence on/off switching with rapid switching speed and high on/off contrast, accompanying the photochromic reactions of **2a**. The dependence of fluorescence on/off switching properties on Förster distance and molar fraction was observed and quantitatively evaluated by a simplified model.

Control of Photomechanical Crystal Twisting by Illumination Direction

Daichi KITAGAWA, Hajime TSUJIOKA, Fei TONG, Xinning DONG, Christopher J. BARDEEN, Seiya KOBATAKE

J. Am. Chem. Soc., Vol. 140(12), pp. 4208-4212 (2018)

Photomechanical molecular crystals have been investigated as mesoscopic photoactuators. Here, we report how the photomechanical twisting of 1,2-bis(2-methyl-5-phenyl-3-thienyl)perfluorocyclopentene crystals depends on illumination direction. The ribbon-like crystal could be successfully prepared by a sublimation method. The crystal exhibited reversible photomechanical twisting upon alternating irradiation with UV and visible light. Moreover, changing the UV illumination direction with respect to the crystal resulted in different twisting modes, ranging from helicoid to cylindrical. Control of photomechanical crystal deformation by illumination direction provides a convenient and useful way to generate a variety of photomechanical motions from a single crystal.

Photomechanically Induced Magnetic Field Response by Controlling Molecular Orientation in 9-Methylantracene Microcrystals

Fei TONG, Wenjing XU, Maram AL-HAIDAR, Daichi KITAGAWA, Rabih O. AL-KAYSI, Christopher J. BARDEEN

Angew. Chem. Int. Ed., Vol. 57(24), pp. 7080-7084 (2018)

A surfactant-assisted seeded-growth method is used to form single-crystal platelets composed of 9-methylantracene with two different internal molecular orientations. The more stable form exhibits a photoinduced twisting, as observed previously for 9-methylantracene microribbons grown by the floating drop method. However, the newly discovered elongated hexagonal platelets undergo a photoinduced rolling-up and unrolling. The ability of the rolled-up cylindrical shape to trap superparamagnetic nanoparticles enables it to be carried along in a magnetic field gradient. The new photoinduced shape change, made possible by a novel surfactant-assisted crystal growth method, opens up the possibility of using light to modulate the crystal translational motion.

Photoinduced Crystal Shape Change Accompanying Thermodynamic Phase Transition (Division Topics, Division of Organic Crystals)

Seiya KOBATAKE

Chemistry & Chemical Industry (Kagaku To Kogyo), Vol. 71(1), p. 25 (2018) (in Japanese)

An unusual photomechanical behavior of a molecular crystal induced by combination of a photochromic reaction and a reversible single-crystal-to-single-crystal phase transition has been introduced in Japanese.

Organic Crystal that Changes its Shape in Response to Light and Heat

Daichi KITAGAWA, Seiya KOBATAKE

Chemical Industry (Kagaku Kogyo), Vol. 69(4), pp. 251-257 (2018) (in Japanese)

The thermodynamic phase transition and photomechanical behavior of diarylethene crystals have been reviewed in Japanese.

Soluble Expression in *Escherichia coli* of a Single-Domain Antibody–Tumor Necrosis Factor α Fusion Protein Specific for Epidermal Growth Factor Receptor

Tomohiro OSAKI, Takeshi NAKANISHI, Motoshi AOKI, Takahiro OMIZU, Daisuke NISHIURA, Masaya KITAMURA

Monoclon. Antib. Immunodiagn. Immunother., Vol. 37, pp. 20–25 (2018)

Tumor-targeted antibody-cytokine fusion proteins, called immunocytokines, are expected to be a useful platform for the development of effective antitumor therapeutic agents; however, their design and cost-efficient production remain as challenges. In this study, we constructed an antibody-cytokine fusion protein (Ia1-TNF α) comprising the single-domain antibody Ia1, which targets epidermal growth factor receptor (EGFR) overexpressed in epithelial tumors and a tumor necrosis factor α (TNF α) domain, which has antitumor activity. Ia1-TNF α was produced in a soluble form by using an *Escherichia coli* expression system, and after affinity purification of the culture supernatant, a yield of ~2 mg/L of cell culture was obtained. Gel filtration analysis showed that Ia1-TNF α existed predominantly as a trimer, which is consistent with the multimerization state of TNF α . Ia1-TNF α exhibited approximately 7-fold lower TNF α biological activity than that of TNF α itself. Flow cytometric analysis revealed that Ia1-TNF α specifically bound to EGFR-expressing tumor cells and that its binding activity was higher than that of monovalent Ia1, suggesting that the fusion protein bound to the tumor cells multivalently. Altogether, these results show that fusion of TNF α with a single-domain antibody could be a cost-efficient means of producing antitumor therapeutic agents.

Affinity Maturation of Humanized Anti-Epidermal Growth Factor Receptor Antibody Using a Modified

Phage-Based Open Sandwich Selection Method

Hideaki SANADA, Kazuki KOBAYASHI, Takamitsu MARU, Takeshi NAKANISHI, Mitsuo UMETSU, Ryutaro ASANO, Izumi KUMAGAI

Sci. Rep., Vol. 8, Article No. 5414 (9 pages) (2018)

Affinity maturation is one of the cardinal strategies for improving antibody function using *in vitro* evolutionary methods; one such well-established method is phage display. To minimise gene deletion, we previously developed an open sandwich (OS) method wherein selection was performed using only phage-displaying VH fragments after mixing with soluble VL fragments. The decrease in anti-EGFR antibody 528 affinity through humanization was successfully recovered by selecting VH mutants using this OS method. However, the affinity was not similar to that of parental 528. For further affinity maturation, we aimed to isolate VL mutants that act in synergy with VH mutants. However, the OS method could not be applied for selecting VL fragments because the preparation of soluble VH fragments was hampered by their instability and insolubility. Therefore, we initially designed a modified OS method based on domain-swapping of VH fragments, from added soluble Fv fragments to phage-displaying VL fragments. Using this novel Fv-added OS selection method, we successfully isolated VL mutants, and one of the Fv comprising VH and VL mutants showed affinity almost equivalent to that of parental 528. This method is applicable for engineering other VL fragments for affinity maturation.

Pharmaceutical Microcrystal Formation by Supersaturation Control with an Electrolyte

Muneki KISHIDA, Koichi IGARASHI, Masayuki AZUMA, Hiroshi OOSHIMA

Journal of Chemical Engineering of Japan, Vol. 51, pp. 1-6 (2018)

Methods to control the particle sizes of active pharmaceutical ingredients were investigated using sodium ecabet (Na-ECA) hydrate, which tends to generate large plate-like crystals, as a model compound. In batch-cooling crystallization in H₂O, the particle size decreased as the cooling rate was increased. Although the particle size reached 97 μm at a cooling rate of 40 °C/h, this may be too large for formulation without further physical processing. A series of semi-batch crystallization experiments was conducted by adding aqueous Na-ECA solution to aqueous NaCl. In these experiments, the particle sizes decreased to less than 7 μm as the NaCl concentration was increased to >1.2% w/w. The particles yielded by semi-batch crystallization showed improved particle size distributions compared to those obtained by the batch-cooling crystallization method. The solubility of Na-ECA hydrate decreased to less than 10% of that in pure water as the NaCl concentration was increased to 3.0% w/w. This solubility change enabled the production of a highly supersaturated environment, allowing facile generation of microcrystals with a narrow particle size distribution.

Behavior of *t*-Butoxycarbonyl-L-asparagine (Boc-Asn) during the Initial Stage of Crystallization

Koichi IGARASHI, Masako AOKI, Yoshiko MASUDA, Masayuki AZUMA, Hiroshi OOSHIMA

Journal of Chemical Engineering of Japan, Vol. 51, pp. 111-115 (2018)

The crystallization mechanism of amino acid derivative *t*-butoxycarbonyl-L-asparagine (Boc-Asn) was investigated. NMR spectroscopy was used to observe the behavior of Boc-Asn molecules in under- and supersaturated solution. Nuclear Overhauser effect (NOE) NMR measurements were performed to provide information concerning the intra- or intermolecular access of a particular hydrogen atom to other hydrogen atoms in solution. We compared the interactions identified by NOE measurements for under- and supersaturated solutions of Boc-Asn with those in the crystal, as determined by X-ray analysis. According to the X-ray analysis, intramolecular NOE should not be observed, but intermolecular NOE might be observed between the methyl protons of the *t*-butoxycarbonyl group and the protons belonging to other functional groups. The time course of the NOE intensity was followed for three solutions with different saturation ratios S (= concentration of solute/solubility). For undersaturated and nearly saturated conditions ($S = 0.8$ and 1.12 at 0 °C), the NOE intensity did not change for at least for 250 h. However, for the supersaturated solution ($S = 1.62$ at 10 °C), the NOE intensity increased suddenly and rapidly after about 120 h, and no crystals were observed during the NOE measurements. As the observed NOEs agreed with those expected from the arrangement of molecules in the

crystal, it was suggested that Boc-Asn molecules aggregated after about 120 h with the same structure as that in the crystal. In addition to the behavior of the Boc-Asn solution before nucleation, we also investigated the effect of aggregation on the crystallization process. Solutions that were preincubated at 10 °C for various periods were further cooled and crystallized at -30 °C. It was found that when the solution was preincubated under the supersaturated condition for a long time before crystallization, nucleation was enhanced, and consequently, the crystal size distribution became homogeneous.

S-allyl-glutathione improves experimental liver fibrosis by regulating Kupffer cell activation in rats

Shigekazu TAKEMURA, Hideki AZUMA, Mayuko OSADA-OKA, Shoji KUBO, Toshihiko SHIBATA, Yukiko MINAMIYAMA

Am. J. Physiol Gastrointest. Liver Physiol., Vol. 314(2), pp. G150-G163 (2018)

S-allyl-glutathione (SAG) is one of the metabolites of diallyl sulfide (DAS), a component of garlic. DAS has shown preventative effects on carcinogenesis in animal models. However, whether synthetic SAG can improve liver fibrosis has not been investigated. We examined the potential preventive effects of SAG on acute and chronic models of liver fibrosis by chronic carbon tetrachloride (CCl₄) administration. SAG inhibited liver fibrogenesis induced by CCl₄ in a dose-dependent manner and reduced heat shock protein-47 (HSP47), a collagen-specific chaperone, and other fibrosis markers. In fibrosis regression models, after administration of either CCl₄ for 9 wk or dimethyl nitrosamine (DMN) for 6 wk, SAG markedly accelerated fibrolysis in both models. In the regression stage of DMN-treated liver, SAG normalized the ratio of M2 phenotype (expression of mannose receptor) in Kupffer cells (KCs). Consistent with these results, the culture supernatants of SAG-treated M2-phenotype KCs inhibited collagen- α_1 (I) chain (COL1A1) mRNA expression in primary culture-activated rat hepatic stellate cells (HSCs). However, SAG did not directly inhibit HSC activation. In an acute model of CCl₄ single injection, SAG inhibited hepatic injury dose dependently consistent with the inhibited the elevation of the bilirubin and ALT levels. These findings suggest that SAG could improve the fibrogenic and fibrolysis cascade via the regulation of excess activated and polarized KCs. SAG may also serve as a preventive and therapeutic agent in fibrosis of other organs for which current clinical therapy is unavailable. **NEW & NOTEWORTHY** S-allyl-glutathione (SAG) is a metabolite of diallyl sulfide, a component of garlic. SAG increased hepatic glutathione levels and GSH-to-GSSG ratio in normal rats. SAG treatment before or after liver fibrosis from chronic CCl₄ administration improved liver fibrosis and regression. SAG decreased heat shock protein-47 (HSP47), a collagen-specific chaperone, and other fibrosis markers in CCl₄-treated livers. SAG-treated Kupffer cell conditioned medium also inhibited collagen- α_1 (I) chain (COL1A1) mRNA expression and other markers in primary culture hepatic stellate cells.

A new method to purify poly- γ -glutamic acid using gemini quaternary ammonium salts and characterization of its ionic complex.

Tao LIU, Hirobumi NOBESHIMA, Yoshihiro OJIMA, Masayuki AZUMA,

J. Chem. Eng. Jpn., Vol. 51(5), pp. 431-437 (2018)

Poly- γ -glutamic acid (γ -PGA) is a water-soluble, nontoxic biodegradable polymer. It is extensively utilized in medicines, foodstuffs, and cosmetics, as well as in water treatment. Highly pure γ -PGA is required for various purposes. In many cases, γ -PGA is produced by microbes of *Bacillus* sp. However, an increase in the viscosity of the culture broth is one of the major problems of γ -PGA production as higher viscosity makes the separation and purification steps difficult. Herein we propose a novel method to obtain pure γ -PGA using gemini quaternary ammonium salts (GQASs). The quaternary ammonium cation of GQASs binds to the carboxylic acid group of γ -PGA via an ionic bond, following which water-insoluble and antimicrobial complexes are formed. These complexes are obtained in the aqueous solution, which were resolved in ethanol solution. With an increase in the added amount of GQAS, the negative charge of the complex decreased in the aqueous solution. Subsequently, the GQAS within the complexes was dissociated by the addition of NaCl, affording pure γ -PGA in a high yield.

Moreover, the complexes were shown to have antibacterial activity and adhered to glass, indicating that the complex itself has a utility value.

Characterization of D-succinylase from *Cupriavidus* sp. P4-10-C and its application in D-amino acid synthesis.

Yosuke SUMIDA, Sachio IWAI, Yoshiaki NISHIYA, Shinya KUMAGAI, Toshihide YAMADA, Masayuki AZUMA,

J. Biosci. Bioeng., Vol. 125(3), pp. 282-286 (2018)

D-amino acids are important building blocks for various compounds, such as pharmaceuticals and agrochemicals. A more cost-effective enzymatic method for D-amino acid production is needed in the industry. We improved a one-pot enzymatic method for D-amino acid production by the dynamic kinetic resolution of *N*-succinyl amino acids using two enzymes: D-succinylase (DSA) from *Cupriavidus* sp. P4-10-C, which hydrolyzes *N*-succinyl-D-amino acids enantioselectively to their corresponding D-amino acid, and *N*-succinyl amino acid racemase (NSAR, EC.4.2.1.113) from *Geobacillus stearothermophilus* NCA1503. In this study, DSA and NSAR were purified and their properties were investigated. The optimum temperature of DSA was 50°C and it was stable up to 55°C. The optimum pH of DSA and NSAR was around 7.5. In D-phenylalanine production, the optical purity of product was improved to 91.6% ee from the examination about enzyme concentration. Moreover, 100 mM *N*-succinyl-DL-tryptophan was converted to D-tryptophan at 81.8% yield with 94.7% ee. This enzymatic method could be useful for the industrial production of various D-amino acids.

Large-scale culture of a megakaryocytic progenitor cell line with a single-use bioreactor system.

Retno W. NURHAYATI, Yoshihiro OJIMA, Takeaki DOHDA, Masahiro KINO-OKA,

Biotechnol. Prog., Vol. 34(2), pp. 362-369 (2018)

The increasing application of regenerative medicine has generated a growing demand for stem cells and their derivatives. Single-use bioreactors offer an attractive platform for stem cell expansion owing to their scalability for large-scale production and feasibility of meeting clinical-grade standards. The current work evaluated the capacity of a single-use bioreactor system (1 L working volume) for expanding Meg01 cells, a megakaryocytic (MK) progenitor cell line. Oxygen supply was provided by surface aeration to minimize foaming and orbital shaking was used to promote oxygen transfer. Oxygen transfer rates (k_{La}) of shaking speeds 50, 100, and 125 rpm were estimated to be 0.39, 1.12, and 10.45 h⁻¹, respectively. Shaking speed was a critical factor for optimizing cell growth. At 50 rpm, Meg01 cells exhibited restricted growth due to insufficient mixing. A negative effect occurred when the shaking speed was increased to 125 rpm, likely caused by high hydrodynamic shear stress. The bioreactor culture achieved the highest growth profile when shaken at 100 rpm, achieving a total expansion rate up to 5.7-fold with a total cell number of $1.2 \pm 0.2 \times 10^9$ cells L⁻¹. In addition, cells expanded using the bioreactor system could maintain their potency to differentiate following the MK lineage, as analyzed from specific surface protein and morphological similarity with the cells grown in the conventional culturing system. Our study reports the impact of operational variables such as shaking speed for growth profile and MK differentiation potential of a progenitor cell line in a single-use bioreactor.

Metabolic Engineering of *Escherichia coli* KO11 with NADH regeneration system for enhancing ethanol production.

Fernanda M. KASHIWAGI, Yoshihiro OJIMA, Masahito TAYA,

J. Chem. Eng. Jpn., Vol. 51(3), pp. 264-268 (2018)

Cofactor regulation for the production of reduced metabolites, such as ethanol, plays an important role regarding the metabolic pathways of microorganisms. In this study, intracellular NADH/NAD⁺ ratio in the ethanologenic strain *Escherichia coli* KO11 was increased by overexpression of formate dehydrogenase from *Mycobacterium vaccae*. In order to avoid the generation of pyruvate-derived byproducts, genes coding for lactate and acetate producing pathways were successfully deleted using the genome editing based on a CRISPR-Cas9 system. In the

culture of constructed strain, NADH regeneration system caused an increase in intracellular NADH/NAD⁺ ratio in the presence of formate, leading to enhanced ethanol production 36% more than the original KO11 strain in culture for 24 h. The detailed investigation revealed that the transient pyruvate accumulation plays a key role for the enhanced ethanol production by NADH regeneration system.

EB1-binding-myomegalin protein complex promotes centrosomal microtubules functions

Habib BOUGUENINA, Daniele SALAUN, Aurelie MANGON, Leslie MULLER, Emilie BAUDELET, Luc CAMOIN, Taro TACHIBANA, Sarah CIANFERANI, Stephane AUDEBERT, Pascal VERDIER-PINARD, Ali BADACHE

Proc. Natl. Acad. Sci. USA., Vol. 114(50), pp. E10687-E10696 (2017)

Control of microtubule dynamics underlies several fundamental processes such as cell polarity, cell division, and cell motility. To gain insights into the mechanisms that control microtubule dynamics during cell motility, we investigated the interactome of the microtubule plus-end-binding protein end-binding 1 (EB1). Via molecular mapping and cross-linking mass spectrometry we identified and characterized a large complex associating a specific isoform of myomegalin termed "SMYLE" (for short myomegalin-like EB1 binding protein), the PKA scaffolding protein AKAP9, and the pericentrosomal protein CDK5RAP2. SMYLE was associated through an evolutionarily conserved N-terminal domain with AKAP9, which in turn was anchored at the centrosome via CDK5RAP2. SMYLE connected the pericentrosomal complex to the microtubule-nucleating complex (γ -TuRC) via Galectin-3-binding protein. SMYLE associated with nascent centrosomal microtubules to promote microtubule assembly and acetylation. Disruption of SMYLE interaction with EB1 or AKAP9 prevented microtubule nucleation and their stabilization at the leading edge of migrating cells. In addition, SMYLE depletion led to defective astral microtubules and abnormal orientation of the mitotic spindle and triggered G1 cell-cycle arrest, which might be due to defective centrosome integrity. As a consequence, SMYLE loss of function had a profound impact on tumor cell motility and proliferation, suggesting that SMYLE might be an important player in tumor progression.

A statistical image analysis framework for pore-free islands derived from heterogeneity distribution of nuclear pore complexes

Yasuhiro MIURA, Satoko TAKEMOTO, Taro TACHIBANA, Yutaka OGAWA, Masaomi NISHIMURA, Hideo YOKOTA, Naoko IMAMOTO

Sci. Rep., Vol. 7, Article No. 16315 (14 pages) (2017)

Nuclear pore complexes (NPCs) maintain cellular homeostasis by mediating nucleocytoplasmic transport. Although cyclin-dependent kinases (CDKs) regulate NPC assembly in interphase, the location of NPC assembly on the nuclear envelope is not clear. CDKs also regulate the disappearance of pore-free islands, which are nuclear envelope subdomains; this subdomain gradually disappears with increase in homogeneity of the NPC in response to CDK activity. However, a causal relationship between pore-free islands and NPC assembly remains unclear. Here, we elucidated mechanisms underlying NPC assembly from a new perspective by focusing on pore-free islands. We proposed a novel framework for image-based analysis to automatically determine the detailed 'landscape' of pore-free islands from a large quantity of images, leading to the identification of NPC intermediates that appear in pore-free islands with increased frequency in response to CDK activity. Comparison of the spatial distribution between simulated and the observed NPC intermediates within pore-free islands showed that their distribution was spatially biased. These results suggested that the disappearance of pore-free islands is highly related to de novo NPC assembly and indicated the existence of specific regulatory mechanisms for the spatial arrangement of NPC assembly on nuclear envelopes.

The STK35 locus contributes to normal gametogenesis and encodes a lncRNA responsive to oxidative stress

Yoichi MIYAMOTO, Penny AF WHILEY, Hoey Y GOH, Chin WONG, Gavin HIGGINS, Taro TACHIBANA, Paul MCMENAMIN, Lynne MAYNE, Kate L LOVELAND

Biol. Open., Vol. 7(8), pii: bio032631. doi: 10.1242/bio.032631. (2018)

Serine/threonine kinase 35 (STK35) is a recently identified human kinase with an autophosphorylation function, linked functionally to actin stress fibers, cell cycle progression and survival. *STK35* has previously been shown to be highly expressed in human testis, and we demonstrated its regulation by nuclear-localized importin α 2 in HeLa cells. The present study identifies progressive expression from the *STK35* locus of two coding mRNA isoforms and one long non-coding RNA (lncRNA) in mouse testis during spermatogenesis, indicating their tightly controlled synthesis. Additionally, lncRNA transcripts are increased by exposure to oxidative stress in mouse GC-1 germ cell line. *STK35* knockout (KO) mice lacking all three RNAs are born at sub-Mendelian frequency, and adults manifest both male and female germline deficiency. KO males exhibit no or partial spermatogenesis in most testis tubule cross-sections; KO ovaries are smaller and contain fewer follicles. Eyes of KO mice display phenotypes ranging from gross deformity to mild goniodysgenesis or iridocorneal angle malformation, to overtly normal. These findings demonstrate the tight regulation of transcription from the *STK35* locus and its central importance to fertility, eye development and cell responses to oxidative stress.

Architecture and Building Engineering

COMPARISON STUDY OF ELASTO-PLASTIC BEHAVIOR ON STATIC AND DYNAMIC RESPONSES FOR SINGLE LAYER LATTICE DOMES UNDER VERTICAL LOADING

Yoshiya TANIGUCHI, Tomoya MATSUI and Susumu YOSHINAKA

J. Struct. Constr. Eng., AIJ, Vol. 83 No. 747, 709-716, May, 2018

This paper focuses on the elasto - plastic behavior of static and dynamic responses for single layer lattice domes, which are subjected to vertical loads. The purpose is to make clear the relationship between seismic responses and static responses from the view point of input strain energy properties after and before yielding, and to estimate bearable seismic levels with the information of static elasto - plastic behaviors. The static response compared is the relationships between equivalent velocities of strain energies and displacements. The dynamic response compared is that between earthquake input acceleration PGA and equivalent velocities of strain energies.

Impact test of an arch model using TMDs with initial displacement

Susumu YOSHINAKA and Yoshiya TANIGUCHI

Proceedings of the IASS Annual Symposium 2017, "Interfaces: architecture. engineering. science", September 25 - 28th, 2017, Hamburg, Germany, Session #27, ID 9205, pp.1-10, (2017)

TMDs (Tuned Mass Dampers) show superior control performance for harmonic responses, but have limited capacity for transient responses. To control transient responses effectively, we propose TMDs with initial displacement. In our previous study, we formulated an equation for initial conditions to release initial TMD displacement. This equation is based on the principle that, under a specific structural initial condition, by giving specific initial displacement to a TMD, the first modal response with low modal damping is eliminated while the second modal response with high modal damping is only oscillated on a two-degree-of-freedom system. This paper describes a vibration test using an arch model under impulse loading to verify the control performance of the proposed method experimentally. From test results, we can see that the TMD model showed high control performance. On the other hand, the control performance is very sensitive to the length and the release moment of the TMD's initial displacement.

Examination of failure wind speed for roof structure of wooden houses in the Enhanced-Fujita scale

Eri GAVANSKI, Gregory A. KOPP (Univ. of Western Ontario)

Proc. of 9th Asia-Pacific Conference on Wind Engineering, (3-7 December 2017, Auckland, New Zealand)

Under tornadic wind events, residential houses are frequently damaged and one of the components of houses which commonly fail are roof-to-wall-connections (RTWC). RTWC failure needs to be mitigated because of its significant damage on insured loss. The Enhanced-Fujita (EF) scale, which is utilized to identify the tornado scale, has only a single damage indicator (DI) for residential houses with little description of structural details of the houses. Since it is well known that building shape and dimensions affect wind pressure acting on the house, more structural description of houses may need to be specified for the Degrees-of-Damage (DOD) in the EF-Scale. In order to examine this point, the present study performed fragility analysis for RTWC failure of residential house considering a wide variety of parameters believed to affect failure wind speeds, which include parameters of roof slope, shape and height, surrounding terrain, neighbouring houses and the presence of dominant opening on a wall.

Surrounding effect on internal wind pressure and correlation between external-internal pressures on low-rise buildings

Eri GAVANSKI, Daisuke KONNO (National Institute of Technology, Hachinohe College), Yasushi Uematsu (Tohoku Univ.)

International Workshop on Wind-Related Disasters and Mitigation, (11-14 March 2018, Sendai, Japan)

The effect of surrounding buildings on internal pressure coefficient, C_{pi} , and the correlation between C_{pi} and external pressure coefficient, γ , were examined by performing wind tunnel tests using a flat-roofed low-rise building model. It is found that its effect is mainly shielding and is significant especially on C_{pi} . Simple fragility analysis was performed in order to understand its effect more clearly. This result indicates that the use of C_{pi} and γ obtained from the isolated building underestimates the roof panel failure wind speed for surrounded building by the degree that it can affect the tornado rating using the EF-scale.

Numerical investigation and accuracy verification of indoor environment for an impinging jet ventilated room using computational fluid dynamics

Tomohiro KOBAYASHI, Kazuki SUGITA, Noriko UMEMIYA, Takashi KISHIMOTO (Kinden Corporation), Mats SANDBERG (University of Gavle, Sweden)

Building and Environment, Vol.115, 251-268, (2017)

The impinging jet ventilation (IJV) system has been proposed as an air distribution strategy to provide a better thermal environment with a medium supply momentum than displacement ventilation (DV) system. However, no simplified prediction method that is practically applicable has been established to date. The ultimate goal of this study is to establish a calculation model to predict the vertical temperature profile in an IJV system. The authors aim to propose a one-dimensional model, where the room is divided into several control volumes. To perform this, the turbulent thermal diffusion between control volumes needs to be well understood. Therefore, a knowledge about the effect of each design factor such as the supply air velocity on the turbulent thermal diffusivity needs to be acquired through a parametric study. Computational Fluid Dynamics (CFD) is effective for this purpose. As first step, the accuracy of CFD simulations is verified by conducting a full-scale experiment. The velocity profiles inside the impinging jet and the indoor temperatures are measured and compared with the CFD results. It is shown that the shear-stress transport- ω model has a sufficient accuracy to analyse the target room, and an appropriate grid layout is established as well. The convection–radiation coupling CDF prediction where the external temperature is used as a boundary condition is adopted as the best method for numerical study in this research. Finally, a parametric study on the supply air velocity is performed based on this setting and its effect on the thermal stratification is presented.

Light environment evaluation under different orders and speeds of illuminance change

Noriko UMEMIYA, Tetsuro ARAI, Tamami SUZUKI and Tomohiro KOBAYASHI

Proceedings of the 10th Asia Lighting Conference, 72-77, Shanghai, (2017)

For this study, the light environment and subjective impressions of observers are evaluated and compared as the illuminance level of an experimental room is changed between light and dark with different orders and speeds. Effects of mood states on the evaluation were also assessed. Results of statistical analyses indicated the following results. 1) In darkening experiments, deterioration of comfort, preference and sense of coziness are less by instantaneous change than by gradual change. 2) In brightening experiments, improvement of comfort, preference, sense of coziness and clearness are greater by instantaneous change than by gradual change. 3) When changed gradually, comfort and preference deteriorate after darkening. The sense of brightness decreases and the sense of glare increases after lightening for subjects of high vigour in mood states. 4) When changed instantaneously, a mood state does not affect the light environment

Light evaluation in high and low mood states

Noriko UMEMIYA and Tamami SUZUKI

Proceedings of the Midterm Conference of CIE, 687-693, Jeju, (2017)

Effects of mood states on evaluation of light environment evaluation were inspected in this study. Light conditions were set in two levels, light (2200 lux) and dark (340 lux). Light level was changed from light to dark or dark to light in an experiment and effects of change order were also considered. Mood states were calculated by Profile of Mood States score which was developed for clinical use. Subjects were classified into high and low mood states by limits of 25, 50 and 75 percentile values of mood score. As a results, tension–anxiety mood was related to the evaluation of glare and comfort. Vigour mood was related to the brightness, comfort, preference and performance. Anger-hostility mood was related to the glare and performance. Depression mood was related to the brightness and glare. However, fatigue and confusion mood were not related to the evaluation of light environment at all.

Comparison of thermal environment, thermal sensation and sleep quality among thermal control patterns in summer sleeping rooms

Noriko UMEMIYA, Yoshiki TACHIBANA, Tomohiro KOBAYASHI, Yusuke NAKAYAMA and Hirona BESSHO

Abstract book of the 17th International Conference on Environmental Engineering, 131, Kobe, (2017)

This survey, with 75 respondents on a total of 343 peak summer days for three years in apartments in Osaka, Japan, compared sleep quality for three thermal control patterns: air-conditioning through the night, window opening through the night, and partial air-conditioning using a timer. Results revealed the following: 1) The outdoor temperature was higher in PA than in WO ($p < 0.01$) and higher in AC than WO ($p < 0.05$). 2) The indoor SET*_{total} was higher in WO than in PA ($p < 0.01$) and higher in PA than in AC ($p < 0.01$). Nevertheless, no significant difference was found among thermal sensations associated with the three conditions. Moreover, sleep quality measured by OSA test was higher, it means that the sleep quality was better, in WO than in AC ($p < 0.01$). 3) As Figure 1 shows, OSA score was low and unrelated to the indoor SET*_{total} in AC. It worsened as the indoor thermal environment

became hotter in WO. But it became better in PA when indoor SET*_total exceeded 31°C. 4) Sleep quality was better in PA than in WO and AC when the outdoor temperature exceeded 27.9°C.

Urban Design and Engineering

Extending the Verbal Map Navigation System for Visually-impaired People Focusing on Byway Information and NFC Interface

Yuki ADACHI, Takashi UCHIDA, Yoshiki SUGA and Yumie SAWADA

Japan Society of Traffic Engineers, Papers on Traffic Engineering, No. 37, pp. 367-372 (2017) (in Japanese)

A System of Assisting Verbal Map Description of Pedestrian Town Navigation for Universal Situations

Yumie SAWADA, Takashi UCHIDA and Yuki ADACHI

Japan Society of Civil Engineers, Proceedings of Infrastructure Planning, No. 56, pp.125_1-7 (2017) (in Japanese)

It is very hard to use walking navigation by smartphones and AR app for visually-impaired people unlike sighted people. Visually-impaired people can't walk a strange land alone. They can't enjoy walking even the well know land because of not knowing the information of the facilities not to usually use and scene of a town changing every day. Voice AR navigation has been studied from the point of view of safety, pace of mind and enjoying walk in order to overcome this disparity.

This study builds a system that allows anyone to easily description Verbal Map. These are helping expansion of navigation area and make more useful AR app for visually-impaired people.

Posterior Evaluation of the Small-Size River Development for the Nature- Friendly Environment and the Water Amenity in the Built-Up Area— Analyses Based on the Actual Use Situation

Yasumasa FUKUSHIMA and Takashi UCHIDA

Japan Society of Civil Engineers, Proceedings of Infrastructure Planning, No. 56, pp. 218_1-10 (2017) (in Japanese)

In recent years the development of the urban river has been focusing on efforts for the environment and the water amenity besides the flood control and the water utilization, in some cases however, the residents along the river have failed to value and then water amenity has made little progress.

This paper takes a case of the waterfront development of the small size river in an emerging built-up area. Going through several years after the project implementation, we take hold of the actual condition and the attitudes of residents by means of hearing survey to the inhabitants. This study performs analyses on the results of actual condition survey towards the smooth implementation of the enterprise and the consensus formation and in urban riverside development considering development methods in order to promote the utilization with high evaluations from the inhabitants as concrete strategies.

Method of Evaluating Dialogue Robots for Visually Impaired and Elderly People

Hiroko MATSUMOTO, Takashi UCHIDA and Kanami BESSYO

Osaka City University, Memoirs of the Faculty of Engineering, Vol. 58, pp.13-24 (2017)

To support the daily living of visually impaired people, we have been conducting research on pedestrian navigation, mainly audio guidance by a "Verbal map." In collaboration with "Verbal map," we plan a dialogue robot that can guide a person in a plaza space. As the first step, this study establishes an evaluation experiment to quantify the degree of pleasant feeling a person has when talking with a robot.

This paper first presents the research background and objectives. Chapter 2 describes the evaluation experiment method. In chapter 3, using results of the experiment conducted, we specifically examine a function evaluation questionnaire and measurements of the psychological load. Finally, this report provides a summary of the research.

Actual Conditions and Major Issues on Basic Scheme of Public Transportation

Yusuke TAKAHASHI, Yasuo HINO, Takashi UCHIDA and Ayaka ARIMOTO

Japan Society of Traffic Engineers, Papers on Traffic Engineering, No. 37, pp.561-564 (2017) (in Japanese)

Effects and Major Issues of Arranging for Bicycle Parking Problems in Residential and Commercial Mixed Area

Yuriko YOSHIKANE, Yasuo HINO, Takashi UCHIDA and Yurie ISHIMURA

Japan Society of Civil Engineers, Proceedings of Infrastructure Planning, No. 56, pp.217_1-4 (2017) (in Japanese)

Illegal parked bicycle problem near rail station area has improved by both supplying bicycle parking spaces and removing illegal parked bicycles. On the other hand, in city center it has not still improved. In these areas, as there are many stakeholders such as residents, shop owners, employee and visitors, it may be not easy to improve the bicycle problems, because of differences of their needs. Therefore, it must be essential to investigate the possibility of public involvement among them.

As a result of a series of studies in corporation with local government and local community, an activity of arranging parked bicycles by “cycle supporter” has introduced based on some workshop activities as a typical public involvement. Then, in this paper, we not only investigated the awareness and effect of the activity of arranging parked bicycles, but also made the desirable issues and presented the possibility of further activities, in future.

Effects and Further Required Issues on Progressing Measures to Promote Safer Use of Bicycles by Enacting the Ordinance in Local Government

Yasuyuki TAKEDA, Yasuo HINO, Takashi UCHIDA and Daiki DOUBATA

Japan Society of Civil Engineers, Proceedings of Infrastructure Planning, No. 56, pp.80_1-5 (2017) (in Japanese)

Recently the movement of enacting the ordinance for promoting safer use of bicycles has been progressing in local government, because of increasing the ration of traffic accidents and illegal parking and so on. However, the background and purpose and effects for enacting ordinance, and further required issues in future, according to feature of each local government, have not been yet clear. Then in this study, in corporation with the local governments enacted the ordinance for safer use of bicycles, the background and purpose effects for enacting ordinance, the important items, the possibility of progressing measures and so on were investigated by questionnaire survey. As a result, it was revealed that the role of relevant organizations and progress of road safety education were not only most important but also they have not been developed in common. In addition, further required issues were proposed based on these findings.

A Study on Identifying Opportunities and Barriers to Use Adaptive Cycle For People with Travel Difficulties

Takuya KONISHI and Nagahiro YOSHIDA

Japan Society of Civil Engineers, Proceedings of Infrastructure Planning, No. 56, pp. 218_1-10 (2017) (in Japanese)

In late years, a tool for traffic to be similar to a bicycle has been developed, and there are the things which two-crew is possible, which have an electric assist, and which have three wheels. The activity in the scene which is not usable by car including the case to go to the small place that a case and the car which do not have a driver's license do not put is expected, and it is thought possibility as the new transportation of the people for with travel difficulties. However, there are few examples that is examined about the use of adaptive cycling by the people for with travel difficulties is possible, and it is necessary to study about the possibility. In this study, I do a hearing survey to the welfare company and experiment with using adaptive cycling, and I decided to grasp the situation that were hard to go out, the potential use opportunity of adaptive cycling, and the problem for using it.

Latent opportunities for the use of two-rider bicycles and associated challenges based on assessments of its use by people with reduced mobility

Takuya KONISHI and Nagahiro YOSHIDA

The 6th Japan Cycling Congress, Poster session, (2017) (in Japanese)

A Case Study on the Issues of Bicycle Safety Education for Children from the Comparative Views of Responsible Organization

Syuta HOSHIRO and Nagahiro YOSHIDA

The 6th Japan Cycling Congress, Poster session, (2017) (in Japanese)

Traffic Accident Risk Analysis Along Trunk Roads using Emergency Braking Event from Floating Car Data

Toshiki KUBOTA, Nagahiro YOSHIDA

The Annual Meeting of Traffic Science, 2 Pages, (2017) (in Japanese)

A Study on Safety Education of Bicycle for Parents with Infants and Elderly People

Kumiko TANIUCHI, Itaru FUJIE, Nagahiro YOSHIDA, Takao YANAGIHARA, Noriaki FUJIMOTO, and Nobuhiko MATSUMURA

Traffic Science, Vol. 48, No. 2, pp.25-29, (2017) (in Japanese)

Understanding the Nature of Walking and Cycling for Transport in Japan

Pola BERENT and Nagahiro YOSHIDA

Osaka City University, Memoirs of the Faculty of Engineering, Vol. 58, pp.25-43 (2017)

The following document is a summary of the existing academic articles available in English. The literature review was conducted for the purpose of gaining an understanding of cycling and walking behaviors in Japan. This was background research in order to acquire theoretical knowledge for the further study, which aimed to establish whether people in Japan (where cyclists regularly mix with pedestrians on sidewalks) show different attitudes and perceptions of comfort while travelling on segregated or unsegregated shared-use paths and to identify whether it is dependable purely on technical aspects of path design (i.e. physical characteristics) or/and whether the travel behavior generated by traffic law has impacts on it.

Experimental Study on Measuring Level of Stress for Bicycle Facilities using Vital Reactions

Katsumasa TATSUNO and Nagahiro YOSHIDA

Japan Society of Civil Engineers, Proceedings of the annual meeting in Kansai, 2 pages (CD-ROM) (2018) (in Japanese)

Evaluation of Road Space Reallocation for Pedestrian and Cyclists using Level of Service Concept at Midosuji Street in Osaka

Haruka KAWACHI, Takashi UCHIDA and Nagahiro YOSHIDA

Japan Society of Civil Engineers, Proceedings of the annual meeting in Kansai, 2 pages (CD-ROM) (2018) (in Japanese)

A Case Study about the Impact of Traffic Signal Installation on Mixed Traffic Conditions in Phnom Penh, Cambodia

Kazuto IMAI and Nagahiro YOSHIDA

Japan Society of Civil Engineers, Proceedings of the annual meeting in Kansai, 2 pages (CD-ROM) (2018) (in Japanese)

Basic Analysis of On-Street Parking Behaviors using Floating Car Data in Osaka Central Areas

Kensuke MEGUMI and Nagahiro YOSHIDA

Japan Society of Civil Engineers, Proceedings of the annual meeting in Kansai, 2 pages (CD-ROM) (2018) (in Japanese)

Evaluation of Road Space Reallocation for Pedestrian and Cyclists using level of service concept at Midosuji Street in Osaka

Haruka KAWACHI and Nagahiro YOSHIDA

The City Planning Institute of Japan, Kansai Branch, Proceedings of The City Planning Institute of Japan, Kansai Branch, 2018, Volume 16, Pages 29-32, (2018) (in Japanese)

The road space reallocation project in the main street of Osaka, Midosuji has started since 2017 to realize the concept of human-centered urban space in response to the change of social trend and conditions. The initial pilot project has been undertaken in the way of increasing the space for pedestrians and cyclists. In addition, a comfortable space in the reallocated section has been created as an experimental study. While the Level of Service concept was widely employed to evaluate user comfort issues in the transportation field but it is unknown that the LOS concept could apply to these space differences and evaluate the reallocation effect correctly. Therefore the objective of this study is to evaluate the effect of space reallocation on street users using the LOS concept through questionnaire and observational surveys. 3 different street sections including a narrow mixed pavement, a wide shared pavement, and a wide shared pavement with comfortable space were compared focusing on the difference between subjective and objective comfort.

Introduction of Inclusive Cycling and Cycle Training in London

Itaru FUJIE, Takao YANAGIHARA, Takuya KONISHI and Nagahiro YOSHIDA

The 7th Japan Cycling Congress, Poster session, (2018) (in Japanese)

Latent opportunities for the use of two-rider bicycles and associated challenges based on assessments of its use by people with reduced mobility

Takuya KONISHI and Nagahiro YOSHIDA

The 7th Japan Cycling Congress, Poster session, (2018) (in Japanese)

A Study on a Numerical Model of Two-Phase Gas-Liquid Flow Induced by a Moving Solid with High Accuracy

Hiroshi MATSUMOTO, Takaaki SHIGEMATSU

Journal of Japan Society of Civil Engineers, Ser. B2 (Coastal Engineering), Vol. 73(2), pp. I_865-I_870 (2017)

In this study, a numerical model for calculation of fluid motion induced by an object penetrating the gas-liquid interface by combining the Immersed Boundary Method and the Level Set Method was presented. A new method of satisfying the boundary condition at the Lagrange points near the gas-liquid interface with high accuracy is described. After validating of tracing method of the gas-liquid interface by calculated result on sloshing in rectangular tank, it is presented that calculated result of the Strouhal number and distribution of time-mean velocity in wake of a circular cylinder agrees to experimental result with reasonable accuracy. Finally, calculated results of vortex pattern induced around a horizontally-oscillating vertical circular cylinder in stationary fluid under the condition of the Keulegan-Carpenter number = 9 and the Reynolds number = 1,000 is presented.

A Study on Splash Generated by Breaking Wave Acting on a Vertical Wall

Yuki YASUHIRA, Takaaki SHIGEMATSU, Masahide TAKEDA

Journal of Japan Society of Civil Engineers, Ser. B2 (Coastal Engineering), Vol. 73(2), pp. I_835-I_840 (2017)

In order to take countermeasures against salt damage of pier superstructure economically and efficiently, it is indispensable to clarify the wave conditions of splash generation at the vertical wall, and to grasp the characteristics of the splash. Using a series of images capturing splash generation process by a high speed camera, characteristics of splash such as the number of droplet, diameter and splashing velocity of each splashing speed, and so on are measured by the PIV and PTV technique and the relationship between splash and wave characteristics was investigated.

A Numerical Study on Effect of Inducing Slow Flow on the Bottom Sediment Environment in Closed Water Area

Hiroaki SUKENAGA, Takaaki SHIGEMATSU, Akio SOHMA, Naotaka YOSHIMURA, Ken HIRAI

Journal of Japan Society of Civil Engineers, Ser. B2 (Coastal Engineering), Vol. 73(2), pp. I_1333-I_1338 (2017)

It is thought that even very slow flow may be useful for environmental improvement of closed watersheds. This study aims to quantitatively evaluate seawater conduction to improve the environment of the Doi River, which is a part of the old moat and therefore is a river without flow. The field survey was carried out. After parameter tuning based on the field survey, a numerical calculation using the ecological model which can treat circulation of nutrients, organic carbon, oxygen, oxygen demand units and so on. It is presented that the effect of promoting slow flow and oxygen concentration on the profile of nutrient and oxygen demand units and oxygen in the sediment material.

A Fundamental Study on the Characteristics of a Local Scour Under a Vertical Plate and Its Countermeasure in Wave Field

Yusuke NAKAHARA, Takaaki SHIGEMATSU, and Takashi YAMANO

Journal of Japan Society of Civil Engineers, Ser. B3 (Ocean Engineering), Vol. 74(2), pp. I_814-I_819 (2018)

Since the local scour, which occurs at the foot of the structure for controlling the drift sand and the flow, greatly affect the stability of the structure, the appropriate countermeasure should be taken based on the prediction of scale of the scour. In this study, the flow and sand migration phenomena formed in the vicinity of the vertical flat plate were observed in detail by using a high speed camera and the effect of the height of the vertical plate on the characteristics of the local scour at the foot of the plate was investigated in hydraulic

experiment. On the basis of the observation the mechanisms of the occurrence of scour was inferred. Further the countermeasures of penetration of the vertical plate into sand bed and embankment at the foot of the vertical plate were proposed and the effectiveness of them were investigated.

An Experimental Study on the Interaction between Oscillatory Flow and Idealized Porous Bed

Takaaki SHIGEMATSU, Sota NAKAJO, and Yuya OKADA

Journal of Coastal Research,: Special Issue 85 - Proceedings of the 15th International Coastal Symposium: pp. 981 – 985 (2018)

The microscopic structures of over and inside flow of a porous medium placed in oscillatory flow was measured by the Particle Tracking Velocimetry with the refractive index matching method in order to investigate interaction between them. The strong shear flow was observed over the surface of the porous medium and the thickness of shear flow varied with the phase of the oscillatory flow. It was found that the thickness of non-dimensional shear flow was almost constant and that it did not depend on the Reynolds number. It was found that the thickness of non-dimensional shear flow was almost constant and it independent with the Reynolds number. Besides, it was also found that the phase difference between flows over and inside the porous bed occurred. The characteristics of the spatial variance of velocity components were shown in detail with the time phase variance. Further, the flow properties around the particle constitutes porous body were measured and investigated in detail.

The Future Prediction of the One-Dimensional Topography of the Estuary Delta of the Shirakawa River

Sota NAKAJO, Kohei NAKANISHI and Hikaru OTA

Coastal Engineering Journal, Volume 59, Issue 2, Special Issue on Climate Impacts on Coastal Engineering, pp. 1740008-1-174008-24 (2018)

Predicting the long-term topographical change based on results of a time-slice experiment using a General Circulation Model (GCM) is difficult because actual change is a result of the continuum of events occurring in succession leading from the past to the future. We developed a one-dimensional topographical model of an estuary delta as the first step of assessing climate change effects. Three major effects, i.e. tidal flow, waves and sediment supply from the river, were included in this model. In order to estimate the sensitivity of these effects, simulations with virtual conditions were conducted. These simulations show equilibrium profiles that are close to the results of Roberts et al. [2000] “Predicting the profile of intertidal mudflats formed by cross-shore tidal currents,” *Proc. Marine Sci.* 3, 263–285.]. The simulation results were validated with observation data from the Shirakawa River delta. As a long-term prediction (about 37 years), the propagation of the rollover point was less than the actual data showed. The gradient of the subtidal zone was gentler than that observed. However, the short-term prediction (about 17 years) agrees with the observation data. These results show that old, unreliable, observation data used as a boundary condition significantly affects the reproducibility of the actual tidal flat profile. Finally, the effect of continuous Sea Level Rise (SLR) over 100 years from the present was investigated. As expected, the simulation results show a shift of the shoreline landward. The water depths in the intertidal and subtidal zones increase compared to a no-SLR condition. Therefore, the topset area grows as a consequence of SLR. Additionally, it was shown that future accumulation in the subtidal zone is reduced with SLR.

On the Effects of Absence of a Member of Porous Media Based on Microscopic Flow Simulation

Sota NAKAJO, Yuya WATANABE, and Takaaki SHIGEMATSU

Journal of Japan Society of Civil Engineers, Ser. B2 (Coastal Engineering), Vol. 73(2), pp. I_877-I_882 (2017)

Simulation results of microscopic flow through porous media used Immersed Boundary method have been validated by comparison with previous experimental studies about the macroscopic pressure drop during passing porous media, the drag force acting on sphere body and so on. The constant rate of pressure drop in case of regular arrangement of porous media members shows suitability of conventional macroscopic method. However, the heterogeneity of pores caused by absence of a member of porous media would induce the difficulty of application of the conventional model. We discussed about the evidences of its difficulty by showing the pressure drop distribution inside porous media, the drag coefficient acting on each porous members, and the distribution of sectional average of intrinsic velocity in porous media.

Morphological Changes and Sediment Discharge at the Mouth of SHIRAKAWA River after

Kumamoto Earthquake

Gozo TSUJIMOTO, Takaomi HOKAMURA, Kengo TABATA, Hikaru OHTA, Sota NAKAJYO, Yasuhide TAKANO

Journal of Japan Society of Civil Engineers, Ser. B2 (Coastal Engineering), Vol. 73 (2), pp. I_601-I_606 (2017)

The geomorphological changes of tidal flats adjacent to Shirakawa River mouth due to flush flood after earthquakes on April 14 and 16, 2016 were examined through field observation data. There was about 0.41m ground subsidence around field observation site. Therefore, the cross-shore bottom profiles could not return to the averaged profiles. The measured profiles were analyzed by the three parameters and the correlation among them was so high. The clinoform along the water-route propagated to off-shore approximately 150m during 2014 to 2016 after the earthquake. The estimated sediment discharge was $1.1 \times 10^5 \text{ m}^3/\text{yr}/\text{km}^2$, which correspond to four times during 1978 to 1997.

Probabilistic Evaluation of Storm Surges in Suruga Bay Employing Stochastic Typhoon Model

Tomohiro YASUDA, Katsuhito IWAHARA, Shota HIRAI, Sota NAKAJYO, Soo Youl KIM

Journal of Japan Society of Civil Engineers, Ser. B2 (Coastal Engineering), Vol. 73 (2), pp. I_253-I_258 (2017)

Design procedure of coastal embankment compares tsunami height and storm surge height and employs higher value as a crown level. Estimation of tsunami or storm surge height is usually based on the historical maximum record or the assumed maximum value. This study proposes probabilistic evaluation procedure of storm surges employing stochastic typhoon model and applies to Suruga Bay. Typhoon tracks passed the target area were extracted from the synthetic typhoon tracks dataset for 5000 years. Storm surge simulation and inundation simulation were conducted by nonlinear shallow water models, and occurrence probabilities of storm surge height were estimated along coasts in Suruga Bay. Statistical analysis estimated a return period of the current design storm surge height at Suruga coast is about 270 years.

On the Effects of a Long-Term Yearly Variation of Tropical Cyclones on the Storm Surge Potential in Japanese Three Major Bays

Sota NAKAJYO, Hideyuki FUJIKI, Sooyoul KIM, Gozo TSUJIMOTO

Journal of Japan Society of Civil Engineers, Ser. B2 (Coastal Engineering), Vol. 73 (2), pp. I_211-I_216 (2017)

The different temporal trend of tropical cyclone properties by each latitude has been shown based on analysis of representative value in each latitudinal band. Some variations of tropical cyclone properties are correlated to two oscillation indices of atmosphere and ocean interaction. The data of tropical cyclone was divided into two groups based on these results. Then representative scenarios for boundary conditions of storm surge simulation were estimated by using statistical approach. The phase change of tropical cyclone is not so large around three major bay, therefore the phase change of storm surge was also small. However, the change of tropical cyclone track caused local change of storm surge event in each bay.

Sensitivity Analysis of Storm Surge Height and Inundation Area Around Tokyo Bay by Changing Typhoon Characteristics Due to Climate Change

Yoko SHIBUTANI, Nobuhito MORI, Sooyoul KIM, Sota NAKAJYO, Hajime MASE

Journal of Japan Society of Civil Engineers, Ser. B2 (Coastal Engineering), Vol. 73 (2), pp. I_1399-I_1404 (2017)

It is reported that the tropical cyclones will be strengthened and the course of tropical cyclones will be changed. Impact assessment of storm surge on climate change due to changed tropical cyclones has been carried out by several researchers. In this study, we have carried out a sensitivity tests of storm surge simulations to climate change considering typhoon characteristics and sea level rises in the Tokyo bay. The maximum surge height at Tokyo bay with worst track had been estimated. Next, relationship between inundation area and central pressure change or sea level rise had been examined. It was found that the change of central pressure and the surge height are in a proportional relation. And the inundation at Ota area was confirmed when the surge height or sea level rise is higher than 1.0 m.

Proposal of an Empirical Equation for Storm Surges Employing a Stochastic Typhoon Model in the Sea of Aki and Iyo-Nada

Tomohiro YASUDA, Kanoto YOKOYAMA, Shota HIRAI, Sota NAKAJYO, Sooyoul KIM

Journal of Japan Society of Civil Engineers, Ser. B3 (Ocean Engineering), Vol. 74 (2), pp. I_581-I_586 (2018)

Recently, the climate has become extreme by the influence of global warming, and frequency of strong typhoon attack is getting increase. Particularly, storm surge disasters are influenced by intensified typhoons. The number of observations of storm surges are limited and insufficient because hazardous storm surges are low-frequency events. It is difficult to assess the probability of storm surges only based on observation data. This study simulates storm surges employing a stochastic typhoon model and a non-linear shallow water model, and proposes an empirical equation. Analysis assesses the effect of the number of data and the typhoon route on estimation accuracy by a proposed empirical equation targeting in Hiroshima (Aki-nada sea) and Matsuyama (Iyo-nada sea). As a result, errors and variations are reduced and the accuracy can be improved by increasing the number of data. Also, even if tropical cyclones have the same scale, storm surge are different by the difference of routes, which are dangerous semicircle and navigable semicircle. If compute the coefficient after classifying the routes, the proposed method can estimate storm surges of high accuracy at any locations.

Estimation of Characteristics of Micro-Barometric Wave and Its Effect on Longwave Propagation

Sota NAKAJO, Sooyoul KIM

Journal of Japan Society of Civil Engineers, Ser. B3 (Ocean Engineering), Vol. 74 (2), pp. I_539-I_544 (2018)

The characteristics of micro-barometric waves in Kyushu island estimated from analysis of high resolution stationary data was similar between each station. The propagation speed and direction was estimated based on cross-correlation analysis. Even if synoptic low-pressure development was similar, micro-barometric wave propagation process was different. Numerical simulation results show the possibility of significant meteorological tsunami caused by very small amplitude pressure waves, and importance of group wave characteristics, e.g. number of waves or wave length.

Basic Study on Real-time Prediction of Meteotsunami Using Artificial Neural Network Model Calibrated by Stationary Measurement Data

Sota NAKAJO, Ryuta YAMAGUCHI, Sooyoul KIM and Gozo TSUJIMOTO

Asian and Pacific Coasts 2017: Proceedings of the 9th International Conference on APAC 2017, pp. 292-232(2017)

Around the west-coastal zone of Kyushu island in Japan, the meteotsunami has been observed many times. In previous studies, some researchers ascertained the micro-barometric wave is primary factor of this phenomena. However, a real-time prediction of the meteotsunami is very difficult because the micro-pressure wave is too small and quick to identify from numerical weather forecasting results. In this study, we analyzed the meteotsunami from high time resolution measurement data and examined predictability of it by an artificial neural network model (ANN model). We used measurement data collected by Japan Meteorological Agency for analysis and calibration of ANN model. Target periods are three significant meteotsunami events. (A)2009 Feb. 21st-28th, (B)2009 Jul. 14th-16th, (C)2010 Jan. 31st-Feb. 2nd. We used a hierarchical neural network model. The back propagation method and the Levenberg-Marquardt method were adopted as an optimization algorithm and an error evaluation. Anomaly of tide was defined as difference between observation tide and prediction tide. Micro-pressure variation was calculated from difference between an observation atmospheric pressure and the moving average of it. We used these values and observation data as inputs of ANN model. The output of ANN was anomaly of tide at a target point. The appropriate combination of input data is very important factor in order to make a high-reproducible model. In addition, the number of units of intermediate layer, training epochs and a lead-time are also notable model parameters. We discussed about these effects based on sensitivity analysis of an ANN model. Relation between anomaly of tide and micro-pressure wave has been confirmed from high time resolution observation data. However, it is difficult to predict the meteotsunami from observation of atmospheric pressure at fixed point because not all micro-pressure caused the meteotsunami. Some guidelines of appropriate parameters of ANN model have been estimated from sensitivity analysis, although model results are depending on the number of intermediate units and training epochs. In a present basic model, the appropriate longest lead-time was approximately 2 hours. The combination of learning data and validation data was very important for model accuracy. It would be efficient to use some ensemble models reflecting the effect of different factors for actual prediction. Prediction result has to be considered as one sample of statistical trial.

Modeling a Coastal Ecosystem to Estimate Climate Change Mitigation and a Model Demonstration in Tokyo Bay

Akio SOHMA, Hisashi SHIBUKI (Mizuho Information and Research Inst.), Fumiya NAKAJIMA (The Univ of Tokyo), Atsushi KUBO (Shizuoka Univ.), Tomohiro KUWAE (Port and Airport Research Inst.)
Ecological Modelling, 384 pp. 261-289 (2018)

An ecosystem model called the “EMAGIN-B.C. ver 1.0 (Ecosystem Model for Aquatic Geologic Integrated Network for Blue Carbon)”, describing the Carbon-Nitrogen-Phosphorus-Oxygen-Calcium cycle was developed to estimate/predict carbon capture and storage in estuaries. EMAGIN-B.C. analyzes (1) carbon burial, wherein carbon is captured biologically in the pelagic and benthic ecosystems and stored in deeper sediments, (2) CO₂ uptake at the ocean surface while considering the carbonate chemistry with total alkalinity and Dissolved Inorganic Carbon (DIC) production/consumption due to biochemical processes, (3) DIC capture associated with grazing at the trophic level among phytoplankton, zooplankton, and benthic fauna, (4) the effects of hypoxia on benthic fauna and bacteria by precise modeling of the biochemical oxygen production/consumption and the resultant hypoxia, and (5) the carbon transport by integration with the hydrodynamic model. EMAGIN-B.C. was applied to Tokyo Bay, a eutrophic, shallow coastal area, and reproduced the observations well. From the model outputs, it can be observed that Tokyo Bay shows functions of climate change mitigation. In the one-year carbon budget, Tokyo Bay captured 16.6% of the DIC from the atmosphere and river as organic matter by biological processes, and 3.9% of the total carbon flowing from the atmosphere and river was stored in the deeper sediment layer.

Ecosystem Model Study on Long-term Dynamics of Dissolved Oxygen and Its Factors at the Bottom Water in Tokyo Bay

Akio SOHMA and Takuro HARUTA

Journal of Japan Society of Civil Engineers, Ser. B2 (Coastal Engineering), Vol.74, No.2, pp. I_1273-I_1278, (2018) (in Japanese)

Hypoxia has been improving throughout Tokyo Bay, however, there are still seriously hypoxic areas. In this study, we analyzed the secular change of dissolved oxygen (DO) and consumption mechanism of the sea-floor due to reduction of nutrients and COD inflow from the land from 1979 to 2009, using the benthic-pelagic coupled ecosystem model, EMAGIN-H.P. As a result, the model demonstrated that there were at least three types of areas: zone A, in which DO increases; zone B, in which DO turns from a decrease to an increase; and zone C, where DO decreases. In addition, reduction of nutrients and COD inflow leads to (1) decrease of reduced substances (Mn²⁺, Fe²⁺, and S²⁻) and increase of benthic fauna due to improvement of hypoxia at zone A, (2) decrease of reduced substances due to DO increase and decrease of benthic fauna due to food shortage at zone C, and (3) increase of benthic fauna until 1994 with the improvement of hypoxia and then a decrease due to food shortage at zone B. These results show that the optimal amount of nutrients and COD inflow in view of both the increase of benthic fauna and the improvement of hypoxia differs from area to area.

Annual Variation of Air-Sea CO₂ Flux at the River Mouth Area and Its Factors -Analysis of an Ecosystem Model, EMAGIN_B.C-

Akio SOHMA, Mizuki NAKAI, Atsushi KUBO (Shizuoka Univ.), and Tomohiro KUWAE (Port and Airport Research Inst.)

Journal of Japan Society of Civil Engineers, Ser. B2 (Coastal Engineering), Vol.74, No.2, pp. I_1267-I_1272, (2018) (in Japanese)

The carbon capture and storage in the coastal shallow ecosystem is a hot topic because of its high potential. The release and uptake of atmospheric CO₂ at the air-sea boundary is an important element consisting the series of carbon capture and storage of the shallow waters. In this study, we applied an ecosystem model, EMAGIN_B.C., considering carbonate chemistry, food-web, and Carbon-Nutrients-Oxygen cycling in the benthic-pelagic coupled system to Tokyo Bay, and analyzed the dynamics of air-sea CO₂ flux and its factors especially focusing on the river mouth area. As the result of the model analysis, CO₂ was released from the ocean to air at the river mouth area on an annual average basis, although CO₂ was taken up at other areas in Tokyo Bay. In addition, the CO₂ release and CO₂ uptake are repeated in the period from the end of April to the end of November. The CO₂ absorption period is thought to be dominated by the consumption of DIC by photosynthesis, and the release period is thought to be dominated by consumption of total alkalinity by nitrification.

CO₂ Uptake in the Shallow Coastal Ecosystems Affected by Anthropogenic Impacts

Tomohiro KUWAE (Port and Airport Research Inst.), Jota KANDA Tokyo Univ. of Marine Science and Technology), Atsushi KUBO (Shizuoka Univ.), Fumiyuki NAKAJIMA (The Univ. of Tokyo), Hiroshi OGAWA (The Univ. of Tokyo), Akio SOHMA, Masahiro SUZUMURA (National Inst. Of Advanced Industrial Science and Technology)

Book Chapter In: Blue Carbon in Shallow Coastal Ecosystems: Carbon Dynamics, Policy, and Implementation (eds T. Kuwae, M. Hori), Springer Nature, Singapore, pp.295–319 (2018)

Shallow coastal ecosystems (SCEs) are generally recognized as not only significant organic carbon reservoirs but also as sources for CO₂ emission on the atmosphere, thus posing a dilemma regarding their role in climate change mitigation measures. However, we argue that SCEs can act as sinks for atmospheric CO₂ under a given set of biogeochemical and socioeconomic conditions. The key properties of SCEs that show net uptake of atmospheric CO₂ are often characteristic of human-dominated systems, that is, high nutrient inputs from terrestrial systems, input of treated wastewater in which labile carbon has been mostly removed, and the presence of hypoxic waters. We propose a new perspective on the potential of human-dominated SCEs to contribute to climate change mitigation, both serving as carbon reservoirs and providing direct net uptake of atmospheric CO₂, in light of human systems-ecosystem interactions. Namely, if we view the land and a SCE as an integrated system, with appropriate management of both wastewater treatment and SCE, we will be able to not only suppress CO₂ release but also capture and store carbon.

Quantification of Ecosystem Services at Tidal Flats in Osaka Bay Using Tidal Flat Health Index: Characterization of the Tidal Flats by Comparison Between Tokyo Bay and Osaka Bay

Tomonari OKADA, Yugo MITO, Takanori SUGANO, Toshiyuki TAKAHASHI, Yoshihiro AKIYAMA, Hiroshi KUROIWA, Toru ENDO, Sosuke OTANI, Susumu YAMOCHI, Yasunori KOZUKI, Takayuki KUSAKABE, Koji OTSUKA, Ryoichi YAMANAKA, Takaaki SHIGEMATSU, Kazuyuki NAKANO, Makoto USHIRO and Tomohiro KUWAE

Journal of Japan Society of Civil Engineers, Ser.B2 (Coastal Engineering), Vol.74, No.2, pp.1417-1422 (2018) (in Japanese)

In this study, the tidal flat health index (THI) was applied to four tidal flats in Osaka Bay to confirm the versatility of THI and understand the features in each tidal flat by comparing them with four tidal flats in Tokyo Bay. The reference values (the best score of each health index) in the services, such as food supply and water purification, related to the ecosystem states, in Osaka Bay were almost equal to those of Tokyo Bay. The reference values in the services, such as tourism and recreation, influenced by the regional population, were higher in Tokyo Bay than in Osaka Bay. However, the reference value of education was higher in Osaka Bay compared to Tokyo Bay, suggesting that environmental learning is active in Osaka. Principal component analysis of the nine services in the eight tidal flats in Osaka Bay and Tokyo Bay revealed that 74% of the THI scores could be explained by 2 components: "utilization of people" and "biodiversity".

Estimation of Air-sea CO₂ Fluxes in Osaka Bay, Harima-Nada and Ago Bay base on Spatial Distribution Survey of Dissolved Inorganic Carbon

Toru ENDO, Junpei SHIMANO, Kenji IKENAGA and Hideki KOKUBU

Journal of Japan Society of Civil Engineers, Ser.B2 (Coastal Engineering), Vol.74, No.2, pp.1315-1320 (2018) (in Japanese)

To evaluate the air-sea CO₂ flux of Osaka Bay, Harima Nada and Ago Bay, we conducted the spatial distribution surveys of the dissolved inorganic carbon (DIC) and pH. There are low DIC concentration in the inner part of Osaka Bay where external load is large because DIC was consumed by photosynthesis of phytoplankton. On the other hand, there are high DIC concentration in the Ago Bay where much organic carbon was accumulated on the sea floor. We found that CO₂ was absorbed basically in all seas at daytime and, especially, Osaka bay had high CO₂ absorption potential compared with the other seas.

CO₂ fluxes were calculated based on a chemical equilibrium model of carbonic acid from the measurement data of DIC and pH, air to sea CO₂ flux was 12.6 to 14.0 CO₂/m²/hr in Osaka bay, 1.5 to 3.7 CO₂/m²/hr in Harima Nada and 0.8 mg CO₂/m²/hr in Ago Bay. The CO₂ Flux of Osaka Bay was larger than the averaged CO₂ fluxes of coastal seas reported in around the world.

Effect of Fallen Leaves Supply with Sandy Sediment Layer on the Benthic Ecosystem in an Artificial Tidal Flat

Toru ENDO, Tsukasa MORITA, Ataru TAMURA and Hiroyuki OOKA

Journal of Japan Society of Civil Engineers, Ser.B3 (Ocean Engineering), Vol.74, No.2, pp.492-297 (2018) (in Japanese)

Deterioration of ecosystem functions is concerned because the sediment layer is becoming sandy by the lack of organic matter in an artificial tidal flat of Osaka Nanko bird sanctuary. We focused on fallen leaves supply with the sandy sediment layer as part of preservation measures for the benthic ecosystem. In this study, we conducted several experiments (a dissolution test, survival tests about benthic organisms and field experiment) by using the easily decomposable fallen leaves and the humified persistent fallen leaves to confirm the efficacy of the fallen leaves supply.

We found that the easily decomposable fallen leaves supply had a negative effect on the benthic habitat environment because the sediment layer was kept in anaerobic condition by decomposing organic matter. However, for the case of supplying the persistent fallen leaves, sulfide was not almost generated and survive rate of *Perinereis wilsoni* was higher than that without supplying fallen leaves. On the other hand, we confirmed that more species were inhabited in the site supplied fallen leaves with the sediment layer than the site of without supplying fallen leaves from the results of field investigation. Therefore, it was suggested that the persistent fallen leaves supply is effective way for the conservation of the benthic ecosystem in sandy tidal flat.

Relationship between Vertical Distribution of pCO₂ in Sea and Air-sea CO₂ Exchange in Inner Part of Osaka Bay

Toru ENDO, Junpei SHIMANO, Daiki SAKAI and Ryuichi FUJIWARA

Journal of Japan Society of Civil Engineers, Ser.B2 (Coastal Engineering), Vol.73, No.2, pp.1231-1236 (2017) (in Japanese)

Vertical distribution of dissolved inorganic carbon (DIC) and water qualities and CO₂ concentration of air water measured at an inner part of Osaka bay during one year and at around the time of approaching typhoon, in order to grasp relationship between the air-sea CO₂ exchange and the vertical distribution characteristics of pCO₂ in sea. We found that CO₂ was absorbed constantly from air to sea at normal condition despite pCO₂ in sea was larger at high water temperature season when biological activity is high. However, CO₂ was emitted from sea to air in rainy weather because pH of surface water becomes lower due to rain water mixing. In addition, CO₂ was also emitted when the coastal upwelling occurred, or the seawater was mixed by typhoon. Furthermore, we increased at bottom layer at the time of high density stratified season spread to surface layer.

Evaluation of Carbon Absorption of Phytoplankton at the North Salt Marsh of Osaka Nanko Bird Sanctuary

Toru ENDO and Taiki KAWASAKI

Journal of Japan Society of Civil Engineers, Ser.B2 (Coastal Engineering), Vol.73, No.2, pp.1369-1374 (2017) (in Japanese)

Recently, the carbon absorption process of wetland ecosystem is getting a lot of attention as a new ecosystem function. It is important to understand the carbon cycle of salt marsh in urban coastal area for coastal management of future. In this study, an incubation experiment on phytoplankton photosynthesis and field investigations on carbon cycle in salt marsh were conducted at the north salt marsh in Osaka Nanko bird sanctuary in order to evaluate the effect of phytoplankton on the carbon budget of salt marsh. The carbon absorption rate per chlorophyll a was formulated as a function of temperature and photon flux density, and the carbon emission rate of respiration and decomposition in seawater was formulated as a function of temperature by measuring DIC changes in the seawater under light and dark conditions. It was found that the rate of the air-sea carbon exchange is smaller than the carbon absorption rate of phytoplankton, and there was no correlation between them, according to estimation of the rate of air-sea carbon flux and amount of carbon absorption of phytoplankton obtained by the seasonal investigation on phytoplankton biomass and DIC of surface water. Finally, it was suggested that the ratio of photosynthesis to carbon budget of the salt marsh was from 10 to 30 % from comparing the daily variation of the carbon cycle due to the air-sea exchange, the water exchange, the carbon absorption of phytoplankton and the carbon emission of respiration and decomposition in sea water.

Organic pollution loads in municipal solid waste incineration fly ash derived from highly reactive slaked lime in leachate from landfill site

Satoshi MIZUTANI, Katsunori MATOZAKI, Hirofumi SAKANAKURA and Yoshinori KANJO

Proc. of the 10th International Conference on the Environmental and Technical Implications of Construction with Alternative Materials (WASCON2018), Tampere, 6-8 June 2018 (on USB).

High levels of total organic carbon (TOC) are often detected in leachate from landfill sites in Japan, which is

problematic for proper leachate treatment. In this study, TOC and chemical oxygen demand (COD_{Mn}) of leachate from fly ash and slaked lime in Japanese landfill sites were determined. The TOC in leachates from 13 kinds of incineration fly ash from municipal solid waste was measured. Ignition loss (IL) of each type of fly ash was also measured to determine the content of organic matter. There was no relationship between TOC and IL. Higher TOC levels were detected in leachate from fly ash from incinerators with dry-acid gas treatment systems. This suggests that the TOC of the leachate from the fly ash was derived from slaked lime for the neutralization of acid gas. Subsequently, 13 kinds of highly reactive slaked lime were obtained. The TOC of their leachates was measured and was in the range of 600–5,680 mg/kg. In contrast, normal industrial lime and $\text{Ca}(\text{OH})_2$ reagent do not contain organic materials. Generally, there was a positive correlation between COD and TOC in slaked lime. TOC showed 60–80% of COD_{Mn}

List of Presentations

at

International Conferences

Presenters are underlined in the list of authors.

†Undergraduate or graduate students of the Faculty of Engineering, Osaka City University

Mechanical and Physical Engineering

Mechanical Engineering

Damage Behavior of CFRP/Titanium Mesh Laminates under Three-point Bending Loading

Yoshinori SEI[†], Hayato NAKATANI and Katsuhiko OSAKA

The 12th Canada-Japan Workshop on Composites, Takayama, Japan, July 4-7, 2018 (poster).

Evaluation of Resin Impregnation Behavior in Thick FRP with Corner during VaRTM Process

Kyosuke NAKAMURA[†], Hayato NAKATANI and Katsuhiko OSAKA

The 12th Canada-Japan Workshop on Composites, Takayama, Japan, July 4-7, 2018 (poster).

High- and Low-Cycle Fatigue Properties of SUS304L Steel Processed by ECAP

Y. KANEKO, H. KOBAYASHI, K. TSUJIMURA, M. UCHIDA and A. VINOGRADOV

The 15th International Conference on Advanced Materials, Kyoto, Japan, Aug. 27-Sep. 1, 2017 (invited).

Fabrication and Microstructure of Electrodeposited Cu-based Alloy Films Having High Composition Gradient

H. HAGIWARA[†], Y. KANEKO and M. UCHIDA

15th International Symposium on Functionally Graded Materials, Kitakyushu, Japan, Aug. 5-8, 2018.

Nonlocal Multiscale Modeling of Deformation Behavior of Polycrystalline Copper by Second-order Homogenization Method

M. UCHIDA, A. TANIGUCHI[†] and Y. KANEKO

The 9th International Conference on Multiscale Materials Modeling, Osaka, Japan, Oct. 27-Nov. 2, 2018.

Applied Physics and Electronics

Excitation Energy Dependence of Carrier-Induced Terahertz Wave Radiation in a GaAs Epitaxial Film

Takayuki HASEGAWA, Yuta OKUSHIMA, Masaaki NAKAYAMA and Yoshihito TANAKA

12th International Conference on Excitonic and Photonic Processes in Condensed Matter and Nano Materials, Nara, Japan, July 8-13, 2018

Temperature Dependence of Photoluminescence Dynamics of Exciton-Exciton Inelastic Scattering in a GaAs/AlAs Multiple-Quantum-Well Structure

Yuichiro MIYAZAKI[†] and Masaaki NAKAYAMA

12th International Conference on Excitonic and Photonic Processes in Condensed Matter and Nano Materials, Nara, Japan, July 8-13, 2018 (poster)

Photoluminescence Polarization Characteristics of Self-Trapped Excitons in an Undoped β -Ga₂O₃ Single Crystal

Suguru YAMAOKA[†], Yusuke MIKUNI[†] and Masaaki NAKAYAMA

12th International Conference on Excitonic and Photonic Processes in Condensed Matter and Nano Materials, Nara, Japan, July 8-13, 2018 (poster)

Strong Coupling Formation in Organic Crystal Microcavities

Takumi NISHIMURA, Keita IMAI, Shun TAKAHASHI, Kenichi YAMASHITA, Hisao YANAGI and Masaaki NAKAYAMA

12th International Conference on Excitonic and Photonic Processes in Condensed Matter and Nano Materials, Nara, Japan, July 8-13, 2018 (poster)

Investigation of a Pressure Gradient Ar Plasma Sputtering for Metal Thin Film Deposition

Hiroki OOTA, Kiyomi TAKAHASHI, Jun-Seok OH, Kazunori KOGA, Tatsuyuki NAKATANI, Masafumi ITO, Masaharu SHIRATANI, Ken YONEZAWA

16th International Conference on Plasma Surface Engineering, Garmisch-Partenkirchen, Germany, September 17-21, 2018 (poster)

Developing In Vitro Models to Analyze the Metrology of Plasma-Tissue Interactions

Endre SZILI, Jun-Seok OH, Akimitsu HATTA, Masafumi ITO, Hideo FUKUHARA, Keiji INOUE, Sung-Ha HONG, Nishtha GAUR, Rob SHORT

Plasma Processing and Science, Gordon Research Conference, Smithfield, RI, USA, August 5-10, 2018 (invited)

Assessing the Helium Plasma Jet Induction of Apoptosis in an In Vivo Tumor Model

Nishtha GAUR, Endre SZILI, Jun-Seok OH, Hideo FUKUHARA, Rishabh BHATIA, Cuong NGUYEN, Sung-Ha HONG, Satsuki ITO, Kotaro OGAWA, Chiaki KAWADA, Taro SHUIN, Masayuki TSUDA, Mutsuo FURUHATA, Atsushi KURABAYASHI, Hiroshi FURUTA, Masafumi ITO, Keiji INOUE, Akimitsu HATTA, Robert SHORT

Plasma Processing and Science, Gordon Research Conference, Smithfield, RI, USA, August 5-10, 2018 (poster)

Application of Multiphase Media Plasmas to Nano-material Treatment

Tatsuru SHIRAFUJI

The 7th International Conference on Microelectronics and Plasma Technology, Incheon, Korea, July 24-28, 2018 (invited)

Effects of Argon Micro-bubble Assistance on the Performance of 3D Integrated Micro Solution Plasma

Reiya NAKAGAWA[†], Hiroto MASUNAGA[†], Jun-Seok. OH, and Tatsuru SHIRAFUJI

The 7th International Conference on Microelectronics and Plasma Technology, Incheon, Korea July 24-28, 2018 (poster)

Effects of Pulse Voltage Polarity on GNP-embedded Polymer Formation on Aqueous Solution Irradiated with Ar DBD Plasma

Shunta HIRANO[†], Shiori AZUMA[†], Yusuke NAKAMURA[†], Jun-Seok OH, Toshiyuki ISSHIKI, and Tatsuru SHIRAFUJI

The 7th International Conference on Microelectronics and Plasma Technology, Incheon, Korea, July 24-28, 2018 (poster)

Effects of Grounded Electrode on the APPJ Treatment for Improving Water Permeability of a Bone-regeneration Scaffold

Yuki HAMAMOTO[†], Masato OSHIRO[†], Jun-Seok OH, Kumi ORITA, Hiromitsu TOYODA, and Tatsuru SHIRAFUJI

The 7th International Conference on Microelectronics and Plasma Technology, Incheon, Korea, July 24-28, 2018 (poster)

Generation of 3D Integrated Micro Solution Plasma in Water with Micro Bubbles

Reiya NAKAGAWA[†], Hiroto MASUNAGA[†], Jun-Seok. OH, and Tatsuru SHIRAFUJI

The 1st International Symposium on Water Frontier Science & Technology Research Center, Tokyo University of Science, "Water on Materials Surface 2018", Tokyo, Japan, July 25-28, 2018 (poster)

Long-term Investigation of Radical-activated Water

Jun-Seok OH, Naoyuki IWATA, Takayuki OHTA, Masaru HORI, and Masafumi ITO

The 8th International Symposium on Plasma Bioscience, Incheon, Korea, July 24-28, 2018 (invited)

Time-Dependence Monitoring of Sterilization Effects and RONS Concentrations in Radical-Activated Water

Naoyuki IWATA, Jun-Seok OH, Takayuki OHTA, Masaru HORI, and Masafumi ITO

The 8th International Symposium on Plasma Bioscience, Incheon, Korea, July 24-28, 2018 (poster)

Diagnostics of Radicals Generated from Atmospheric-Pressure Radical Source and Their Activated Water Using Ultra-Violet Absorption Spectroscopy

Masafumi ITO, Naoyuki IWATA, Jun-Seok OH, Takayuki OHTA, Masaru HORI

24th Europhysics Conference on Atomic and Molecular Physics of Ionized Gases, Glasgow, UK, July 17-21, 2018 (poster)

Plasma Jet Treatment of Hypoxic Tumours

Endre SZILI, Jun-Seok OH, Hideo FUKUHARA, Keiji INOUE, Akimitsu HATTA, Rob SHORT

The 20th Gaseous Electronics Meeting, Queensland, Australia, June 21-24, 2018 (invited)

Investigation of How Short-Lived and Long-Lived Plasma Species Interact with DNA in Models of Tissue Fluid, Tissue and Cells

Nishtha GAUR, Endre SZILI, Sung Ha HONG, Hirofumi KURITA, Jun-Seok OH, Masafumi ITO, Akira MIZUNO, Akimitsu HATTA, Allison COWIN, David GRAVES, Robert SHORT

The 20th Gaseous Electronics Meeting, Queensland, Australia, June 21-24, 2018

Development of VUV Absorption Spectroscopy for Quantitative Analysis of Plasma Activated Water

Jun-Seok OH, Naoyuki IWATA, Akimitsu HATTA, Tatsuru SHIRAFUJI, and Masafumi ITO

The 6th International Workshop and the 5thrd International Mini Workshop on Solution Plasma and Molecular Technology, Gdansk, Poland, June 4-7, 2018 (invited)

Plasma-on-Chip: An Innovative Microdevice to Direct Cell Fate using A Non-Thermal Atmospheric Pressure Plasma

Shinya KUMAGAI, Mine KOBAYASHI, Jun-Seok OH, Tetsuji SHIMIZU, Minoru SASAKI

10th International Symposium on Organic Molecular Electronics, Saga, Japan, May 31-June 2, 2018

Improvement of Water Permeability of a Scaffold by Irradiating Atmospheric Pressure Plasma Jet

Masato OSHIRO[†], Kumi ORITA, Yoshihiro HIRAKAWA, Hiromitsu TOYODA and Tatsuru SHIRAFUJI

The 19th anniversary International Symposium on Advanced Plasma Science and its Application for Nitrides and Nanomaterials / The 11th International Conference on Plasma-Nano Technology & Science, Nagoya, Japan, March 4-8, 2018 (poster)

Time Evolution of RONS in Water Treated with Air Bubble Plasma

Shoma MIYAMOTO[†], Kentaro NISHIMOTO[†], Shin-ichi IMAI and Tatsuru SHIRAFUJI

The 19th anniversary International Symposium on Advanced Plasma Science and its Application for Nitrides and Nanomaterials / The 11th International Conference on Plasma-Nano Technology & Science, Nagoya, Japan, March 4-8, 2018 (poster)

Effects of Micro-bubble Assistance on the Performance of 3D Integrated Micro Solution Plasma

Hiroto MASUNAGA[†], Yodai ISHIDA[†] and Tatsuru SHIRAFUJI

The 19th anniversary International Symposium on Advanced Plasma Science and its Application for Nitrides and Nanomaterials / The 11th International Conference on Plasma-Nano Technology & Science, Nagoya, Japan, March 4-8, 2018 (poster)

Structural Analysis of Au-Nanoparticle-Embedded Polymer Films Synthesized on HAuCl₄/Gelatin Aqueous Solution Irradiated with Ar DBD Plasma

Shiori AZUMA[†], Yusuke NAKAMURA[†], Toshiyuki ISSHIKI and Tatsuru SHIRAFUJI

The 19th anniversary International Symposium on Advanced Plasma Science and its Application for Nitrides and Nanomaterials / The 11th International Conference on Plasma-Nano Technology & Science, Nagoya, Japan, March 4-8, 2018 (poster)

Efficiency of OH Radical Production in 3D Integrated Micro Solution Plasma

Tatsuru SHIRAFUJI, Junpei YAMAMOTO[†] and Hiroto MASUNAGA[†]

The 19th anniversary International Symposium on Advanced Plasma Science and its Application for Nitrides and Nanomaterials / The 11th International Conference on Plasma-Nano Technology & Science, Nagoya, Japan, March 4-8, 2018 (poster)

Applied Chemistry and Bioengineering

Hydrolysis of Organophosphates Catalyzed by Prussian Blue Analogs

Chihiro TERASHIMA[†], Hiroyasu TABE, Yusuke YAMADA

The 9th OCARINA International Symposium, Osaka, Japan, March 7, 2018 (poster)

Light-Driven Water Oxidation Reaction Catalyzed by Cyano-Bridged Metal Complexes with Core-Shell Structure

Akira KITASE[†], Hiroyasu TABE, Yusuke YAMADA

The 9th OCARINA International Symposium, Osaka, Japan, March 7, 2018 (poster)

Catalytic Activity of Thiocyanato-bridged Polynuclear Metal Complexes for Hydrolysis of Organophosphates

Masaaki MATSUSHIMA[†], Chihiro TERASHIMA[†], Hiroyasu TABE, Yusuke YAMADA

The 9th OCARINA International Symposium, Osaka, Japan, March 7, 2018 (poster)

Construction of Composite Photocatalysts for Water Oxidation Using Silica Nanoparticles Assembly as a Mesoporous Support

Gentaro SAKAMOTO[†], Hiroyasu TABE, Yusuke YAMADA

The 9th OCARINA International Symposium, Osaka, Japan, March 7, 2018 (poster)

Synthesis and Characterization of $\text{Li}_2\text{Co}_{1.8}\text{Ni}_{0.2}\text{O}_4$ as Zero-Strain Lithium Insertion Material

Kensuke KAJIKAWA[†], Yusuke YAMADA, Kingo ARIYOSHI

The 9th OCARINA International Symposium, Osaka, Japan, March 7, 2018 (poster)

Heterogeneous Catalysis of Cyano-Bridged Polynuclear Metal Complexes for Organophosphate Hydrolysis

Hiroyasu TABE[†], Chihiro TERASHIMA, Yusuke YAMADA

43rd International Conference on Coordination Chemistry, Sendai, Japan, July 31, 2018 (poster)

Enhanced Catalysis of Prussian Blue Analogs with CN-Deficient Sites for Hydrolysis of Organophosphates

Mari YAMANE[†], Chihiro TERASHIMA, Hiroyasu TABE, Yusuke YAMADA

43rd International Conference on Coordination Chemistry, Sendai, Japan, July 31, 2018 (poster)

Activity of Core-Shell Nanoparticles Composed of Cyano-Bridged Metal Complexes Containing Co Ions for Photocatalytic Water Oxidation

Akira KITASE[†], Hiroyasu TABE, Yusuke YAMADA

43rd International Conference on Coordination Chemistry, Sendai, Japan, August 1, 2018 (poster)

Catalysts Utilized for Artificial Photosynthesis with a Molecular Light Harvesting Unit

Yusuke YAMADA

OrganiX-2018, An International Conference in Chemistry, Tezpur, India, December 20, 2018 (invited)

Workshop Instructor on “Micro XRF”

K. TSUJI

67th Annual Conference on Applications of X-ray Analysis Denver X-ray Conference, Westminster, Colorado, U.S.A., August 6-10, 2018 (invited)

Workshop Instructor on “Trace Analysis”

K. TSUJI

67th Annual Conference on Applications of X-ray Analysis Denver X-ray Conference, Westminster, Colorado, USA, August 6-10, 2018 (invited)

Recent Advances and Standardization in X-Ray Fluorescence (XRF) Analysis: Confocal 3D-XRF and Total Reflection XRF

K. TSUJI

IUPAC Analytical Chemistry Workshop Advances in Analytical Chemistry II, Nara, Japan, April 27, 2018 (invited)

New Sample Preparation for TXRF Analysis Using Resist Pattern Layer

K. TSUJI, T. FURUSATO[†], N. YOMOGITA[†]

67th Annual Conference on Applications of X-ray Analysis Denver X-ray Conference, Westminster, Colorado, U.S.A., August 6-10, 2018

Observation of Crystal Structure Changes with Full Field X-ray Diffraction Imaging Instrument

M. YAMANASHI[†], K. TSUJI

67th Annual Conference on Applications of X-ray Analysis Denver X-ray Conference, Westminster, Colorado, U.S.A., August 6-10, 2018 (poster)

New Sample Carrier Modified with Low-Z Material Layer for TXRF Analysis

K. TSUJI, T. FURUSATO[†], N. YOMOGITA[†]

European Conference on X-Ray Spectrometry (EXRS2018), Ljubljana, Slovenia, June 24-29, 2018

Elemental Analysis of Human Hair by Confocal Micro-XRF Analysis

T. FURUSATO[†], N. YOMOGITA[†], K. TSUJI

European Conference on X-Ray Spectrometry (EXRS2018), Ljubljana, Slovenia, June 24-29, 2018

Quantitative Elemental Analysis of Human Hairs by Using Desktop X-Ray Fluorescence Analyzer

T. FURUSATO[†], F. INOUE (Nobias), K. TSUJI

European Conference on X-Ray Spectrometry (EXRS2018), Ljubljana, Slovenia, June 24-29, 2018 (poster)

In Situ Observation of the Corrosion Process of Steel Sheets under Bending Stress by Confocal Micro XRF Technique

M. NAKANISHI[†], R. HOSOMI[†], K. TSUJI

European Conference on X-Ray Spectrometry (EXRS2018), Ljubljana, Slovenia, June 24-29, 2018 (poster)

Elemental Distribution Analysis of Copper-based Preservative-treated Woods by Micro XRF Method

M. NAKANISHI[†], Y. FUJIWARA (Kyoto University), Y. FUJII (Kyoto University), K. TSUJI

European Conference on X-Ray Spectrometry (EXRS2018), Ljubljana, Slovenia, June 24-29, 2018 (poster)

Raman Microspectroscopic Study on an Optically Formed Poly(*N*-isopropylacrylamide) Rich Microparticle: Molecular Weight Dependence of a Polymer Concentration in the Particle

Kayo FUJIWARA[†], Tatsuya SHOJI, Mitsuhiro MATSUMOTO, Taka-Aki ASOH, Takashi NISHIYAMA, Hideo HORIBE, Yasuyuki TSUBOI

Optical Manipulation Conference, SPIE Structured Light, Yokohama, Japan, April 25–27, 2018

Oxygen Additive Effects on Decomposition Rate of Poly(Vinyl Phenol)-Based Polymers Using Hydrogen Radicals Produced by a Tungsten Hot-Wire Catalyst

Masashi YAMAMOTO (Kagawa College), Shiro NAGAOKA (Kagawa College), Keisuke OHDAIRA (Japan Advanced Institute of Science and Technology), Hironobu UMEMOTO (Shizuoka University, Osaka City University), Hideo HORIBE

10th International Conference on Hot Wire (Cat) & Initiated Chemical Vapor Deposition, Kitakyushu, Japan, September 3–6, 2018 (poster)

PEGylated Amphiphilic Block Copolymers as Membrane Anchors for Controlled Affinity to Lipid Bilayer Membranes

Yuta KODA (Osaka City University, Kyoto University), Daiki TAKAHASHI (Kyoto University), Yoshihiro SASAKI (Kyoto University), Kazunari AKIYOSHI (Kyoto University, JST-ERATO)

256th ACS National Meeting & Exposition, Boston, U.S.A., August 19–23, 2018

Coumarin Derivative Polymers for Thermo- and Light-Responsive Monofunctional Polymers

Eriko SATO

14th International Conference of Computational Methods in Science and Engineering (ICCMSE 2018), Thessaloniki, Greece, March 14-18, 2018 (invited)

Design of Smart Adhesive Materials based on Well-Defined Reactive Polymers

Eriko SATO

The polymer society of Korea, 2018 Spring Meeting, Korea-Japan Joint Symposium, Smart Interface by Functional Polymers, Daejeon, Korea, April 4-6, 2018 (invited)

Cross-Linked Polyperoxides for Photoremovable Adhesives

Eriko SATO, Chisato OMORI[†], Takashi NISHIYAMA and Hideo HORIBE

The 35th International Conference of Photopolymer Science and Technology, Chiba, Japan, June 25-28, 2018 (invited)

Degradable Polymers for Dismantlable Adhesive Materials

Eriko SATO

The 10th International Conference of Modification, Degradation and Stabilization of Polymers, Tokyo, Japan, September 2-6, 2018 (invited)

Degradable Hyperbranched Polymers for Green Adhesive Materials

Eriko SATO, Yoji YAMASHITA[†], Yuta KODA, Hideo HORIBE

The 12th SPSJ International Polymer Conference, Hiroshima, Japan, December 4-7, 2018

Development of Thermal Latent Reductants for Accelerated Decomposition of Cross-Linked Polyperoxides

Chisato OMORI[†], Eriko SATO, Yuta KODA and Hideo HORIBE

The 12th SPSJ International Polymer Conference, Hiroshima, Japan, December 4-7, 2018 (poster)

Thermo- and Photo-Responsive Behavior of Monofunctional Dual Stimuli-Responsive Organogels

Seidai OKADA[†], Eriko SATO, Yuta KODA and Hideo HORIBE

The 12th SPSJ International Polymer Conference, Hiroshima, Japan, December 4-7, 2018 (poster)

Facile Synthesis of Poly(dialkyl fumarate) Macromonomers by Radical Polymerization using Addition-Fragmentation Chain Transfer Agent

Junichiro KURAHASHI[†], Noboru TAMARI[†], Eriko SATO, Yuta KODA and Hideo HORIBE

The 12th SPSJ International Polymer Conference, Hiroshima, Japan, December 4-7, 2018 (poster)

Photoswitching of Birefringence of Diarylethene Single Crystals by Photochromic Reaction

Kohei MORIMOTO[†], Hajime TSUJIOKA[†], Daichi KITAGAWA, Seiya KOBATAKE

9th OCARINA International Symposium, Osaka, Japan, March 6-7, 2018 (poster)

Dependence of Fluorescence On/Off Switching Properties of Nanoparticles Consisting of Two Types of Diarylethenes on Forster Distance and Molar Fraction

Tatsumoto NAKAHAMA[†], Daichi KITAGAWA, Hikaru SOTOME (Osaka University), Syoji ITO (Osaka University), Hiroshi MIYASAKA (Osaka University), Seiya KOBATAKE

French-Japanese International Associated Laboratory Nano-synergetics: Workshop for Young Researchers on Photo-active materials with Cooperative and Synergetic Responses, Lille, France, March 29-30, 2018

Development of Novel Photomechanical Phenomena of Photoresponsive Molecular Crystals by High-order Photoexcitation

Seiya KOBATAKE

2nd International Symposium on Photosynergetics and 3rd Workshop on Photo-active Materials with Cooperative and Synergetic Responses - Nanosynergetics, International Associated Laboratory (LIA) between France and Japan, Osaka, Japan, May 21-23, 2018 (invited)

Emission Color Tuning and Efficient Emission of BODIPY Polymer in Solid State

Katsuya SHIMIZU[†], Daichi KITAGAWA, Seiya KOBATAKE

27th International Symposium on Photochemistry (PhotoIUPAC 2018), Dublin, Ireland, July 8-13, 2018 (poster)

Photoinduced Crystal Shape Change of Photochromic Diarylethene Crystals

Seiya KOBATAKE

13th International Workshop on Crystal Growth of Organic Materials (CGOM13), Seoul, Korea, August 27-30, 2018 (plenary)

How Illumination Direction Affects Photomechanical Crystal Twisting

Daichi KITAGAWA, Hajime TSUJIOKA[†], Fei TONG (University of California, Riverside), Xinning DONG (University of California, Riverside), Christopher J. BARDEEN (University of California, Riverside), Seiya KOBATAKE

13th International Workshop on Crystal Growth of Organic Materials (CGOM13), Seoul, Korea, August 27-30, 2018

Photo-tuning of Birefringence in Diarylethene Crystals

Kohei MORIMOTO[†], Hajime TSUJIOKA[†], Daichi KITAGAWA, Seiya KOBATAKE

13th International Workshop on Crystal Growth of Organic Materials (CGOM13), Seoul, Korea, August 27-30, 2018 (poster)

Crystallization-induced Emission of 1,2-Bis(3-methyl-5-(4-alkylphenyl)-2-thienyl)perfluoro- cyclopentenes

Tatsumoto NAKAHAMA[†], Daichi KITAGAWA, Hikaru SOTOME (Osaka University), Syoji ITO (Osaka University), Hiroshi MIYASAKA (Osaka University), Seiya KOBATAKE

13th International Workshop on Crystal Growth of Organic Materials (CGOM13), Seoul, Korea, August 27-30, 2018 (poster)

Fluorescence On/Off Switching of Branched Polymer Consisting of Diarylethene and Fluorene Derivatives

Katsuya SHIMIZU[†], Seiya KOBATAKE

Journées GDR Photo Électro Stimulation, Kick-off meeting, Rennes, France, October 2-3, 2018 (poster)

Photochromic Diarylethene Crystals That Exhibit Unusual Photomechanical Behavior

Seiya KOBATAKE, Daichi KITAGAWA

10th Asian Photochemistry Conference (APC 2018), Taipei, Taiwan, December 16-20, 2018 (invited)

Fluorescence Color Tuning and On/Off Switching of BODIPY Polymers in Solid State

Katsuya SHIMIZU[†], Seiya KOBATAKE

10th Asian Photochemistry Conference (APC 2018), Taipei, Taiwan, December 16-20, 2018 (poster)

Photomechanical Crystal Deformation of Diarylethenes with Polarized Light

Akira HIRANO[†], Daichi KITAGAWA, Seiya KOBATAKE

10th Asian Photochemistry Conference (APC 2018), Taipei, Taiwan, December 16-20, 2018 (poster)

Change in Interference Color in Diarylethene Crystals upon Photoirradiation

Kohei MORIMOTO[†], Hajime TSUJIOKA[†], Daichi KITAGAWA, Seiya KOBATAKE

10th Asian Photochemistry Conference (APC 2018), Taipei, Taiwan, December 16-20, 2018 (poster)

Determination of Solubility of Extremely Poor Water Solubility Co-crystal Melamine Cyanurate

K. IGARASHI, R. YANAGITA[†], J. ter HORST (Strathclyde University)

13th International Workshop of the Crystal Growth of Organic Material, Seoul, Korea, August 27-30, 2018 (poster)

Effect of Plastic Piece Moving in the Solution on Crystal Nucleation of L-alanine

K. IGARASHI, T. KOBAYASHI[†], H. OOSHIMA

Asian Crystallization Technology Symposium 2018, Singapore, June 20-22, 2018 (poster)

Control of Crystal Size Distribution Using a mL-Scale Continuous Crystallizer Equipped with a High Speed Agitator

K. IGARASHI, H. OOSHIMA

International Powder and Nanotechnology Forum 2018 in ACHEMA 2018, Frankfurt am Main, Germany, June 12-13, 2018 (invited)

Enhancement of Crystal Nucleation Rate by Reciprocating Plastic Piece in L-alanine Solution

T. KOBAYASHI[†], K. IGARASHI, H. OOSHIMA

11th International Conference on Separation Science and Technology (ICSST17), Busan, Korea, November 9-11, 2017 (poster)

Crystallization of a Tripeptide from the Oil Phase

K. IGARASHI, H. OOSHIMA

11th International Conference on Separation Science and Technology (ICSST17), Busan, Korea, November 9-11, 2017

Development of Large-scale Single-use Bioreactor System for a Megakaryocytic Progenitor Cell Line

Tomohiro TOKURA (Fujimori Kogyo Co., Ltd), Retno Wahyu NURHAYATI (Universitas Indonesian), Hiroyuki MATSUDA (Fujimori Kogyo Co., Ltd), Yoshihiro OJIMA, Takeaki DOHDA (Osaka University), Masahiro KINO-OKA (Osaka University)

Tissue Engineering and Regenerative Medicine International Society (TERMIS) 2018, 03-P530, Kyoto, Japan, September 4-7, 2018 (poster)

Urban Engineering

Urban Design and Engineering

Children's Bicycle Transport Mobility, Development of Safety Education Programs and Their Adaptation for Children with Disabilities

N. YOSHIDA

The International Workshop on Delivering Cycling Training and Activity Sessions for Disabled People, London, The United of Kingdom, October 11, 2018

Bicycle Transportation Policy in Japan and Recent IATSS Project

N. YOSHIDA

Japanese Association of Traffic Psychology (JATP) & International Association of Traffic and Safety Sciences (IATSS), French-Japanese workshop - Present and future of traffic psychology and neighbouring disciplines -, Tokyo, Japan, October 23-24, 2018

The estimation of CO₂ flux in subtropical coastal ecosystems using a numerical model

Hirofumi MOKI (Port and Airport Research Inst.), Akio SOHMA, Hisashi SHIBUKI (Mizuho Information and Research Inst.), Kenji TOYODA (Mizuho Information and Research Inst.), Anirban AKHAND (Port and Airport Research Inst.), Kenta WATANABE (Port and Airport Research Inst.), Tatsuki TOKORO (National Research Institute of Fisheries and Environment of Inland Sea), Tomomi INOUE (National Institute for Environmental Studies), Hiroya YAMANO (National Institute for Environmental Studies), Masayuki BANNO (Port and Airport Research Inst.), Yasuyuki NAKAGAWA (Kyushu Univ.), Hiroyuki MATSUDA (Yokohama National Univ.), and Tomohiro KUAWA (Port and Airport Research Inst.)

Proc. of the Japan Geoscience Union Meeting, ACG43-P06, Chiba, JAPAN, (2018.5) (on USB).

Coastal ecosystems can play a role in climate change mitigation. One of the appropriate way to accurately quantify and predict the role is the utilization of numerical models. The mitigation effects can be facilitated by CO₂ uptake by net primary producers such as mangroves, zooxanthella in coral reef and seagrasses. In this study, we developed a new ecosystem model that incorporates the biogeochemical processes of mangroves, tidal flats, seagrass meadows, lagoons, and coral reefs. We estimated CO₂ fluxes between air and the ecosystems and carbon burial rates in Yaeyama islands, Japan, which is the model site. In the future prediction, we selected two scenarios of representative concentration pathways, low emission (RCP2.6) and high emission (RCP8.5), adopted in IPCC 5th Assessment Report and compared the model results in 2010 and 2100. The output of HadGEM2-ES from CMIP5 models were used as the boundary data. Our model results showed that the mangrove absorbed CO₂ more than other ecosystems because of direct uptake of CO₂ from the air. The maximal carbon burial rate was found in the mangrove. Additionally, the inflowing of open waters affected the air-ecosystem CO₂ flux and carbon burial rate near the open boundary. We will also present the result of comparisons between the model results and observed data.

Ecosystem modelling to estimate blue carbon in a human-dominated estuarine and shallow coastal system

Akio SOHMA, Hisashi SHIBUKI (Mizuho Information and Research Inst.), Fumiyo NAKAJIMA (The Univ of Tokyo), Tomohiro KUAWA (Port and Airport Research Inst.)

Proc. of the International Society for Ecological Modelling Global Conference 2017, (2017.9) (on USB).

Estuarine and shallow coastal systems (ESCS) are recognized as not only significant organic carbon reservoirs but also emitters of CO₂ to the atmosphere through air-sea CO₂ gas exchange, thus posing a dilemma on ESCS's role in climate change mitigation measures. A ecosystem model composed of a benthic and a pelagic system was developed and applied to the Tokyo bay, ESCS, Japan with the goal of (1) understanding the "pattern and variability" of carbon cycle of ESCS in a high CO₂ world, (2) revealing the "key process and interaction" of ESCS as the carbon reservoirs/emitters of CO₂, and (3) evaluating the ideal "management" of ESCS to obtain the best balance among the water quality, biological productivity and carbon storage. The description of biogeochemical processes are derived from model components (i.e. TCO₂, phytoplankton, detritus, DOM, DO, Nutrients, pH and alkalinity). From the model analysis, Tokyo bay is capable of directly absorbed atmospheric CO₂. In the presentation. we summarize key factors for coastal areas to be functioned as a sink for atmospheric CO₂.

